6-12-2018

Investigation of Structure and Dynamics of Deep Eutectic Solvent Using Infrared Spectroscopy

Yaowen Cui
Louisiana State University and Agricultural and Mechanical College

INVESTIGATION OF STRUCTURE AND DYNAMICS OF DEEP EUTECTIC SOLVENT USING INFRARED SPECTROSCOPY

A Thesis

Submitted to the Graduate Faculty of the
Louisiana State University and
Agricultural and Mechanical College
in partial fulfillment of the
requirements for the degree of
Doctor of Philosophy

in

The Department of Chemistry

by
Yaowen Cui
B.E., Harbin University of Science and Technology, 2007
M.S., Western Kentucky University, 2012
August 2018

ACKNOWLEDGEMENTS

I thank and express my gratitude to my advisor Dr. Daniel G. Kuroda. During the past five years, he set a perfect example of being a scientist. He showed me his passion for science with his action. He can always find something interesting in research and be excited about it. He has the ability to make researches exciting. Another lesson I learned from him is his practical ability. He is not only the advisor of our group, but also a technician, mechanical workshop operator, electrician, and programmer, which inspires me to realize I can do more things than I thought. I was so lucky to have the opportunity to be a student under his advising, and I cannot thank him enough for being a fantastic mentor over the years.

I also give special thanks to my committee members, Dr. John Pojman, Dr. Isiah Warner, and Dr. Revati Kumar, for their support and help. Their probing questions motivated me to think about my work in depth.

I am grateful to have the opportunity to work with my wonderful group members. I send my thanks to Dr. Kristen Fulfer, who is always helpful whenever I have any question. I want to thank Susith RG Kankanamge. He is just the right person I would like to share my idea on research with, and get a smarter feedback from. I extend my earnest appreciation to other group members, Xiaoliu Zhang, Xiaobing Chen, and Jeramie Rushing for the help I have received from them. All of you are part of my most precious memory these years.

Lastly, I express appreciation to my wife. Without her, I cannot make it. The love and support is always the motivation to keep me going through the most disheartening moments.

TABLE OF CONTENTS

ABSTRACT

Deep Eutectic Solvents (DES) are liquid mixtures prepared from solids. As a new class of green solvents, DES not only share many properties with ionic liquids, such as low volatility, conductivity, tailorable constituents, but also have some advantages over ionic liquids, like easier preparation, safe and inexpensive materials, biodegradability, low toxicity, and excellent solubility. Because of those attractive properties, DES has been studied in many scientific and engineering fields. However, compared with the great number of studies of the application, many questions about structure and dynamics of DES are unanswered. To shed light on the mystery of solvent or solvation structure and dynamics, we investigated the DES systems with Fourier Transform Infrared (FTIR) and Two-Dimensional Infrared spectroscopy (2DIR). Vibrational transitions measured by infrared spectroscopy serve as sensitive probes to report the local environment and dynamics. We studied the solvation structure and dynamics of choline chloride-based DESs with thiocyanate probe. The interactions between solute and solvation shell were assigned by use of FTIR and confirmed by Molecular Dynamics (MD) simulation. The vibrational mode of infrared probes allowed detection of the solvation dynamics in choline chloride-based DESs as in-place and inter-solvation shell motions within picosecond timescale. Assignments were confirmed by the analysis of MD simulation. In another project, we studied the effects of the molecular structure of hydrogen bond acceptor on the structure and dynamics of acetamide based DES. Our studies show that symmetry of the HBA cation will affect the contribution of slow molecular motion of the environment. The overall dynamics is rationalized in terms of a microscopic heterogeneous structure of the DESs, where the heterogeneities create domains that slow making and breaking of the hydrogen bond. Heterogeneity was further supported by the use of MD simulation. Lastly, we

investigated the interactions and solvent structure of a non-ionic DES composed of N-methylacetamide and lauric acid. The interactions among the components were observed with FTIR and temperature-dependent experiments. Finally, the heterogeneous structure of DES with polar and non-polar domains was proposed, and verified by observed confined dynamics of amide band and probes, which is similar to reported water dynamics in reverse micelles.

CHAPTER 1
INTRODUCTION

1.1. Background

Solvents play an essential role in most areas in chemistry, such as synthetic, analytical, pharmaceutical, and environmental.[1-2] With the rising demands of chemical processes, the current molecular solvents cannot fulfill all new and innovative needs. Conventional solvents, including water and organic solvents, are limited by their fixed physical or chemical properties. In addition, in the case of conventional solvents by their toxicity, high vapor pressure, safety hazards, and waste management issues.[3] With the idea of green chemistry, most of the molecular solvents cannot meet the requirements of the application in green technology due to properties of being environmentally unfriendly and/or having poor recyclability.[3-5] This has spurred researchers to find alternative solvents that will lower the environmental cost of solvent applications and other requirements.

During the last several decades, efforts have been made toward the development of alternative solvents. These efforts include using supercritical fluids, specifically supercritical carbon dioxide ($scCO_2$).[5] Because of its unique properties at the supercritical point, methods using $scCO_2$ are also considered solventless methods. Supercritical CO_2 has been widely employed in the separation and the extraction process.[6-8] Compared with conventional distillation, the efficiency of the supercritical fluid is much higher.[8] However, the limited applied conditions of the supercritical fluid are a drawback for broad application. The other solution for the alternative of molecular solvents is complex solvents, including ionic liquids (ILs) and deep eutectic solvents (DESs).

In salts, even at the liquid phase, only ions exist, which causes low vapor pressure. Ionic liquids are salts with melting temperatures below 100 °C or below room temperature.[9] Even though the first ILs, ethylammonium nitrate ($EtNH_3NO_3$) was reported in 1914,[10] the research of ILs has attracted more attention in the last several decades, and the number of published work concerning ILs was grown exponentially.[11] The primary advantage of ILs is negligible vapor pressure, which allows ILs to be stable even at high temperatures and to be non-flammable. Compared with volatile organic solvents,[12] ILs are also considered to be green solvents.[13] Another excellent advantage of ILs is that the structure of ILs can be tailored by different combinations of cations and anions. This property not only allows the physical or chemical properties of ILs to be tunable but also makes it possible to put catalytic groups into the structure, which combines the roles of solvent and catalysts.[4, 9, 14] Due to the tailorable property, ILs are considered as a class of "Designer Solvent."[15] Moreover, the other advantages, such as conductivity,[16-17] broad electrochemical window,[17-18] and high solvation power, shows that ILs have promising value as an alternative solvent.

Several issues of ILs limit them from wide spread application. First, the cost of starting materials and the synthesis process are issues that cannot be ignored, especially when compared with conventional solvents. Moreover, the relatively small market for ILs leads to their application at the laboratory scale instead of the industrial scale.[19] A second issue with ILs is that they are sensitive to impurities.[20-21] The ILs have to be of very high purity and have to be operated in an inert atmosphere because moisture and CO_2 in the environment will dissolve in ILs,[22] which further increases the cost of ILs applications.

During the last two decades, Deep Eutectic Solvents (DESs) have been discovered as a new class of designer solvents. DESs is the liquid phase mixture of two or more solid components. The interaction between the components, such as hydrogen bonding interaction, depresses the

melting point of the mixture lower than the melting point of each component. The freezing behavior of DESs is presented in figure 1.1.[20] The first DES, a mixture of metal chloride and quaternary ammonium salt, was reported in 2001 by Abbott et al.[23] Later on in 2003, Abbott and coworkers reported the DESs composed of quaternary ammonium salt and urea as Hydrogen Bond Acceptor (HBA) and Hydrogen Bond Donor (HBD), respectively.[24] Since more and more DESs have been discovered, the DESs are classified into four types by Abbott and co-workers in 2007, as shown in table 1.1.[20]

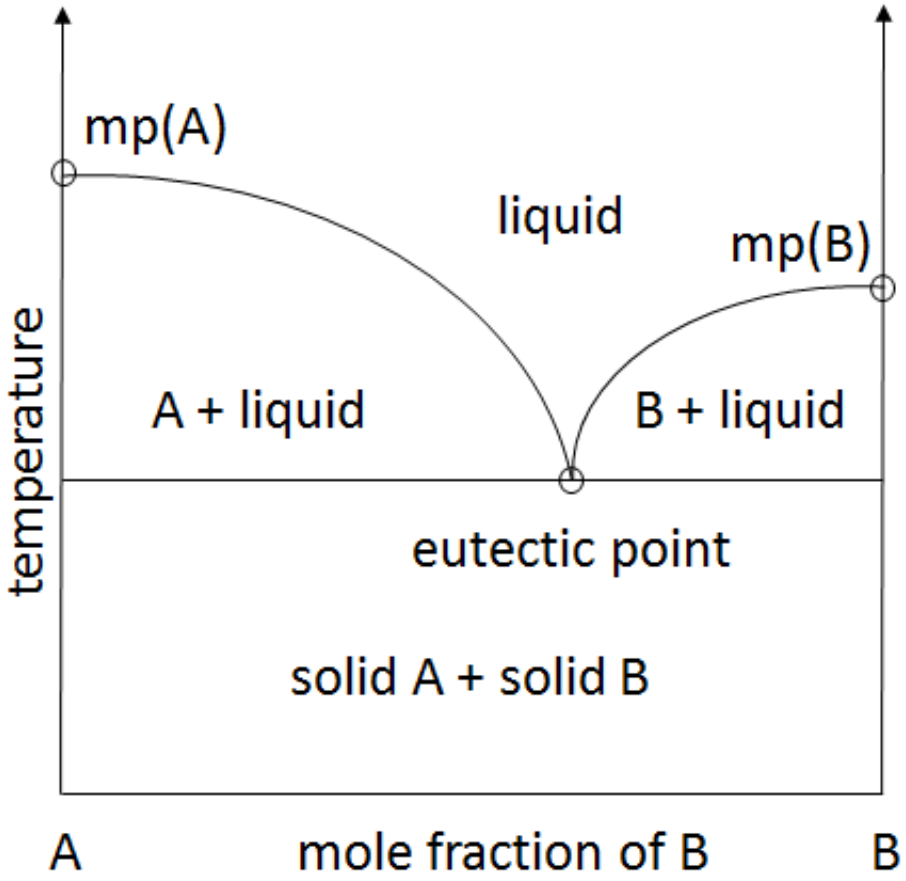

Figure 1.1. Scheme of a two-component phase diagram

Table 1.1. Categories of DESs

Type I	Organic salt + metal salt
Type II	Organic salt + metal salt hydrate
Type III	Organic salt + hydrogen-bond donor
Type IV	Metal salt + hydrogen-bond donor

Because the individual components of DESs are solid at room temperature, the vapor pressure of DESs is extremely low, which is similar to ILs. In addition, DESs share other properties of ILs, like conductivity, nonflammable, and tailorable structure; thus, DESs are considered as an analog of ILs.[20, 25] Besides the similarity to ILs properties, DESs have several advantages over ILs. First, the materials used to make DESs are usually inexpensive and easy to prepare. Choline chloride, (2-hydroxyethyl)trimethylammonium chloride, the most popular hydrogen acceptor in DESs, is a very inexpensive, quaternary ammonium salt, which can be produced at a rate of a few thousand tons per year through a high-efficiency process.[26] The materials used as a hydrogen bond donor are usually simple organic acids, alcohols, or amides, which are also inexpensive and easily acquired. Further, the synthesis simply consists of mixing the components. Compared with the preparation of ILs, ion exchange and inert gas atmosphere are necessary.[20] The preparation of DESs is a 100% atom economy process. These properties ensure the industrial application value of DESs. Secondly, even though ILs are considered as "green solvents," most of the ILs studied are toxic or not biodegradable.[25, 27] The materials in most DESs are non-toxic and biodegradable. For example, choline chloride can be added to chicken feed as a food additive.[28] With the demand of safer materials used, some Natural Deep Eutectic Solvents (NADES) have been reported. They

are composed of natural compounds, especially metabolites, such as organic acids, sugars, and amino acids.[29-30] Moreover, the structure of both DESs and ILs can be tailored to meet different requirements, but DESs allow more freedom than ILs. Not only the type DES can be produced from the combinations of different hydrogen bond donors and acceptors, but also the ratios of components can adjust the solvent properties.[24-25] With the different molar ratios of DESs, the physicochemical properties, like melting point, density, ionic conductivity, viscosity, and solvent structure, can be varied.

1.1.1. Applications

DESs have been studied in various fields including dissolution and separation processes, catalysis, electrochemistry processes, polymerization, and recently oil-spill recovery.[20,25,31-33] Most of DESs are composed of hydrogen bond donors and acceptors through strong hydrogen bond interaction.[34] Because of this feature, DESs can be an excellent solvent with the ability to dissolve a wide variety of materials, such as salts, proteins, drugs, amino acids, sugars, polysaccharides, etc.[35-37] More interestingly, DESs can dissolve various metal oxides, which, when combined with conductivity, can be used in metal recovery, metal deposition, and polishing processes.[38-42] Another benefit of using DESs is drug solubilization. Morrison, et al. reported the dissolution of several poorly soluble drugs (macromolecules) in DESs, reline (choline chloride/urea), and maline (choline chloride/malonic acid).[35] The solubility of studied drugs in pure DESs are one to five orders of magnitude times higher than that in pure water. Even for the aqueous mixture of DES, the solubility of drugs is enhanced. Combining the feature of low toxicity, DESs are accepted as promising carriers for oral dosing of rats during early medicinal investigation.[43]

One industrial application of DESs is glycerol removal from raw biodiesel due to its high polarity. During the transesterification reaction of vegetable oil with either methanol or ethanol, glycerol is produced as a by-product, and even after separation, a non-negligible amount of glycerol remaining in the biodiesel. Abbott et al. used various quaternary ammonium salts into the biodiesel, forming DES to extract glycerol from biodiesel.[44] Because of high polarity, these DESs are immiscible with biodiesel. Later choline chloride/glycerol, at a molar ratio of 1:1, was found to be the best combination of DES to remove residual glycerol from biodiesel.[45] Some other DESs like choline chloride with ethylene glycol and trifluoroacetamide were also reported as an efficient extractor of residual glycerol.[46-47]

DESs have also been applied as electrolytes for electrodeposition or as solvents for electrochemistry reactions. Even though ILs have successfully proved their potential over water and other organic solution,[48-49] the drawback of ILs for electrochemistry application, such as sensitive to water and possible degradation, cannot be ignored. Due to many similarities with ILs, DESs have successfully replaced ILs in electrochemistry application. A variety of choline chloride-based DESs has been reported to be successful electrolyte of electrodeposition.[42,50-52]

DESs have also been studied in polymer synthesis. Mota-Morales have reported frontal polymerization in choline chloride-based DESs in 2011.[53] During the polymerization process, DESs not only play the role of the polymerization medium. The polymerization performance in DESs is proven much better than conventional organic solvents and ionic liquids. The components of DESs is also the monomer in the polymerization process, which is called all-in-one system.[31,54] The polymerization in DESs with HBD,[53,55] and cation of HBA salts[56-57] as monomer were studied, respectively. The containing of monomers can be modified, which can avoid the uncontrolled polymerization problem from using ionic liquids.

A recent application of DESs involves application as a phase-selective gelator in the recovery of the oil after an oil spill.[32] The DES prepared from N-methylacetamide, and lauric acid was found to have the capacity to make oil gelation when added to a mixture of water and oil. When compared with previous synthetic gelators, this DES has a significant advantage because the only required process for preparation of the gelator is mixing. Even though only lauric acid can cause the oil to gel, the structure of DES with a lauric acid makes it easier to apply to an oil-spill, which is confirmed by comparing DES with lauric acid power and a mixture of lauric acid and ethanol.

1.2. Previous study of structure and dynamics of DES

1.2.1. Solvent structure and interactions between components

Reports on applications of DESs are abundant.[20, 25, 33] In contrast, there are only a few studies of structure and dynamics of both solvent and solvation. In 2011, Abbott et al. have reported the molecular motion and ion diffusion in choline chloride-based DESs by time-resolved Nuclear Magnetic Resonance (NMR) spectroscopy.[58] They studied four DESs, which contain choline chloride as the hydrogen bond acceptor for all the DESs with ethylene glycol, glycerol, urea, or malonic acid as hydrogen bond donors, respectively. Through the result of all the DESs from Pulsed Field Gradient NMR (PFG-NMR), the translation of HBDs (alcohols or urea molecules) diffuses faster than choline cation, while in malonic based DES are opposite due to the acid dimer formation. Moreover, the temperature dependent diffusion coefficients of all the samples were measured, and they obey the Arrhenius equation. The diffusion of choline cation is more influenced by temperature than the associated HBD molecules.

Similar DES systems were also studied by Quasielastic Neutron Scattering (QENS) by Mamontov et al.[59] The authors used a DES composed of glycerol and choline chloride to reveal the differential microscopic motion between choline cations and HBD molecules. Because of the strong interaction between chloride anion and the HBDs through hydrogen bonding, the dynamics of HBD are restricted, wherein the interaction of choline and chloride ions are weaker. Thus result the choline cations experience less restrictive local transient confinement than hydrogen bond donor molecules, even though the particle size of choline cation in the DESs is bigger than glycerol.

The interaction of components in the choline chloride-based DESs have also been studied by Molecular Dynamics (MD) simulation combined with FTIR spectra by Colina et al.[60-61] By examining the systems of choline chloride-based DESs with ethylene glycol, glycerol, urea, and malonic acid as HBDs, they highlighted the importance of the strong hydrogen bond interaction between hydrogen bond donor molecules and chloride anions, which takes more than a 50% fraction of the hydrogen bonds in all the DESs. The intermolecular hydrogen bond between HBD molecules also appears, but with less significance. Their FTIR spectra of the DES with malonic acid, along with each component as comparisons, shows that both the hydroxyl and carbonyl region have a vibrational coupling, making the frequencies shift and shapes broader.

The charge delocalization of DESs was also studied with ab-initio molecular dynamics simulation by Mollenhauer et al.[62] The authors compared the charge distribution in choline based DESs with urea, ethylene glycol, and oxalic acid as HBDs, respectively. Also, the strong hydrogen bonding between anions and HBD molecules is confirmed. The author also showed that the varied hydrogen bond strengths between anion and HBDs will change the charge distribution of the cation on nitrogen and oxygen atoms. Finally, the distance between the anion and atoms of the cations

reveals that the major interaction between anion and cation in choline chloride-based DESs is through the anion and OH group of the cation.

Those studies focused on the interactions of cations and HBDs in the pure DES. It is worth noting that in Colina's work, the authors mentioned the interaction through cations and HBDs have the smallest hydrogen bond contribution by the analysis of the Radial Distribution Function (RDF). Also, Mollenhauer's work confirms that the hydrogen bonding through choline OH group by the charge of oxygen in choline is reduced from the gas phase.[62] However, the overall picture of how the interaction through OH group of choline and the interactions between the choline hydroxyl group and HBDs is not provided. Furthermore, the influence of the chemical structure of the cation of HBAs in type III DESs is also a mystery.

1.2.2. Solvation structure and dynamics of DESs

The solvation structure and dynamics are equally important as those of the solvent alone since they can help to understand the interaction between solute and solvent microscopically and lead to developing the application of DESs. Over the last several years, the solvation structure and dynamics of solutes in DESs have been investigated.

Biswas and his co-workers investigated the solvation structure and dynamics of multiple types of DESs via steady-state and time-resolved spectroscopy.[63-69] Among them, the acetamide-electrolyte DES have been extensively studied by femtosecond Raman-induced Kerr effect spectroscopy, steady state, and time-resolved fluorescence spectroscopies. In these studies, the authors used molecular dyes (chromophore) as the solute to report the solute-solvent interaction. The dye molecules of fluorescence can emit light upon light excitation. With this method, the translation and rotation of the deep eutectic mixture of acetamide and different alkali metal

electrolytes or their combinations are explored.[66,69] Their results showed that pronounced solution heterogeneity exists in the deep eutectic mixtures of acetamide with alkali metal inorganic salts.

The same group also studied the reactive and nonreactive dynamics of the most popular type III DESs, choline chloride with urea, by steady and time-resolved fluorescence spectroscopy.[70] According to their study, the system choline chloride-urea presents moderate spatial and dynamical heterogeneity. Interestingly, the solvation and rotation times in the DES have different correlations while changing components, while that correlation conventional molecular solvent and ionic liquid are considered to be the same. This phenomenon shows that the differential rotation and solvation dynamics with the medium. Plus, this study provides evidence of deep eutectic solvent differing significantly from ionic liquids.

1.2.3. The solvent structure of non-ionic DES

DESs are classified into four types as mentioned,[20] but there are several non-ionic based DESs that have been reported.[32,63,71] these DESs fall outside of the four classes of DES defined by Abbott. The structure and dynamics of one of these DESs, composed of acetamide and urea, was studied by Biswas et al.[63] The non-ionic DES has a spatial and dynamical homogeneity, which differs from the same group of measured ionic DESs, with either moderate or pronounced spatial and dynamical heterogeneity. The homogeneous solution structure was also supported by the analysis of all-atom MD simulation.

Later, the hydrophobic DESs composed of menthol and carboxylic acid were reported.[71] The author explored menthol based DES and found the eutectic mixing ratios of each constituent and examined the physical properties. It is worth noting that, their viscosity and density are lower

than regular ionic DESs. The FTIR spectra of each eutectic mixture confirmed the hydrogen bond interaction between menthol and hydrogen bond donor (carboxylic acid).

Another hydrophobic non-ionic DES, the mixture of NMA-LA, was reported in 2017, which is similar to the menthol based DES.[32] This DES has a lot of similarity with the menthol based DES, including low density and viscosity, hydrophobicity, and also has hydrogen bond interaction between the two components. However, unlike the menthol-based DES, because both NMA and lauric acid contain carbonyl group and a OH or NH group, they both have the capacity to be considered as a hydrogen bond acceptor and donor. Currently, there is no work investigating the interaction between amide and carboxylic acid in the DES system. Interestingly, from the polarity view, the NMA molecule is polar and hydrophilic, and because of the long alkane chain, lauric acid is hydrophobic. Moreover, their mixture is also hydrophobic. The questions on what is the position of NMA in the DES, and will that cause a heterogeneous microstructure in the DES are unanswered.

1.3. Structural and dynamical study with infrared spectroscopy

The structure and dynamics of DESs can be studied experimentally by adding a chromophore that can sense the structure or dynamics directly or indirectly. For infrared spectroscopy, some groups, like carbonyl, and nitrile groups, are widely employed to study the structure and dynamics of the condensed phase.[72-79] Compared to molecular dyes previously mentioned, the infrared probe is sensitive to the local environmental change because of the small size, while common molecular dyes are a large molecules. Moreover, the low energy of the light source of time-resolved infrared spectroscopy causes a negligible change in temperature, which

ensures that the system equilibrium remains unchanged.[80-81]. Therefore, the investigation of structure and dynamics of DESs are carried out with the steady-state and time-resolved infrared spectra of probes in DESs.

In addition to Fourier Infrared Spectroscopy as a steady-state spectroscopy, Two-Dimensional Infrared Spectroscopy is another major technique used in this work. 2DIR spectroscopy is the infrared analogue of 2D NMR. The advantage of 2DIR is that it is capable of measuring the evolution of vibrational transitions of structures in picosecond or even sub-picosecond timescale. The first femtosecond three pulse infrared photon echo was measured by Hochstrasser and co-workers favored from the advent of femtosecond laser.[82] The following decades 2DIR spectroscopy was used to investigate structure and dynamics in many fields, including aqueous systems,[83-89] biochemistry,[90-93] ionic liquid,[94-97] polymer,[98], electrolyte,[99-100] and interface of nanoparticles.[101-102]

The signal of 2DIR, vibrational photon echo, is produced by the interaction of three femtosecond infrared pulses with a sample. The photon echo generated at the phase-matching direction, is measured with heterodyne detection by overlapped with a forth phase-locked pulse, called local oscillator. The raw data collected at varied coherence time and detection time but constant delay time, will be transferred with Fourier Transform to frequency-domain as coherence and detection frequency, respectively. A 2DIR spectrum is contoured intensity of ω_τ versus ω_t as different T. By comparing the correlation between ω_τ and ω_t with different T, the dynamics such as chemical exchange, energy transfer, and spectral diffusion can be extracted.

1.4. Outline of this thesis

The focus of the work described in this thesis is to investigate solvent and solvation structure and dynamics of Deep Eutectic Solvents using FTIR and 2DIR spectroscopy assisted with Molecular Dynamics simulation. In chapter 2, the theory of third-order nonlinear response, signal treatment after-acquired, and Liouville pathways are described with the diagrammatic approach. The experimental details of 2DIR, like data collecting and methods of data analysis, are also described.

In chapter 3, the solvation dynamics of three choline based DESs with ethylene glycol, glycerol, and urea, respectively, were investigated. The nitrile stretching mode in thiocyanate ion as an infrared probe detected the solvation dynamics in all the DESs as in-place and inter-solvation shell motions within a picosecond timescale. The assignment was confirmed by use of MD simulation and ab initio computations. Finally, frequency fluctuations of the probe in DESs calculated from the combination FTIR and 2DIR data showed the DES with urea has better organized molecular structure than the other two DESs.

In Chapter 4, my studies focus on the effect of the side chain of hydrogen bond acceptor in the amide-based DES. The differential dynamics was extracted from the 2DIR spectra of the carbonyl of naturally contained isotope ^{13}C in each DES as a probe. All DESs were observed to have hydrogen bond making and breaking dynamics. The symmetry of HBA cation affects the contribution of slow molecular motion of the environment. The overall dynamics is rationalized in terms of a microscopic heterogeneous structure of the DESs, where the heterogeneities create domains that slow the hydrogen bond making and breaking. The heterogeneity was further supported by molecular dynamics simulation.

Chapter 5 is a presentation of an investigation of the interactions between constituents of a non-ionic DES composed of N-methylacetamide (NMA) and lauric acid (LA). In the DES, interactions between self-species and inter-species of the two components are observed. The heterogeneous structure of DES with polar and non-polar domains was proposed and verified by observing confined dynamics of amide I band and probes, which is similar to reported water dynamics in reverse micelles.

1.5. References

1. Kerton, F., Renewable Solvents in Alternative Solvents for Green Chemistry. Fm Kerton. Cambridge, Royal Society of Chemistry: 2009.

2. Hu, Z.; Oskam, G.; Searson, P. C., Influence of Solvent on the Growth of Zno Nanoparticles. *Journal of Colloid and Interface Science* **2003**, *263*, 454-460.

3. Gani, R.; Jiménez-González, C.; Constable, D. J., Method for Selection of Solvents for Promotion of Organic Reactions. *Computers & Chemical Engineering* **2005**, *29*, 1661-1676.

4. Welton, T., Room-Temperature Ionic Liquids. Solvents for Synthesis and Catalysis. *Chemical reviews* **1999**, *99*, 2071-2084.

5. Clark, J. H.; Tavener, S. J., Alternative Solvents: Shades of Green. *Organic process research & development* **2007**, *11*, 149-155.

6. Erkey, C., Supercritical Carbon Dioxide Extraction of Metals from Aqueous Solutions: A Review. *The Journal of Supercritical Fluids* **2000**, *17*, 259-287.

7. Yamaguchi, K.; Murakami, M.; Nakano, H.; Konosu, S.; Kokura, T.; Yamamoto, H.; Kosaka, M.; Hata, K., Supercritical Carbon Dioxide Extraction of Oils from Antarctic Krill. *Journal of Agricultural and Food Chemistry* **1986**, *34*, 904-907.

8. Díaz-Maroto, M. C.; Perez-Coello, M. S.; Cabezudo, M. D., Supercritical Carbon Dioxide Extraction of Volatiles from Spices: Comparison with Simultaneous Distillation–Extraction. *Journal of Chromatography A* **2002**, *947*, 23-29.

9. Wasserscheid, P.; Welton, T., *Ionic Liquids in Synthesis*; John Wiley & Sons, 2008.

10. Walden, P., Molecular Weights and Electrical Conductivity of Several Fused Salts. *Bull. Acad. Imper. Sci.(St. Petersburg)* **1914**, *1800*.

11. Petkovic, M.; Seddon, K. R.; Rebelo, L. P. N.; Pereira, C. S., Ionic Liquids: A Pathway to Environmental Acceptability. *Chemical Society Reviews* **2011**, *40*, 1383-1403.

12. Moniruzzaman, M.; Ono, T., Ionic Liquid Assisted Enzymatic Delignification of Wood Biomass: A New 'Green'and Efficient Approach for Isolating of Cellulose Fibers. *Biochemical Engineering Journal* **2012**, *60*, 156-160.

13. Earle, M. J.; Seddon, K. R., Ionic Liquids. Green Solvents for the Future. *Pure and applied chemistry* **2000**, *72*, 1391-1398.

14. Sheldon, R., Catalytic Reactions in Ionic Liquids. *Chemical Communications* **2001**, 2399-2407.

15. Plechkova, N. V.; Seddon, K. R., Ionic Liquids:"Designer" Solvents for Green Chemistry. *Methods and Reagents for Green Chemistry* **2007**, 105-130.

16. Galiński, M.; Lewandowski, A.; Stępniak, I., Ionic Liquids as Electrolytes. *Electrochimica acta* **2006**, *51*, 5567-5580.

17. Ohno, H., *Electrochemical Aspects of Ionic Liquids*; John Wiley & Sons, 2005.

18. Armand, M.; Endres, F.; MacFarlane, D. R.; Ohno, H.; Scrosati, B., Ionic-Liquid Materials for the Electrochemical Challenges of the Future. *Nature materials* **2009**, *8*, 621-629.

19. Wypych, G., *Handbook of Solvents*; ChemTec Publishing, 2001.

20. Smith, E. L.; Abbott, A. P.; Ryder, K. S., Deep Eutectic Solvents (Dess) and Their Applications. *Chemical reviews* **2014**, *114*, 11060-11082.

21. Widegren, J. A.; Saurer, E. M.; Marsh, K. N.; Magee, J. W., Electrolytic Conductivity of Four Imidazolium-Based Room-Temperature Ionic Liquids and the Effect of a Water Impurity. *The Journal of Chemical Thermodynamics* **2005**, *37*, 569-575.

22. Camper, D.; Scovazzo, P.; Koval, C.; Noble, R., Gas Solubilities in Room-Temperature Ionic Liquids. *Industrial & Engineering Chemistry Research* **2004**, *43*, 3049-3054.

23. Abbott, A. P.; Capper, G.; Davies, D. L.; Munro, H. L.; Rasheed, R. K.; Tambyrajah, V., Preparation of Novel, Moisture-Stable, Lewis-Acidic Ionic Liquids Containing Quaternary Ammonium Salts with Functional Side Chainselectronic, *Chemical Communications* **2001**, 2010-2011.

24. Abbott, A. P.; Capper, G.; Davies, D. L.; Rasheed, R. K.; Tambyrajah, V., Novel Solvent Properties of Choline Chloride/Urea Mixtures. *Chemical Communications* **2003**, 70-71.

25. Zhang, Q.; Vigier, K. D. O.; Royer, S.; Jérôme, F., Deep Eutectic Solvents: Syntheses, Properties and Applications. *Chemical Society Reviews* **2012**, *41*, 7108-7146.

26. Liu, F.; Audemar, M.; Vigier, K. D. O.; Cartigny, D.; Clacens, J.-M.; Gomes, M. F. C.; Pádua, A. A.; De Campo, F.; Jérôme, F., Selectivity Enhancement in the Aqueous Acid-Catalyzed Conversion of Glucose to 5-Hydroxymethylfurfural Induced by Choline Chloride. *Green Chemistry* **2013**, *15*, 3205-3213.

27. Couling, D. J.; Bernot, R. J.; Docherty, K. M.; Dixon, J. K.; Maginn, E. J., Assessing the Factors Responsible for Ionic Liquid Toxicity to Aquatic Organisms Via Quantitative Structure–Property Relationship Modeling. *Green Chemistry* **2006**, *8*, 82-90.

28. Daghir, N.; Marion, W.; Balloun, S., Influence of Dietary Fat and Choline on Serum and Egg Yolk Cholesterol in the Laying Chicken. *Poultry Science* **1960**, *39*, 1459-1466.

29. Choi, Y. H.; van Spronsen, J.; Dai, Y.; Verberne, M.; Hollmann, F.; Arends, I. W.; Witkamp, G.-J.; Verpoorte, R., Are Natural Deep Eutectic Solvents the Missing Link in Understanding Cellular Metabolism and Physiology? *Plant physiology* **2011**, *156*, 1701-1705.

30. Dai, Y.; van Spronsen, J.; Witkamp, G.-J.; Verpoorte, R.; Choi, Y. H., Natural Deep Eutectic Solvents as New Potential Media for Green Technology. *Analytica chimica acta* **2013**, *766*, 61-68.

31. Carriazo, D.; Serrano, M. C.; Gutiérrez, M. C.; Ferrer, M. L.; del Monte, F., Deep-Eutectic Solvents Playing Multiple Roles in the Synthesis of Polymers and Related Materials. *Chemical Society Reviews* **2012**, *41*, 4996-5014.

32. Cui, Y.; Li, M.-C.; Wu, Q.; Pojman, J. A.; Kuroda, D. G., Synthesis-Free Phase-Selective Gelator for Oil-Spill Remediation. *ACS applied materials & interfaces* **2017**, *9*, 33549-33553.

33. Tang, B.; Row, K. H., Recent Developments in Deep Eutectic Solvents in Chemical Sciences. *Monatshefte für Chemie-Chemical Monthly* **2013**, *144*, 1427-1454.

34. Abbott, A. P.; Frisch, G.; Hartley, J.; Ryder, K. S., Processing of Metals and Metal Oxides Using Ionic Liquids. *Green Chemistry* **2011**, *13*, 471-481.

35. Morrison, H. G.; Sun, C. C.; Neervannan, S., Characterization of Thermal Behavior of Deep Eutectic Solvents and Their Potential as Drug Solubilization Vehicles. *International journal of pharmaceutics* **2009**, *378*, 136-139.

36. Mamajanov, I.; Engelhart, A. E.; Bean, H. D.; Hud, N. V., DNA and Rna in Anhydrous Media: Duplex, Triplex, and G-Quadruplex Secondary Structures in a Deep Eutectic Solvent. *Angewandte Chemie International Edition* **2010**, *49*, 6310-6314.

37. Guo, W.; Hou, Y.; Wu, W.; Ren, S.; Tian, S.; Marsh, K. N., Separation of Phenol from Model Oils with Quaternary Ammonium Salts Via Forming Deep Eutectic Solvents. *Green Chemistry* **2013**, *15*, 226-229.

38. Shivagan, D.; Dale, P.; Samantilleke, A.; Peter, L., Electrodeposition of Chalcopyrite Films from Ionic Liquid Electrolytes. *Thin Solid Films* **2007**, *515*, 5899-5903.

39. Abbott, A. P.; Capper, G.; McKenzie, K. J.; Ryder, K. S., Electrodeposition of Zinc–Tin Alloys from Deep Eutectic Solvents Based on Choline Chloride. *Journal of Electroanalytical Chemistry* **2007**, *599*, 288-294.

40. Abbott, A. P.; El Ttaib, K.; Frisch, G.; McKenzie, K. J.; Ryder, K. S., Electrodeposition of Copper Composites from Deep Eutectic Solvents Based on Choline Chloride. *Physical Chemistry Chemical Physics* **2009**, *11*, 4269-4277.

41. Popescu, A.-M.; Constantin, V.; Cojocaru, A.; Olteanu, M., Electrochemical Behaviour of Copper (Ii) Chloride in Choline Chloride-Urea Deep Eutectic Solvent. *Rev. Chim.(Bucharest)* **2011**, *62*, 206-211.

42. Gómez, E.; Cojocaru, P.; Magagnin, L.; Valles, E., Electrodeposition of Co, Sm and Smco from a Deep Eutectic Solvent. *Journal of electroanalytical chemistry* **2011**, *658*, 18-24.

43. Morrison, H. G.; Sun, C. C.; Neervannan, S., Characterization of Thermal Behavior of Deep Eutectic Solvents and Their Potential as Drug Solubilization Vehicles. *International journal of pharmaceutics* **2009**, *378*, 136-139.

44. Abbott, A. P.; Cullis, P. M.; Gibson, M. J.; Harris, R. C.; Raven, E., Extraction of Glycerol from Biodiesel into a Eutectic Based Ionic Liquid. *Green Chemistry* **2007**, *9*, 868-872.

45. Hayyan, M.; Mjalli, F. S.; Hashim, M. A.; AlNashef, I. M., A Novel Technique for Separating Glycerine from Palm Oil-Based Biodiesel Using Ionic Liquids. *Fuel Processing Technology* **2010**, *91*, 116-120.

46. Shahbaz, K.; Mjalli, F. S.; Hashim, M.; Al-Nashef, I. M., Using Deep Eutectic Solvents for the Removal of Glycerol from Palm Oil-Based Biodiesel. *Journal of Applied Sciences* **2010**, *10*, 3349-3354.

47. Shahbaz, K.; Mjalli, F.; Hashim, M.; AlNashef, I., Using Deep Eutectic Solvents Based on Methyl Triphenyl Phosphunium Bromide for the Removal of Glycerol from Palm-Oil-Based Biodiesel. *Energy & Fuels* **2011**, *25*, 2671-2678.

48. Abbott, A. P.; Capper, G.; Davies, D. L.; Rasheed, R., Ionic Liquids Based Upon Metal Halide/Substituted Quaternary Ammonium Salt Mixtures. *Inorganic Chemistry* **2004**, *43*, 3447-3452.

49. Yang, J.-Z.; Tian, P.; He, L.-L.; Xu, W.-G., Studies on Room Temperature Ionic Liquid Incl 3–Emic. *Fluid Phase Equilibria* **2003**, *204*, 295-302.

50. Smith, E. L.; Barron, J. C.; Abbott, A. P.; Ryder, K. S., Time Resolved in Situ Liquid Atomic Force Microscopy and Simultaneous Acoustic Impedance Electrochemical Quartz Crystal Microbalance Measurements: A Study of Zn Deposition. *Analytical chemistry* **2009**, *81*, 8466-8471.

51. Figueiredo, M.; Gomes, C.; Costa, R.; Martins, A.; Pereira, C. M.; Silva, F., Differential Capacity of a Deep Eutectic Solvent Based on Choline Chloride and Glycerol on Solid Electrodes. *Electrochimica Acta* **2009**, *54*, 2630-2634.

52. Nkuku, C. A.; LeSuer, R. J., Electrochemistry in Deep Eutectic Solvents. *The Journal of Physical Chemistry B* **2007**, *111*, 13271-13277.

53. Mota-Morales, J. D.; Gutiérrez, M. C.; Sanchez, I. C.; Luna-Barcenas, G.; del Monte, F., Frontal Polymerizations Carried out in Deep-Eutectic Mixtures Providing Both the Monomers and the Polymerization Medium. *Chemical Communications* **2011**, *47*, 5328-5330.

54. Carriazo, D.; Gutiérrez, M. a. C.; Ferrer, M. L.; del Monte, F., Resorcinol-Based Deep Eutectic Solvents as Both Carbonaceous Precursors and Templating Agents in the Synthesis of Hierarchical Porous Carbon Monoliths. *Chemistry of Materials* **2010**, *22*, 6146-6152.

55. Fazende, K. F.; Phachansitthi, M.; Mota-Morales, J. D.; Pojman, J. A., Frontal Polymerization of Deep Eutectic Solvents Composed of Acrylic and Methacrylic Acids. *Journal of Polymer Science Part A: Polymer Chemistry* **2017**, *55*, 4046-4050.

56. Isik, M.; Ruiperez, F.; Sardon, H.; Gonzalez, A.; Zulfiqar, S.; Mecerreyes, D., Innovative Poly (Ionic Liquid) S by the Polymerization of Deep Eutectic Monomers. *Macromolecular rapid communications* **2016**, *37*, 1135-1142.

57. Serrano, M. C.; Gutiérrez, M. C.; Jiménez, R.; Ferrer, M. L.; del Monte, F., Synthesis of Novel Lidocaine-Releasing Poly (Diol-Co-Citrate) Elastomers by Using Deep Eutectic Solvents. *Chemical Communications* **2012**, *48*, 579-581.

58. D'Agostino, C.; Harris, R. C.; Abbott, A. P.; Gladden, L. F.; Mantle, M. D., Molecular Motion and Ion Diffusion in Choline Chloride Based Deep Eutectic Solvents Studied by 1 H Pulsed Field Gradient Nmr Spectroscopy. *Physical Chemistry Chemical Physics* **2011**, *13*, 21383-21391.

59. Wagle, D. V.; Baker, G. A.; Mamontov, E., Differential Microscopic Mobility of Components within a Deep Eutectic Solvent. *The journal of physical chemistry letters* **2015**, *6*, 2924-2928.

60. Perkins, S. L.; Painter, P.; Colina, C. M., Experimental and Computational Studies of Choline Chloride-Based Deep Eutectic Solvents. *Journal of Chemical & Engineering Data* **2014**, *59*, 3652-3662.

61. Perkins, S. L.; Painter, P.; Colina, C. M., Molecular Dynamic Simulations and Vibrational Analysis of an Ionic Liquid Analogue. *The Journal of Physical Chemistry B* **2013**, *117*, 10250-10260.

62. Zahn, S.; Kirchner, B.; Mollenhauer, D., Charge Spreading in Deep Eutectic Solvents. *ChemPhysChem* **2016**, *17*, 3354-3358.

63. Das, A.; Das, S.; Biswas, R., Density Relaxation and Particle Motion Characteristics in a Non-Ionic Deep Eutectic Solvent (Acetamide+ Urea): Time-Resolved Fluorescence Measurements and All-Atom Molecular Dynamics Simulations. *The Journal of chemical physics* **2015**, *142*, 034505.

64. Indra, S.; Biswas, R., How Heterogeneous Are Trehalose/Glycerol Cryoprotectant Mixtures? A Combined Time-Resolved Fluorescence and Computer Simulation Investigation. *The Journal of Physical Chemistry B* **2016**, *120*, 11214-11228.

65. Biswas, R.; Das, A.; Shirota, H., Low-Frequency Collective Dynamics in Deep Eutectic Solvents of Acetamide and Electrolytes: A Femtosecond Raman-Induced Kerr Effect Spectroscopic Study. *The Journal of chemical physics* **2014**, *141*, 134506.

66. Das, A.; Das, S.; Biswas, R., Fast Fluctuations in Deep Eutectic Melts: Multi-Probe Fluorescence Measurements and All-Atom Molecular Dynamics Simulation Study. *Chemical Physics Letters* **2013**, *581*, 47-51.

67. Guchhait, B.; Al Rasid Gazi, H.; Kashyap, H. K.; Biswas, R., Fluorescence Spectroscopic Studies of (Acetamide+ Sodium/Potassium Thiocyanates) Molten Mixtures: Composition and Temperature Dependence. *The Journal of Physical Chemistry B* **2010**, *114*, 5066-5081.

68. Gazi, H. A. R.; Guchhait, B.; Daschakraborty, S.; Biswas, R., Fluorescence Dynamics in Supercooled (Acetamide+ Calcium Nitrate) Molten Mixtures. *Chemical Physics Letters* **2011**, *501*, 358-363.

69. Guchhait, B.; Daschakraborty, S.; Biswas, R., Medium Decoupling of Dynamics at Temperatures∼ 100 K above Glass-Transition Temperature: A Case Study with (Acetamide+ Lithium Bromide/Nitrate) Melts. *The Journal of chemical physics* **2012**, *136*, 174503.

70. Das, A.; Biswas, R., Dynamic Solvent Control of a Reaction in Ionic Deep Eutectic Solvents: Time-Resolved Fluorescence Measurements of Reactive and Nonreactive Dynamics in (Choline Chloride+ Urea) Melts. *The Journal of Physical Chemistry B* **2015**, *119*, 10102-10113.

71. Ribeiro, B. D.; Florindo, C.; Iff, L. C.; Coelho, M. A.; Marrucho, I. M., Menthol-Based Eutectic Mixtures: Hydrophobic Low Viscosity Solvents. *ACS Sustainable Chemistry & Engineering* **2015**, *3*, 2469-2477.

72. Ohta, K.; Maekawa, H.; Saito, S.; Tominaga, K., Probing the Spectral Diffusion of Vibrational Transitions of Ocn-and Scn-in Methanol by Three-Pulse Infrared Photon Echo Spectroscopy. *The Journal of Physical Chemistry A* **2003**, *107*, 5643-5649.

73. Thøgersen, J.; Rehault, J.; Odelius, M.; Ogden, T.; Jena, N. K.; Jensen, S. J. K.; Keiding, S. R.; Helbing, J., Hydration Dynamics of Aqueous Nitrate. *The Journal of Physical Chemistry B* **2013**, *117*, 3376-3388.

74. Kuroda, D. G.; Vorobyev, D. Y.; Hochstrasser, R. M., Ultrafast Relaxation and 2d Ir of the Aqueous Trifluorocarboxylate Ion. *The Journal of chemical physics* **2010**, *132*, 044501.

75. Singh, P. K.; Kuroda, D. G.; Hochstrasser, R. M., An Ion's Perspective on the Molecular Motions of Nanoconfined Water: A Two-Dimensional Infrared Spectroscopy Study. *The Journal of Physical Chemistry B* **2013**, *117*, 9775-9784.

76. Dahl, K.; Sando, G. M.; Fox, D. M.; Sutto, T. E.; Owrutsky, J. C., Vibrational Spectroscopy and Dynamics of Small Anions in Ionic Liquid Solutions. *The Journal of chemical physics* **2005**, *123*, 084504.

77. Mandal, A.; Ramasesha, K.; De Marco, L.; Tokmakoff, A., Collective Vibrations of Water-Solvated Hydroxide Ions Investigated with Broadband 2dir Spectroscopy. *The Journal of chemical physics* **2014**, *140*, 204508.

78. Moilanen, D. E.; Wong, D.; Rosenfeld, D. E.; Fenn, E. E.; Fayer, M., Ion–Water Hydrogen-Bond Switching Observed with 2d Ir Vibrational Echo Chemical Exchange Spectroscopy. *Proceedings of the National Academy of Sciences* **2009**, *106*, 375-380.

79. Park, K. H.; Choi, S. R.; Choi, J. H.; Park, S.; Cho, M., Real-Time Probing of Ion Pairing Dynamics with 2dir Spectroscopy. *ChemPhysChem* **2010**, *11*, 3632-3637.

80. Nienhuys, H.-K.; Woutersen, S.; van Santen, R. A.; Bakker, H. J., Mechanism for Vibrational Relaxation in Water Investigated by Femtosecond Infrared Spectroscopy. *The Journal of chemical physics* **1999**, *111*, 1494-1500.

81. Chuntonov, L.; Kumar, R.; Kuroda, D. G., Non-Linear Infrared Spectroscopy of the Water Bending Mode: Direct Experimental Evidence of Hydration Shell Reorganization? *Physical Chemistry Chemical Physics* **2014**, *16*, 13172-13181.

82. Hamm, P.; Lim, M.; Hochstrasser, R. M., Non-Markovian Dynamics of the Vibrations of Ions in Water from Femtosecond Infrared Three-Pulse Photon Echoes. *Physical review letters* **1998**, *81*, 5326.

83. Nicodemus, R. A.; Ramasesha, K.; Roberts, S. T.; Tokmakoff, A., Hydrogen Bond Rearrangements in Water Probed with Temperature-Dependent 2d Ir. *The Journal of Physical Chemistry Letters* **2010**, *1*, 1068-1072.

84. Fayer, M. D.; Moilanen, D. E.; Wong, D.; Rosenfeld, D. E.; Fenn, E. E.; Park, S., Water Dynamics in Salt Solutions Studied with Ultrafast Two-Dimensional Infrared (2d Ir) Vibrational Echo Spectroscopy. *Accounts of chemical research* **2009**, *42*, 1210-1219.

85. King, J. T.; Ross, M. R.; Kubarych, K. J., Water-Assisted Vibrational Relaxation of a Metal Carbonyl Complex Studied with Ultrafast 2d-Ir. *The Journal of Physical Chemistry B* **2012**, *116*, 3754-3759.

86. Thämer, M.; De Marco, L.; Ramasesha, K.; Mandal, A.; Tokmakoff, A., Ultrafast 2d Ir Spectroscopy of the Excess Proton in Liquid Water. *Science* **2015**, *350*, 78-82.

87. Ramasesha, K.; Roberts, S. T.; Nicodemus, R. A.; Mandal, A.; Tokmakoff, A., Ultrafast 2d Ir Anisotropy of Water Reveals Reorientation During Hydrogen-Bond Switching. *The Journal of chemical physics* **2011**, *135*, 054509.

88. Eaves, J.; Loparo, J.; Fecko, C. J.; Roberts, S.; Tokmakoff, A.; Geissler, P., Hydrogen Bonds in Liquid Water Are Broken Only Fleetingly. *Proceedings of the National Academy of Sciences of the United States of America* **2005**, *102*, 13019-13022.

89. Kim, Y. S.; Hochstrasser, R. M., The 2d Ir Responses of Amide and Carbonyl Modes in Water Cannot Be Described by Gaussian Frequency Fluctuations. *The Journal of Physical Chemistry B* **2007**, *111*, 9697-9701.

90. Kim, Y. S.; Hochstrasser, R. M., Applications of 2d Ir Spectroscopy to Peptides, Proteins, and Hydrogen-Bond Dynamics. *The Journal of Physical Chemistry B* **2009**, *113*, 8231-8251.

91. DeFlores, L. P.; Ganim, Z.; Nicodemus, R. A.; Tokmakoff, A., Amide I′− Ii′ 2d Ir Spectroscopy Provides Enhanced Protein Secondary Structural Sensitivity. *Journal of the American Chemical Society* **2009**, *131*, 3385-3391.

92. Ganim, Z.; Chung, H. S.; Smith, A. W.; DeFlores, L. P.; Jones, K. C.; Tokmakoff, A., Amide I Two-Dimensional Infrared Spectroscopy of Proteins. *Accounts of chemical research* **2008**, *41*, 432-441.

93. Chung, J. K.; Thielges, M. C.; Bowman, S. E.; Bren, K. L.; Fayer, M., Temperature Dependent Equilibrium Native to Unfolded Protein Dynamics and Properties Observed with Ir Absorption and 2d Ir Vibrational Echo Experiments. *Journal of the American Chemical Society* **2011**, *133*, 6681-6691.

94. Ren, Z.; Ivanova, A. S.; Couchot-Vore, D.; Garrett-Roe, S., Ultrafast Structure and Dynamics in Ionic Liquids: 2d-Ir Spectroscopy Probes the Molecular Origin of Viscosity. *The journal of physical chemistry letters* **2014**, *5*, 1541-1546.

95. Tamimi, A.; Fayer, M. D., Ionic Liquid Dynamics Measured with 2d Ir and Ir Pump–Probe Experiments on a Linear Anion and the Influence of Potassium Cations. *The Journal of Physical Chemistry B* **2016**, *120*, 5842-5854.

96. Brinzer, T.; Berquist, E. J.; Ren, Z.; 任哲; Dutta, S.; Johnson, C. A.; Krisher, C. S.; Lambrecht, D. S.; Garrett-Roe, S., Ultrafast Vibrational Spectroscopy (2d-Ir) of Co2 in Ionic Liquids: Carbon Capture from Carbon Dioxide's Point of View. *The Journal of chemical physics* **2015**, *142*, 212425.

97. Kramer, P. L.; Giammanco, C. H.; Fayer, M. D., Dynamics of Water, Methanol, and Ethanol in a Room Temperature Ionic Liquid. *The Journal of chemical physics* **2015**, *142*, 212408.

98. Ma, J.; Xuan, S.; Guerin, A. C.; Yu, T.; Zhang, D.; Kuroda, D. G., Unusual Molecular Mechanism Behind the Thermal Response of Polypeptoids in Aqueous Solutions. *Physical Chemistry Chemical Physics* **2017**, *19*, 10878-10888.

99. Fulfer, K. D.; Kuroda, D. G., Solvation Structure and Dynamics of the Lithium Ion in Organic Carbonate-Based Electrolytes: A Time-Dependent Infrared Spectroscopy Study. *The Journal of Physical Chemistry C* **2016**, *120*, 24011-24022.

100. Li, K.; Galle Kankanamge, S. R.; Weldeghiorghis, T. K.; Jorn, R.; Kuroda, D. G.; Kumar, R., Predicting Ion Association in Sodium Electrolytes: A Transferrable Model for Investigating Glymes. *The Journal of Physical Chemistry C* **2017**.

101. Donaldson, P. M.; Hamm, P., Gold Nanoparticle Capping Layers: Structure, Dynamics, and Surface Enhancement Measured Using 2d-Ir Spectroscopy. *Angewandte Chemie* **2013**, *125*, 662-666.

102. Huber, C. J.; Egger, S. M.; Spector, I. C.; Juelfs, A. R.; Haynes, C. L.; Massari, A. M., 2d-Ir Spectroscopy of Porous Silica Nanoparticles: Measuring the Distance Sensitivity of Spectral Diffusion. *The Journal of Physical Chemistry C* **2015**, *119*, 25135-25144.

CHAPTER 2
LINEAR AND NONLINEAR INFRARED SPECTROSCOPY

The following chapter focuses on the theory of linear and two-dimensional infrared spectroscopies. The signal of infrared absorption spectroscopy is related to macroscopic polarization, which is generated by the interaction of electrical fields and chromophores as a light-matter response. The polarization was described through several theoretical approaches.[1-5] In this chapter, a semi-classical approach was adopted, where the chromophore is treated quantum mechanically, and the electromagnetic field is considered classically. Vibrational lineshape will be discussed quantitatively through a stochastic model. The details about the 2DIR experiment including photon echo generation, heterodyne detection, experimental setup, and data collection including analysis will be provided. Finally, the experimental details of 2DIR, such as femtosecond infrared laser generation and heterodyne detection, will be described.

2.1. Theoretical molecular response

The time-dependent Hamiltonian of an isolated vibrator is expressed as:

$$H(t) = \hat{H}_0 + \hat{V}(t) \tag{1}$$

where H_0 is time independent molecular Hamiltonian and $\hat{V}(t)$ is time-dependent potential, which describes the interaction with the time-dependent electric field. The potential $\hat{V}(t)$ can be written as:

$$\hat{V}(t) = -\vec{\mu} \cdot \vec{E}(t) \tag{2}$$

where $\vec{\mu}$ is the transition dipole operator, and $\vec{E}(t)$ is time dependent electric field. The solution is a wave function that fulfills the time dependent Schrodinger equation as

$$\frac{\partial}{\partial t}|\psi\rangle = -\frac{i}{\hbar}\hat{H}(t)|\psi\rangle. \tag{3}$$

$$\frac{\partial}{\partial t}\langle\psi| = \frac{i}{\hbar}\langle\psi|\hat{H}(t). \tag{4}$$

The density operator of a pure quantum state $|\psi\rangle$ is defined as:

$$\rho \equiv |\psi\rangle\langle\psi|. \tag{5}$$

Thus the time evolution of the density operator evolves is given by

$$\frac{d}{dt}\rho = -\frac{i}{\hbar}\hat{H}(t)\rho + \frac{i}{\hbar}\rho\hat{H}(t) = -\frac{i}{\hbar}\left[\hat{H}(t), \rho\right]. \tag{6}$$

Equation 6 is the *Liouville-von Neumann* equation. The equation above considers the density matrix of a pure state, which is described by a single wavefunction. While in condensed-phase systems, the density matrix of the ensemble is defined as:

$$\rho = \sum_s p_s|\psi_s\rangle\langle\psi_s| \tag{7}$$

where p_s is the probability of the state $|\psi_s\rangle$, and $\sum_s p_s = 1$.

The wavefunction in the interaction picture:

$$|\psi(t)\rangle \equiv e^{-\frac{i}{\hbar}\hat{H}_0(t-t_0)}|\psi_I(t)\rangle \tag{8}$$

with the reference time t_0. The time dependence of wavefunction in interaction picture is caused by the perturbation $\hat{V}(t)$. If the perturbation is zero, the wave function is

$$|\psi_I(t)\rangle = |\psi(t_0)\rangle. \tag{9}$$

Otherwise,

$$\frac{\partial}{\partial t}|\psi_I(t)\rangle = -\frac{i}{\hbar}\hat{V}_I(t)|\psi_I(t)\rangle. \tag{10}$$

where the perturbation $\hat{V}_I(t)$ in the interaction picture is defined as:

$$\hat{V}_I(t) \equiv e^{\frac{i}{\hbar}\hat{H}_0(t-t_0)}\hat{V}(t_0)e^{-\frac{i}{\hbar}\hat{H}_0(t-t_0)}. \tag{11}$$

In the interaction picture, the density matrix is defined as:

$$|\psi(t)\rangle\langle\psi(t)| = e^{-\frac{i}{\hbar}\hat{H}_0(t-t_0)}|\psi(t)\rangle\langle\psi(t)|e^{\frac{i}{\hbar}\hat{H}_0(t-t_0)} \tag{12}$$

or

$$\rho = e^{-\frac{i}{\hbar}\hat{H}_0(t-t_0)}\rho_I(t)e^{\frac{i}{\hbar}\hat{H}_0(t-t_0)}. \tag{13}$$

In addition, the time-dependent Schrödinger Equation translated to the Liouville-von Neumann equation is

$$\frac{d}{dt}\rho_I(t) = -\frac{i}{\hbar}\left[\hat{V}_I(t), \rho_I(t)\right]. \tag{14}$$

The power expansion of the density matrix in the interaction picture is

$$\rho_I(t) = \rho_I(t_0) + \sum_{n=1}^{\infty}\left(-\frac{i}{\hbar}\right)^n \int_{t_0}^{t} d\tau_n \int_{t_0}^{\tau_n} d\tau_{n-1} \dots \int_{t_0}^{\tau_2} d\tau_1$$

$$\left[\hat{V}_I(\tau_n), \left[\hat{V}_I(\tau_{n-1}), \dots \left[\hat{V}_I(\tau_1), \rho_I(t)\right] \dots\right]\right]. \tag{15}$$

When the equation above is substituted into equation (13), the density matrix of Schrodinger picture is

$$\rho(t) = \rho(t_0) + \sum_{n=1}^{\infty}\left(-\frac{i}{\hbar}\right)^n \int_{t_0}^{t} d\tau_n \int_{t_0}^{\tau_n} d\tau_{n-1} \dots \int_{t_0}^{\tau_2} d\tau_1$$

$$e^{-\frac{i}{\hbar}\hat{H}_0(t-t_0)}\left[\hat{V}_I(\tau_n), \left[\hat{V}_I(\tau_{n-1}), \dots \left[\hat{V}_I(\tau_1), \rho(t_0)\right] \dots\right]\right] e^{\frac{i}{\hbar}\hat{H}_0(t-t_0)}$$

$$\equiv \rho^{(0)}(t) + \sum_{n=1}^{\infty}\rho^{(n)}(t). \tag{16}$$

Here, the first term is the 0^{th}-order density matrix. Plugging equation (2) into above equation will lead the density matrix n^{th}-order density matrix to:

$$\rho^{(n)}(t) = -\left(-\frac{i}{\hbar}\right)^n \int_{t_0}^{t} d\tau_n \int_{t_0}^{\tau_n} d\tau_{n-1} \dots \int_{t_0}^{\tau_2} d\tau_1 \, E(\tau_n)E(\tau_{n-1}) \dots E(\tau_1)$$

$$e^{-\frac{i}{\hbar}\hat{H}_0(t-t_0)}\left[\hat{\mu}_I(\tau_n), [\hat{\mu}_I(\tau_{n-1}), \dots [\hat{\mu}_I(\tau_1), \rho(t_0)] \dots]\right] e^{\frac{i}{\hbar}\hat{H}_0(t-t_0)} \quad (17)$$

A macroscopic polarization is generated after interaction with the radiation. The polarization and emitted signal electric field have a 90 degree phase difference, which is expressed as $E_{sig}(t) = iP(t)$,

where the polarization is given according to the matrix density as:

$$P(t) = Tr\left(\hat{\mu}\rho(t)\right) \equiv \langle\hat{\mu}\rho(t)\rangle. \quad (18)$$

Then the n[th]-order polarization can be expressed as:

$$P^{(n)}(t) = -\left(-\frac{i}{\hbar}\right)^n \int_{t_0}^{t} d\tau_n \int_{t_0}^{\tau_n} d\tau_{n-1} \dots \int_{t_0}^{\tau_2} d\tau_1 \, E(\tau_n)E(\tau_{n-1}) \dots E(\tau_1)$$

$$\langle\hat{\mu}(t)\left[\hat{\mu}(\tau_n), [\hat{\mu}(\tau_{n-1}), \dots [\hat{\mu}(\tau_1), \rho(t_0)] \dots]\right]\rangle \quad (19)$$

where the dipole operator is defined as:

$$\hat{\mu}(t) = e^{\frac{i}{\hbar}\hat{H}_0(t-t_0)}\hat{\mu}e^{-\frac{i}{\hbar}\hat{H}_0(t-t_0)}. \quad (20)$$

When the time in equation (19) is replaced by the time step interval,

$$\begin{aligned} t_0 &= -\infty \\ \tau_1 &= 0 \\ t_1 &= \tau_2 - \tau_1 \\ t_2 &= \tau_3 - \tau_2 \\ &\dots\dots \\ t_n &= t - \tau_n \end{aligned} \quad (21)$$

the equation (19) can be rewritten as:

$$P^{(n)}(t) = -\left(-\frac{i}{\hbar}\right)^n \int_0^\infty dt_n \int_0^\infty dt_{n-1} \dots \int_0^\infty dt_1$$

$$E(t-t_n)E(t-t_n-t_{n-1}) \dots E(t-t_n-t_{n-1}-\cdots-t_1) \cdot$$

$$\langle \hat{\mu}(t_n+t_{n-1}+\cdots+t_1)\left[\hat{\mu}(t_{n-1}+\cdots+t_1), \dots \left[\hat{\mu}(0), \rho_{eq}\right] \dots\right]\rangle \qquad (22)$$

Therefore, the n[th]-order nonlinear response function has the form as:

$$R^{(n)}(t_n, \dots, t_1) =$$

$$-(-\tfrac{i}{\hbar})^n \theta(t) \langle \hat{\mu}(t_n+\cdots+t_1)[\hat{\mu}(t_{n-1}+\cdots+t_1), \dots, \left[\hat{\mu}(0), \rho_{eq}\right] \dots]\rangle. \qquad (23)$$

To explicitly include causality, Heaviside step function $\theta(t)$ is inserted. The response function is proportional to the polarization. According to the response function, first and third order spectroscopy can be accessed.

2.2. Linear response

The first order or linear response function is expressed as a function of the molecular system and its interaction, equation (23), with an incident field:

$$R^{(1)} = -(-\frac{i}{\hbar})\theta(t)\langle \hat{\mu}(t), [\hat{\mu}(0), \rho_{eq}]\rangle$$

$$= (\frac{i}{\hbar})\theta(t) Tr\left(\hat{\mu}(t)\hat{\mu}(0)\rho_{eq} - \hat{\mu}(t)\rho_{eq}\hat{\mu}(0)\right) \qquad (24)$$

$$= (\frac{i}{\hbar})\theta(t)\left(C_\mu(t) - C_\mu^*(t)\right)$$

where $C_\mu(t)$ is the dipole correlation function. Because the dipole operator is Hermitian, the first order response function is the imaginary part of the dipole correlation function.

2.3. Third-order response

Using the similar method of the linear response function, the third order response function can be obtained as eight terms, four terms and their complex conjugates.

$$R^{(3)}(t_3,t_2,t_1) = -\left(-\frac{i}{\hbar}\right)^3 \theta(t_1)\theta(t_2)\theta(t_3)\sum_{i=1}^{4} R_i(t_3,t_2,t_1) - R_i^*(t_3,t_2,t_1)\,; \quad (25)$$

where the response R_i is written as:

$$R_1(t_3,t_2,t_1) = Tr(\hat{\mu}(0)\hat{\mu}(t_1+t_2)\hat{\mu}(t_1+t_2+t_3)\hat{\mu}(t_1)\rho_{eq}) \quad (26)$$

$$R_2(t_3,t_2,t_1) = Tr(\hat{\mu}(0)\hat{\mu}(t_1)\hat{\mu}(t_1+t_2+t_3)\hat{\mu}(t_1+t_2)\rho_{eq}) \quad (27)$$

$$R_3(t_3,t_2,t_1) = Tr(\hat{\mu}(t_1)\hat{\mu}(t_1+t_2)\hat{\mu}(t_1+t_2+t_3)\hat{\mu}(0)\rho_{eq}) \quad (28)$$

$$R_4(t_3,t_2,t_1) = Tr(\hat{\mu}(t_1+t_2+t_3)\hat{\mu}(t_1+t_2)\hat{\mu}(t_1)\hat{\mu}(0)\rho_{eq}) \quad (29)$$

Considering the time evolution of the system, response function R_1can be described as:

$$\begin{aligned} R_1(t_3,t_2,t_1) &= \langle\hat{\mu}(0)\hat{\mu}(t_1+t_2)\hat{\mu}(t_1+t_2+t_3)\hat{\mu}(t_1)\rho_{eq}\rangle \\ &= \langle\hat{\mu}(t_1+t_2)\hat{\mu}(t_1+t_2+t_3)\hat{\mu}(t_1)\rho_{eq}\hat{\mu}(0)\rangle \\ &= \langle U_0^\dagger(t_1+t_2)\hat{\mu}U_0(t_1+t_2)U_0^\dagger(t_1+t_2+t_3)\hat{\mu}U_0(t_1+t_2 \\ &\qquad + t_3)U_0^\dagger(t_1)\hat{\mu}U_0\rho_{eq}\hat{\mu}(0)\rangle \\ &= \langle\hat{\mu}U_0(t_3)U_0(t_2)\hat{\mu}U_0(t_1)\rho_{eq}\hat{\mu}(0)U_0^\dagger(t_1)U_0^\dagger(t_2)\hat{\mu}U_0^\dagger(t_3)\rangle \end{aligned} \quad (30)$$

The evolution of the systems can be seen as:

- At $t = 0$, the dipole operator acts on the *bra* side of density matrix.
- The system evolves under H_0 during t_1, t_2, and t_3.
- At $t = t_1$, the dipole operator acts on the *ket* side of density matrix.
- At $t = t_1 + t_2$, the dipole operator acts on the *bra* side of density matrix.

- At $t = t_1 + t_2 + t_3$, the polarization is generated by multiplying dipole operator on the *ket* side of density matrix and taking the trace.

2.4. Rotating wave approximation and phase matching

2.4.1. Rotating-wave approximation

The macroscopic polarization $P(t)$ is also a function of the electric field $E(t)$. The precise way to include $E(t)$ is obtained by solving the time dependent Schrodinger equation (1). Equation (19) shows that the electric field of the third order polarization at given a time is:

$$E(t) = E'(t-\tau_1)e^{-i\omega_0(t-\tau_1)+i\vec{k}_1\vec{r}} + E'(t-\tau_2)e^{-i\omega_0(t-\tau_2)+i\vec{k}_2\vec{r}} + E'(t-\tau_3)e^{-i\omega_0(t-\tau_3)+i\vec{k}_3\vec{r}} + c.c. \tag{31}$$

where E' is the envelop of electric field, which is a δ-function in time. The electric field are described by assuming that all the electric fields have the same center frequency and envelop. Therefore, the product of $E(t-t_1)E(t-t_1-t_2)E(t-t_1-t_2-t_3)$ in equation (19) for third order response will have $6^3 = 216$ terms.

When the center frequency of the pulses are close enough to the vibrational transition frequency of the chromophore, some of the phase factors can be canceled. After integration, the contribution of the left fast oscillatory factor is much smaller than slowly varying terms. Therefore, the fast oscillating term can be neglected, which is known as a rotating-wave approximation. Take the linear polarization for example,

$$P^{(1)}(t) = \left(\frac{i}{\hbar}\right)\int_0^\infty \theta(\tau)\, d\tau E(t-\tau)\langle\hat{\mu}(\tau)\hat{\mu}(0)\rho_{eq} - \rho_{eq}\hat{\mu}(0)\hat{\mu}(\tau)\rangle \tag{32}$$

$$= \left(\frac{i}{\hbar}\right)\int_0^\infty \theta(\tau)\, d\tau \left[E'(t-\tau)e^{-i\omega_0(t-\tau)+i\vec{k}_1\vec{r}}\right.$$

$$\left. + E'^{*}(t-\tau)e^{+i\omega_0(t-\tau)+i\vec{k}_1\vec{r}}\right]\langle\hat{\mu}(\tau)\hat{\mu}(0)\rho_{eq}\rangle + c.c.$$

And for a two-level system, the linear polarization is given by,

$$P^{(1)}(t) = \left(\frac{i}{\hbar}\right)\int_0^\infty \theta(\tau)\, d\tau \left[E'(t-\tau)e^{-i\omega_0(t-\tau)+i\vec{k}_1\vec{r}+i\omega_0\tau}\right.$$

$$\left. + E'^{*}(t-\tau)e^{+i\omega_0(t-\tau)+i\vec{k}_1\vec{r}-i\omega_0\tau}\right]\langle\hat{\mu}(\tau)\hat{\mu}(0)\rho_{eq}\rangle + c.c. \quad (33)$$

The second term of electric field expression is highly oscillatory and is ignored according to rotating-wave approximation. Thus, only the first term appears in the polarization.

2.4.2. Phase matching

The electric field is also the function of the wavevector and phase, the expression of the electric field is described as:

$$E_n(t) = E_n'(t)\cos\left(\vec{k}\cdot\vec{r} - \omega t + \phi\right). \quad (34)$$

In this case, the rotating-wave approximation also dictates phase and wavevector through an electric field, $E(t) \propto e^{-i\omega t+i\emptyset+i\vec{k}\cdot\vec{r}}$ or $E^*(t) \propto e^{+i\omega t-i\emptyset-i\vec{k}\cdot\vec{r}}$. Then the polarization $P_1^{(3)}$ as a function of wavevector, phase, and R_1 is:

$$P_1^{(3)} \propto e^{i\left(-\vec{k}_1+\vec{k}_2+\vec{k}_3\right)\cdot\vec{r}} e^{i(-\phi_1+\phi_2+\phi_3)} \int_0^\infty dt_3 \int_0^\infty dt_2 \int_0^\infty dt_1\, E_3''(t-t_3)$$

$$\cdot E_2''(t-t_3-t_2)\cdot E_1''^{*}(t-t_3-t_2-t_1)R_1(t_1,t_2,t_3) \quad (35)$$

and $P_4^{(3)}$ is

$$P_4^{(3)} \propto e^{i(\vec{k}_1-\vec{k}_2+\vec{k}_3)\cdot\vec{r}} e^{i(\phi_1-\phi_2+\phi_3)} \int_0^\infty dt_3 \int_0^\infty dt_2 \int_0^\infty dt_1 \, E_3''(t-t_3) \cdot E_2''^*(t-t_3-t_2) \cdot E_1''(t-t_3-t_2-t_1) R_4(t_1,t_2,t_3) \quad (36)$$

where E_n'' is the envelop and time dependent of the electric field.

The response function $R_n^{(3)} \neq 0$ only when $t_1 \geq 0, t_2 \geq 0$, and $t_3 \geq 0$. When the pulses separate in time, only one set of response functions will be measured in the corresponding phase-matching direction. When $t_1 = 0$, the $-\vec{k}_1 + \vec{k}_2 + \vec{k}_3$ and $+\vec{k}_1 - \vec{k}_2 + \vec{k}_3$ directions contain the same information, but the response function is not the same.

Among all the combinations of phase matching direction with three pulse wavevectors, only beams in $-\vec{k}_1 + \vec{k}_2 + \vec{k}_3$ and $+\vec{k}_1 - \vec{k}_2 + \vec{k}_3$ direction are used in 2DIR spectroscopy, and the directions are illustrated figure 2.1.

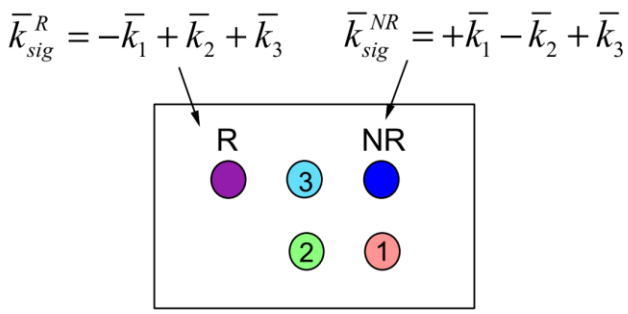

Figure 2.1. Phase matching direction selected in 2DIR spectroscopy. The number 1, 2, and 3 indicate the input pulses. Through a lens, the non-rephasing (NR) and rephasing (R) are generated in the given direction.

2.5. Diagrammatic Perturbation Theory: Feynman Diagram approach

Diagrammatic Perturbation Theory is a simplified way to track the contribution of the nonlinear signal in a set of states of the system probed during the experiment. Double-side Feynman diagrams are the easiest representation for tracking the state of coherence in different

times. Feynman diagram interprets the microscopic origin of the signal by presenting the evolution of the density matrix under interaction with the electric field followed by time-propagation. The rule of drawing Feynman diagram is summarized as:

- The vertical line on the left and right indicates the time evolution of the *ket* and *bra* of the density matrix. Time is increased from bottom to top.
- Interactions with the light field are presented as arrows. An inward arrow to the vertical line represents absorption, and an outward arrow presents emission.
- Each diagram has a sign $(-1)^n$, where n is the number of interaction on the *bra* side. The minus sign exists because of the interaction on right side in the commutator carrying a minus sign. The last interaction is not counted in this sign-rule because it is not a part of the commutator.
- The arrow pointing to the right represents an electric field with $e^{-i(\vec{k}\cdot\vec{r}-\omega t+\phi)}$, whereas the arrow pointing to the left represents electric field with $e^{i(\vec{k}\cdot\vec{r}-\omega t+\phi)}$.
- An arrow pointing towards the system represents an up-climbing of the *bra* or *ket* of the density matrix.
- The last interaction must end in a population state.

The Feynman diagram of corresponding possible Liouville pathways for the two-level system is shown in figure 2.2. In the diagram, the time interval of t_1, t_2, and t_3 are replaced with τ, T, and t, respectively. In the pathway of R_1 and R_2, the sign of the phase accumulated in τ and t are opposite, which are called rephasing pathways. On the contrary, in the pathway represented by R_3 and R_4, the sign of the phase is unaltered and are named nonrephasing pathways. The signal emitted through rephasing and nonrephasing pathways in $-\vec{k}_1+\vec{k}_2+\vec{k}_3$ and $+\vec{k}_1-\vec{k}_2+\vec{k}_3$ phase matching directions, respectively. The signal emitted at the phase matching direction of

$-\vec{k}_1+\vec{k}_2+\vec{k}_3$ when the time order of $\vec{k}_2$ preceding $\vec{k}_1$ is the same as the signal at the phase matching direction of $+\vec{k}_1-\vec{k}_2+\vec{k}_3$ when the time order of $\vec{k}_1$ preceding $\vec{k}_2$. Therefore, at the direction of $-\vec{k}_1+\vec{k}_2+\vec{k}_3$, both rephasing and nonrephasing signal can be detected by switching the pulse ordering $(\vec{k}_1,\vec{k}_2,\vec{k}_3)$ and $(\vec{k}_2,\vec{k}_1,\vec{k}_3)$.

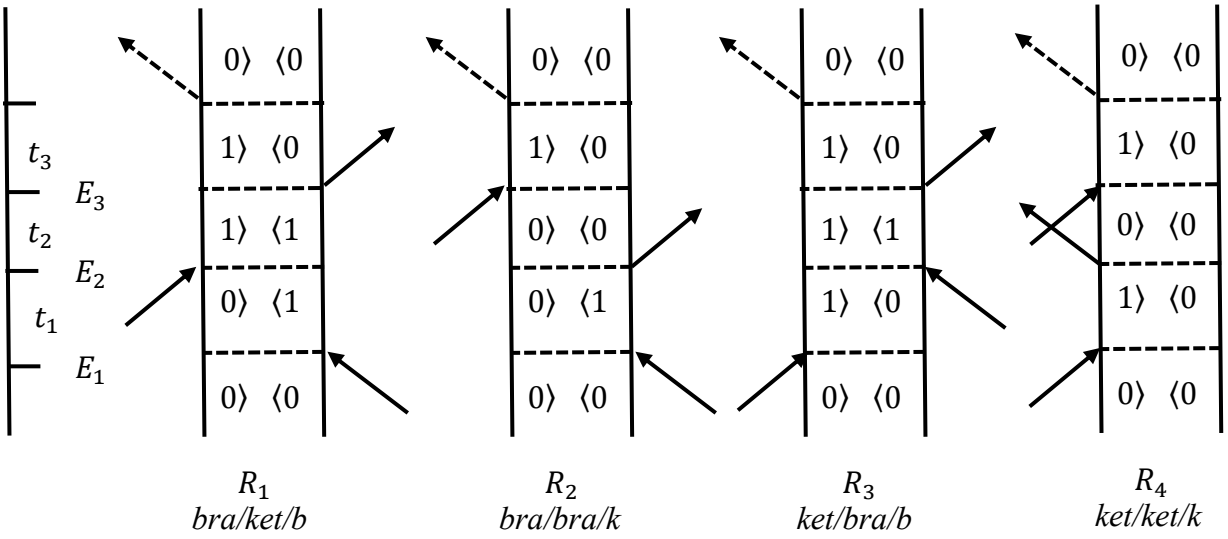

Figure 2.2. Feynman diagram of a two-level system

Similarly, the Liouville pathways for three-level system at $-\vec{k}_1+\vec{k}_2+\vec{k}_3$ phase matching direction are shown in figure 2.3. The response functions corresponding to the pathways are described as:

$$R_1(\tau,T,t)=\langle\hat{\mu}_{01}(0)\hat{\mu}_{01}(\tau+T)\hat{\mu}_{01}(\tau+T+t)\hat{\mu}_{01}(\tau)\rangle \quad (37)$$

$$R_2(\tau,T,t)=\langle\hat{\mu}_{01}(0)\hat{\mu}_{01}(\tau)\hat{\mu}_{01}(\tau+T+t)\hat{\mu}_{01}(\tau+T)\rangle \quad (38)$$

$$R_3(\tau,T,t)=-\langle\hat{\mu}_{01}(0)\hat{\mu}_{21}(\tau+T+t)\hat{\mu}_{21}(\tau+T)\hat{\mu}_{01}(\tau)\rangle \quad (39)$$

$$R_4(\tau,T,t)=\langle\hat{\mu}_{01}(\tau)\hat{\mu}_{01}(\tau+T)\hat{\mu}_{01}(\tau+T+t)\hat{\mu}_{01}(0)\rangle \quad (40)$$

$$R_5(\tau,T,t) = \langle \hat{\mu}_{01}(\tau+T+t)\hat{\mu}_{01}(\tau+T)\hat{\mu}_{01}(\tau)\hat{\mu}_{01}(0)\rangle \quad (41)$$

$$R_6(\tau,T,t) = -\langle \hat{\mu}_{01}(\tau)\hat{\mu}_{21}(\tau+T+t)\hat{\mu}_{21}(\tau+T)\hat{\mu}_{01}(0)\rangle \quad (42)$$

The sign of R_3 and R_6 are negative, and the frequency of coherence state during time t are ω_{21}.

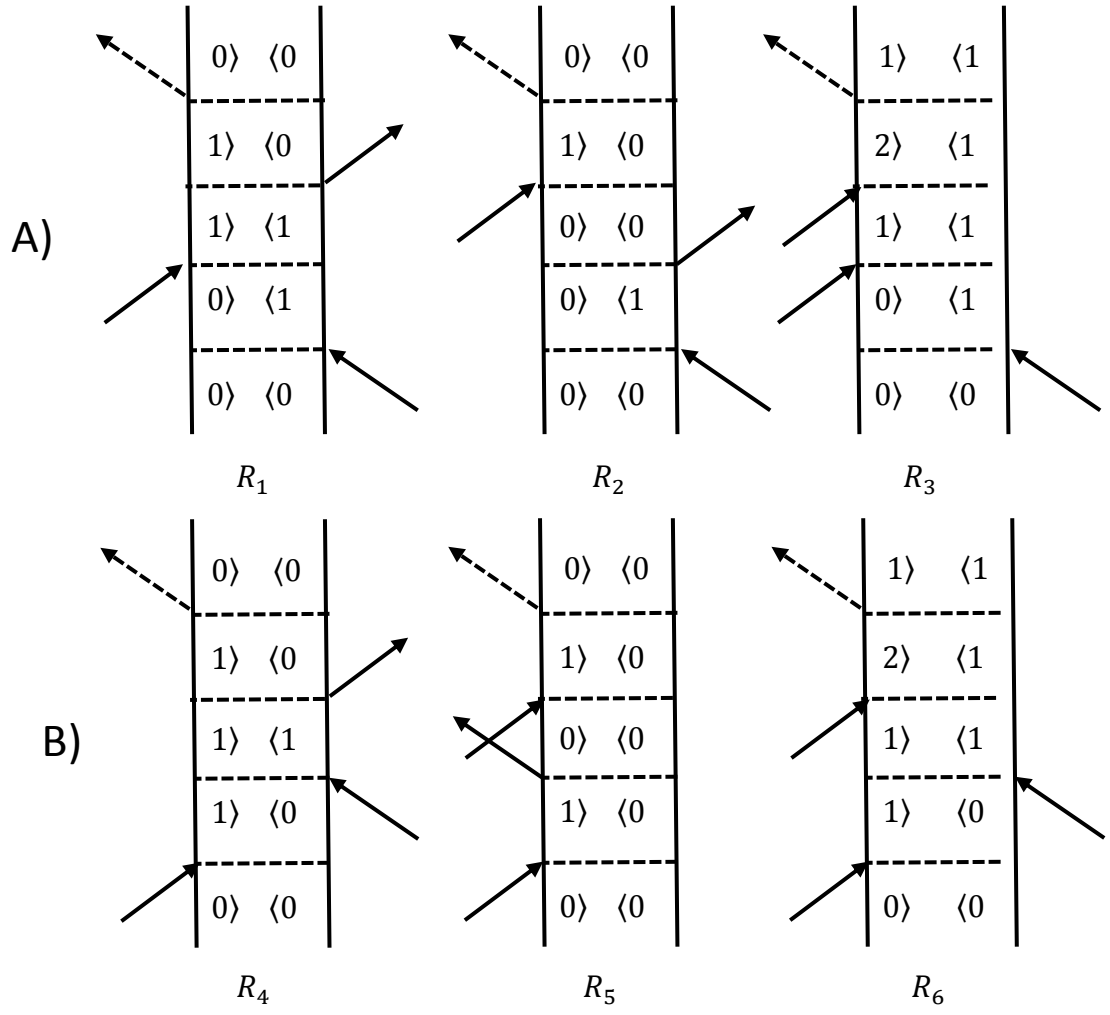

Figure 2.3. Feynman diagram of a three-level system

2.6. Vibrational lineshape

In vacuum, the vibrational transition is presented as a line without width. However, the interaction of probed dipole with a fluctuation environment makes the IR lineshape broader in the

condense phase. It is the time scale and amplitude of fluctuation that determines the width of the peak. In this section, the lineshape affected by vibrational dephasing is discussed classically, which was first illustrated by Ryogo Kubo over forty years ago.[6] The stochastic force of the environment acting on the molecule causes the vibrational frequencies to fluctuate randomly with time. Thus the frequency of the dipole is considered as time-dependent, $\omega(t)$, which is assumed to have a Gaussian distribution. The time-dependent transition frequency is described as:

$$\begin{aligned} \omega(t) &= \bar{\omega} + \delta\omega(t) \\ \langle \delta\omega(t) \rangle &= 0 \\ P\big(\delta\omega(t)\big) &= \frac{1}{\sigma\sqrt{2\pi}} e^{-\delta\omega(t)^2/2\sigma^2} \\ \sigma &= \langle \delta\omega(t)^2 \rangle \end{aligned} \tag{43}$$

The classical transition dipole also can be described as the linear relationship with the time-dependent frequency as:

$$\frac{\partial \mu}{\partial t} = -i\omega(t)\mu \tag{44}$$

And the time-dependent dipole can be solved through

$$\begin{aligned} \mu(t) &= \mu(0) e^{-i\int_0^t d\tau \omega(\tau)} \\ &= \mu(0) e^{-i\bar{\omega}t - i\int_0^t d\tau \delta\omega(\tau)} \end{aligned} \tag{45}$$

Substituting equation (45) into the dipole correlation function result in,

$$\langle \mu(t)\mu(0) \rangle = \langle |\mu(0)|^2 e^{-i\bar{\omega}t - i\int_0^t d\tau \delta\omega(\tau)} \rangle \tag{46}$$

When the treatment is applied with the *Condon approximation*, assume the magnitude of dipole is time-independent. It should be noted here; the dipole is treated without considering the vectorial nature. Therefore, the dipole can be taken out from the average as:

$$\langle \mu(t)\mu(0)\rangle = C_\mu(t) = \mu^2 e^{-i\bar{\omega}t}\Phi(t) \tag{47}$$

where $\Phi(t)$ is the dephasing function as:

$$\Phi(t) = \langle e^{-i\int_0^t d\tau \delta\omega(\tau)}\rangle. \tag{48}$$

Further, for a system with Gaussian statistics, the dephasing function can be simplified by the cumulant expansion of the average as:

$$\Phi(t) = e^{-i\int_0^t dt_1\langle\delta\omega(t_1)\rangle + \frac{i^2}{2!}\int_0^t t_1\int_0^t t_2\langle\delta\omega(t_1)\delta\omega(t_2)\rangle + \cdots}. \tag{49}$$

In the above equation, the first term of the exponential is zero, and only the second term survives for a system with Gaussian statistics. Then the dephasing function can be rewritten with $\tau = t_1 - t_2$ as:

$$\begin{aligned}\Phi(t) &= e^{-\frac{1}{2}\int_0^t t_1\int_0^t t_2\langle\delta\omega(t_1)\delta\omega(t_2)\rangle} \\ &= e^{-\int_0^t t_1\int_0^t t_2\langle\delta\omega(t_1-t_2)\delta\omega(0)\rangle} \\ &= e^{-\int_0^t d\tau(t-\tau)\langle\delta\omega(\tau)\delta\omega(0)\rangle} = e^{-g(t)} \\ C_{\delta\omega\delta\omega}(t) &= \langle\delta\omega(t)\delta\omega(0)\rangle\end{aligned} \tag{50}$$

$C_{\delta\omega\delta\omega}(t)$ is the frequency-frequency correlation function. Adding the phenomenological vibrational lifetime faction $\frac{1}{2T_1}$, the vibrational lineshape through dipole correlation function is:

$$C_\mu(t) = \mu^2 e^{-i\bar{\omega}t - \frac{t}{2T_1} - g(t)}. \tag{51}$$

Thus, the Gaussian stochastic model describes the influence of the frequency fluctuation on the vibrational lineshape.

The nonlinear response can be treated using the similar approach, and the third-order response in equations (37) to (42) as:

$$R(01|11|10) = R_1^r(t,\tau;T) = \mu_{01}^4 e^{i\omega_{10}\tau - g(\tau)} e^{-i\omega_{10}t - g(t)} e^{\delta G_1(t,\tau,T)} \tag{52}$$

$$R(01|00|10) = R_2^r(t,\tau;T) = R_1^r(t,\tau;T) \tag{53}$$

$$\begin{aligned} &R(01|11|21) = R_3^r(t,\tau;T) \\ &= \mu_{12}^2\mu_{01}^2 e^{i\omega_{10}\tau - g(\tau)} e^{-i(\omega_{10}-\Delta)t-(g(\tau)+g_\Delta(t)-2g_{1\Delta}(t))} e^{\delta G_1(t,\tau,T)+\delta G_2(t,\tau,T)} \end{aligned} \tag{54}$$

$$R(10|11|10) = R_4^{nr}(t,\tau;T) = \mu_{01}^4 e^{-i\omega_{10}\tau - g(\tau)} e^{-i\omega_{10}t - g(t)} e^{-\delta G_1(t,\tau,T)} \tag{55}$$

$$R(10|00|10) = R_5^{nr}(t,\tau;T) = R_4^{nr}(t,\tau;T) \tag{56}$$

$$\begin{aligned} &R(10|11|21) = R_6^{nr}(t,\tau;T) \\ &= \mu_{12}^2\mu_{01}^2 e^{-i\omega_{10}\tau - g(\tau)} e^{-i(\omega_{10}-\Delta)t-(g(\tau)+g_\Delta(t)-2g_{1\Delta}(t))} e^{-\delta G_1(t,\tau,T)-\delta G_2(t,\tau,T)} \end{aligned} \tag{57}$$

where Δ is the anharmonicity of the vibrational transition. $R(ij|kl|mn)$ indicates the Liouville pathway from ρ_{ij} to ρ_{kl} to ρ_{mn}. And the function $\delta G_1(t,\tau,T)$ and $\delta G_2(t,\tau,T)$ are indicated

$$\delta G_1(t,\tau,T) = g(T) - g(\tau+T) - g(t+T) + g(\tau+t+T) \tag{58}$$

$$\delta G_2(t,\tau,T) = -g_{1\Delta}(T) + g_{1\Delta}(\tau+T) + g_{1\Delta}(t+T) - g_{1\Delta}(\tau+t+T) \tag{59}$$

respectively. The functions $g_\Delta(x)$ and $g_{1\Delta}(x)$ indicate the autocorrelation of $\langle\delta\Delta(x)\delta\Delta(0)\rangle$ and $\langle\delta\omega_{10}(x)\delta\Delta(0)\rangle$, respectively, where $\delta\Delta(x)$ is the anharmonicity fluctuation from its mean at time x. The two-dimensional infrared spectroscopy spectrum is defined as:

$$S(\omega_t,\omega_{\tau,}T) = \int_0^\infty d\tau \int_0^\infty dt\,[i\sum_{j=1}^{6} R_j(t,\tau,T)]e^{i(\omega_t t+\omega_\tau\tau)} \tag{60}$$

with the overall phase to zero for simplicity.

2.7. Dynamics from 2DIR: spectral diffusion

The process of the frequency evolution in the condense phase can be described by the Gauss-Markov process, in which the frequency correlation function decays exponentially as

$$\langle\delta\omega(t)\delta\omega(0)\rangle = \Delta^2 e^{-\frac{t}{\tau}} \tag{61}$$

where Δ^2 is the variance of frequency fluctuation, and τ is the correlation time constant. So $g(t)$ can be rewritten as:

$$g(t) = \Delta^2\tau^2(e^{-\frac{t}{\tau}} + \frac{t}{\tau} - 1) \tag{62}$$

Here $g(t)$ will be discussed with different limits.

2.7.1. Long correlation times

When $t \gg \tau$, which indicates a homogeneous case where $e^{-\frac{t}{\tau}} \approx 0$, $t/\tau \gg 1$ and

$$g(t) = -\Delta^2\tau t. \tag{63}$$

Define the homogeneous dephasing time as

$$T_2 = \frac{1}{\Gamma} = \frac{1}{\Delta^2\tau}. \tag{64}$$

Therefore, the dephasing function decays exponentially as

$$\Phi(t) = e^{-\frac{t}{T_2^*}} \tag{65}$$

The lineshape after Fourier transformation is a Lorentzian function as:

$$Re\sigma(\omega) \propto \frac{1}{(\omega - \bar{\omega})^2 - \frac{1}{{T_2}^2}} \tag{66}$$

So, when the system with the frequency fluctuation time scale much faster than the inverse of the distribution, $\tau \ll \frac{1}{\Delta}$, the resonance will be "motionally narrowed" into Lorentzian lineshape.

2.7.2. Short correlation times

If the $\tau \gg t$, which corresponding inhomogeneous case, $C_{\delta\omega\delta\omega}(t) = \Delta^2$, a constant. Expand the exponential term as

$$e^{-\frac{t}{\tau}} \approx 1 - \frac{t}{\tau} + \frac{t^2}{2\tau^2} + \cdots \tag{67}$$

Then we can get

$$g(t) = \frac{\Delta^2 \tau^2}{2} \tag{68}$$

Thus the dephasing function is a Gaussian function. After Fourier transforming, the inhomogeneous broadening presents a Gaussian distribution centered at the mean frequency, which is opposite to the homogeneous case. When the correlation time is much longer than the inverse of distribution, $\tau \gg \frac{1}{\Delta}$, the spectrum presents as Gaussian lineshape. Usually, the case is between homogeneous and inhomogeneous case, the lineshape are the mixture of Gaussian and Lorentzian distribution.

2.7.3. Spectral Diffusion

The frequency fluctuation is the phenomenon of spectral diffusion. Previously, we have illustrated the frequency fluctuation of the chromophore. The frequency evolution can originate from more than one physical process. For example, the nitrile stretching mode in solution can experience solvation shell oscillation and diffusion processes. If one assumes that the frequency fluctuation is a Markov process, the frequency correlation should decay exponentially.[7] In this case, the correlation function is the sum of each exponential component, where each exponent represents a specific physical process with definite time.

The frequency-frequency correlation function can be obtained from an experiment from the evolution of the frequency of two-Dimensional Infrared spectroscopy. Cho et al. first showed that the frequency correlation function is directly proportional to the nodal line slope of the positive and negative peaks in the 2DIR spectra.[8] Later, Fayer's group proposed the central line slope

(which is using maximum point instead of the nodal point of Cho's work) as the metric to estimate the correlation function.[9]

2.8. Heterodyne detection

The transformation of the photon echo signal from the time domain to the frequency domain allows us to measure the intensity and phase of the signal needed to characterize the system. Thus, we use a heterodyned detection, which overlaps the photon echo signal with a reference field to produce the interference signal. This so-called heterodyne detection is widely used in nonlinear spectroscopy.[10-13] The reference field employed has the same frequency as the signal and it is called the local oscillator. When heterodyned, both the photon echo signal field $E_{sig}^{(3)}(t)$ and local oscillator field $E_{LO}(t-t_{LO})$ are incident on a square-law detector,

$$\tilde{E}_{sig}(\omega) = \int_{-\infty}^{\infty} dt E'_{sig}(t)\, e^{i\phi_{sig}-i\omega t} = E'_{sig}(\omega) e^{i\phi_{sig}-i\omega t} \tag{69}$$

$$\tilde{E}_{LO}(\omega) = \int_{-\infty}^{\infty} d(t-t_{LO}) E'_{LO}(t)\, e^{i(\phi_{sig}-\phi_{LO})+i\omega t_{LO}} = E'_{LO}(\omega) e^{i\phi_{sig}+i\omega t_{LO}} \tag{70}$$

where t_{LO} is the time interval between last pulse of three incident pulses and local oscillator. Thus the resulting signal in frequency domain is

$$\begin{aligned} S(\omega) &= \left| E'_{sig}(\omega) e^{i\phi_{sig}} + E'_{LO}(\omega) e^{i(\phi_{LO}+\omega t_{LO})} \right| \\ &= \left| E'_{sig}(\omega) \right|^2 + |E'_{LO}(\omega)|^2 + 2E'_{sig}(\omega) E'_{LO}(\omega) \cos(\Delta\phi + \omega t_{LO}) \end{aligned} \tag{71}$$

The term of $\left|E'_{sig}(\omega)\right|^2$ is ignored due to too low intensity compared with the other terms. And $|E'_{LO}(\omega)|^2$ can be measured by blocking the signal with a chopper. Thus the $|E'_{LO}(\omega)|^2$ can be subtracted from heterodyned signal. Compared the intensity of photon echo signal, the third term in equation (71) is much amplified than before heterodyned.

2.9. Experimental setup

2.9.1. Femtosecond infrared pulse generation

Our experiment used a femtosecond laser pulse generated from Mai-Tai SP with Spitfire Ace high-performance Ti-Sapphire system. Each ultrashort pulse is generated by passive mode locking. Mode locking is based on the Kerr-Lens effect of a Ti-Sapphire crystal.[14] A pair of prisms in the cavity shorten the duration of the pulse and produce the pulse centered at ~800 nm. The resulting pulse servers as the seed pulse to be amplified. In the amplifier, the seed pulses are amplified through chirped pulse amplification.[15] The amplifier is composed of a stretcher, an amplification cavity, and a compressor. The seed pulse is initially stretched to sub-nanosecond to avoid damaging thresholds of amplification cavity by reducing the peak power. The stretched pulse is amplified in amplification cavity. After compressor, the output laser is 800 nm pulse with 5 kHz repetition rate with an average power of 1.0 W.

An Optical Parametric Amplifier[15-17] is used to generate the pulse at the mid-infrared region from the amplified 800 nm pulse. The schematic layout is shown in figure 2.4. The 800 nm pulse is split into three parts: two pump beams and one as the white light seed. The white light is generated by the white light seed focusing on a 2 mm thick sapphire plate. First, the white light and one of the two pump pulses (~50 μJ) focus on a β-BaB_2O_4 (BBO, type II, 2 mm crystal thickness) crystal to preamplify the frequency component. Second, the other pump beam (~270 μJ) is overlapped with the preamplified continuum on the same BBO crystal but on a different spot to generate a signal and an idler. Through a dichroic mirror, the signal and idler delay time can be adjusted to provide higher stability. At last, the collimated signal and idler can generate the pulse in infrared frequency region through an BBO (Type II, 1 mm) Difference Frequency Generation (DFG) crystal. The

pulses other than infrared pulse will be filtered by germanium filter so that only infrared laser can be transmitted.

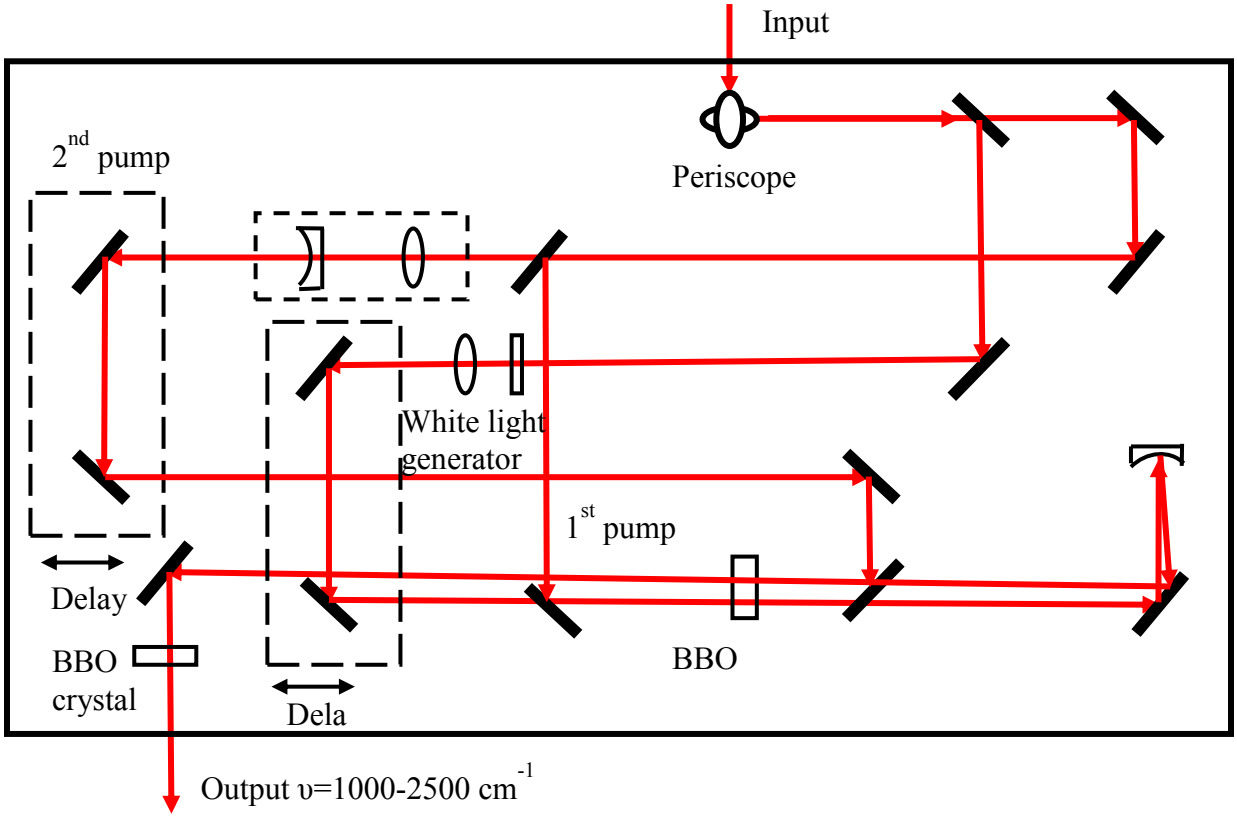

Figure 2.4. Optical layout of OPA used for IR pulse.

2.9.2. 2DIR experimental setup

There are several ways to design the experimental setup for measuring a heterodyned photon echo signal generated by three incident pulses.[10, 18-21] The 2DIR spectroscopy can have a collinear or pump-probe configuration, where the probe pulse overlapped with phone echo as a local oscillator. The most 2DIR experiment pulses are arranged using box-CARS phase-matching geometry. The three incident pulse and oscillator pulse are generated through the setup shown in figure 2.5. The path of each beam is modified by a computer controlled translation stages, which can move at the

nanometer scale. Thus the accuracy of the time interval between pulses can be controlled with femtosecond time resolution. A synchronized chopper at frequency of 5 kHz is placed on the path of $\vec{k}_3$ to collect local oscillator signal which is used in heterodyned detection for subtraction from interference. The three incident pulses $\vec{k}_1$, $\vec{k}_2$, and $\vec{k}_3$ focus on the sample with a lens. The liquid sample is contained between two 25 mm CaF_2 windows separated with Teflon spacer with different thickness in a mounted liquid sample cell. The photon echo signal is heterodyned with the local oscillator by overlapping them on a 5:95 CaF_2 beamsplitter. The interfered signal detected by a nitrogen cooled 64-element MCT array detector through a monochromator. The 2DIR setup is enclosed in an air tight hand-made box, which is purged with CO_2 filtered dry air to eliminate the influence from moisture and CO_2. Most of the experiments are performed by collecting scanned τ and wavelength λ in the detector from -4 ps to 4 ps as a 5 fs per step rate for each waiting time. .

2.10. Determination of time zero between pulses

Before the 2DIR measurement, the time zero between pulse $\vec{k}_1$, $\vec{k}_2$, and $\vec{k}_3$ should be determined with sub-cycle accuracy (for wavelength of 5 μm, one cycle is ~17 fs) for artifact-free 2DIR spectra. Although using the IR-FROG approach one can get accurate time zero,[22] for the solution in a protic solvent, the approach of using thermal grating signal of solvent molecules is widely employed. When all the pulses overlap in time, the D_2O exhibits a weak, pulsewidth limited non-resonant signal. The relative time between two pulses can be determined by fixing the third pulse much later than them, for example, 10 ps, and fitted the thermal grating signal vs. time with Gaussian function.

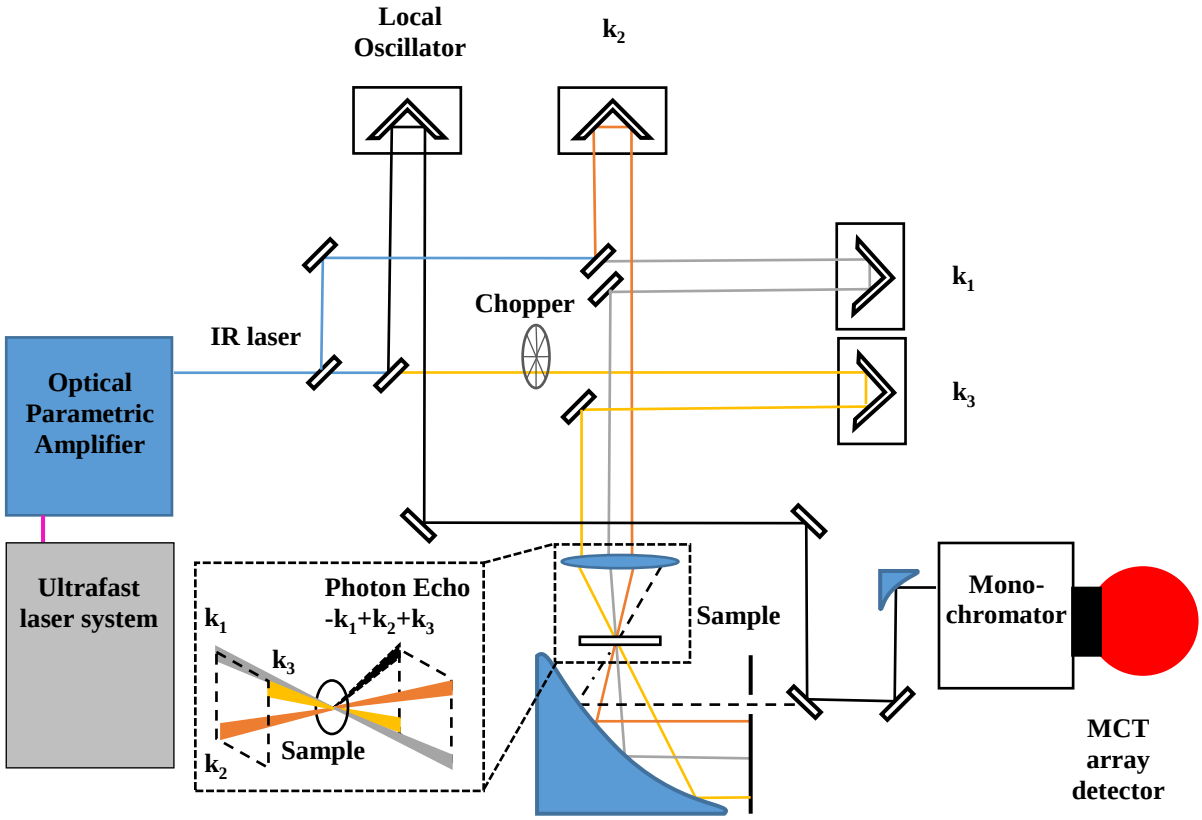

Figure 2.5. Schematic of the 2DIR spectroscopy setup

2.11. Obtain frequency domain 2DIR data

As we mentioned previously, the raw data collected by the detector is in the form of scanning time τ and wavelength λ. The postprocessing step is inverse Fourier transforming the raw data from $I(\tau, \lambda_k)$ to $I(\tau, \omega_t)$,[10, 12-13] where λ_k is the wavelength corresponding the kth detector element and ω is evenly spaced frequencies. The inverse Fourier transform is performed as:

$$S(\tau, T, t) = \sum_{k=1}^{64} \tilde{S}(\tau, T, \lambda_k) e^{-i\omega_k t} \Delta\omega_k \tag{72}$$

where

$$\omega_k = \frac{2\pi c}{\lambda_k} \tag{73}$$

and

$$\Delta\omega_k = \frac{2\pi c}{\lambda_k - \frac{1}{2}\Delta\lambda} - \frac{2\pi c}{\lambda_k + \frac{1}{2}\Delta\lambda} \tag{74}$$

$\Delta\lambda$ is the wavelength different between two neighboring elements in the detector. The detection time t can be obtained from a known time zero. Then, Fourier transform the time domain data twice to frequency domain as:

$$\tilde{S}(\tau, \omega_t, T) = \sum_t S(\tau, t, T) e^{i\omega_t t} \Delta t \tag{75}$$

$$\tilde{S}(\omega_\tau, \omega_t, T) = \sum_t S(\tau, \omega_t, T) e^{i\omega_\tau \tau} \Delta\tau \tag{76}$$

The data analysis process above is followed for both rephrasing and nonrephasing data. The resulting frequency domain data need to be corrected by relative phase between the rephrasing and nonrephasing signal.

2.12. Conclusion

In this section, the theoretical formalism of first order and third order nonlinear spectroscopy was derived for the interaction between light and matter. Under-rotating wave approximation, the linear and third-order response function are derived, and the Feynman diagram was introduced. During the electric field-dipole interaction process, the influence of dephasing to spectral lineshape was discussed. Also, the 2DIR experimental setup was described in this chapter.

The details about femtosecond infrared laser generation, apparatus setup, and heterodyne detection, and post-processing of spectra data was provided.

2.13. References

1. Mukamel, S., *Principles of Nonlinear Optical Spectroscopy*; Oxford University Press on Demand, 1999.

2. Hamm, P.; Zanni, M., *Concepts and Methods of 2d Infrared Spectroscopy*; Cambridge University Press, 2011.

3. Sung, J.; Silbey, R. J., Optical Four Wave Mixing Spectroscopy for Multilevel Systems Coupled to Multimode Brownian Oscillators. *The Journal of chemical physics* **2003**, *118*, 2443-2445.

4. Sung, J.; Silbey, R. J., Four Wave Mixing Spectroscopy for a Multilevel System. *The Journal of Chemical Physics* **2001**, *115*, 9266-9287.

5. Cho, M., *Two-Dimensional Optical Spectroscopy*; CRC press, 2009.

6. Kubo, R., A Stochastic Theory of Line Shape. *Stochastic Processes in Chemical Physics* **1969**, *15*, 101-127.

7. Wang, M. C.; Uhlenbeck, G. E., On the Theory of the Brownian Motion Ii. *Reviews of modern physics* **1945**, *17*, 323.

8. Kwac, K.; Cho, M., Molecular Dynamics Simulation Study of N-Methylacetamide in Water. Ii. Two-Dimensional Infrared Pump–Probe Spectra. *The Journal of chemical physics* **2003**, *119*, 2256-2263.

9. Kwak, K.; Park, S.; Finkelstein, I. J.; Fayer, M., Frequency-Frequency Correlation Functions and Apodization in Two-Dimensional Infrared Vibrational Echo Spectroscopy: A New Approach. *The Journal of chemical physics* **2007**, *127*, 124503.

10. Lepetit, L.; Chériaux, G.; Joffre, M., Linear Techniques of Phase Measurement by Femtosecond Spectral Interferometry for Applications in Spectroscopy. *JOSA B* **1995**, *12*, 2467-2474.

11. Hochstrasser, R. M., Dynamical Models for Two-Dimensional Infrared Spectroscopy of Peptides. *Adv Chem Phys* **2005**, *132*, 1-56.

12. Dorrer, C.; Belabas, N.; Likforman, J.-P.; Joffre, M., Spectral Resolution and Sampling Issues in Fourier-Transform Spectral Interferometry. *JOSA B* **2000**, *17*, 1795-1802.

13. Dorrer, C.; Belabas, N.; Likforman, J.; Joffre, M., Experimental Implementation of Fourier-Transform Spectral Interferometry and Its Application to the Study of Spectrometers. *Applied Physics B* **2000**, *70*, S99-S107.

14. Backus, S.; Durfee III, C. G.; Murnane, M. M.; Kapteyn, H. C., High Power Ultrafast Lasers. *Review of scientific instruments* **1998**, *69*, 1207-1223.

15. Wynne, K.; Reid, G. D.; Hochstrasser, R. M., Regenerative Amplification of 30-Fs Pulses in Ti: Sapphire at 5 Khz. *Optics letters* **1994**, *19*, 895-897.

16. Cerullo, G.; De Silvestri, S., Ultrafast Optical Parametric Amplifiers. *Review of scientific instruments* **2003**, *74*, 1-18.

17. Shen, Y., Principles of Nonlinear Optics (Wiley Series in Pure and Applied Optics). **2009**.

18. DeFlores, L. P.; Nicodemus, R. A.; Tokmakoff, A., Two-Dimensional Fourier Transform Spectroscopy in the Pump-Probe Geometry. *Optics letters* **2007**, *32*, 2966-2968.

19. Shim, S.-H.; Zanni, M. T., How to Turn Your Pump–Probe Instrument into a Multidimensional Spectrometer: 2d Ir and Vis Spectroscopies Via Pulse Shaping. *Physical Chemistry Chemical Physics* **2009**, *11*, 748-761.

20. Helbing, J.; Hamm, P., Compact Implementation of Fourier Transform Two-Dimensional Ir Spectroscopy without Phase Ambiguity. *JOSA B* **2011**, *28*, 171-178.

21. Hamm, P.; Lim, M.; Hochstrasser, R. M., Non-Markovian Dynamics of the Vibrations of Ions in Water from Femtosecond Infrared Three-Pulse Photon Echoes. *Physical review letters* **1998**, *81*, 5326.

22. Fecko, C.; Loparo, J.; Tokmakoff, A., Generation of 45 Femtosecond Pulses at 3 Mm with a Knbo3 Optical Parametric Amplifier. *Optics communications* **2004**, *241*, 521-528.

CHAPTER 3
SOLVATION DYNAMICS OF AN IONIC PROBE IN CHOLINE CHLORIDE-BASED DEEP EUTECTIC SOLVENTS

3.1. Introduction

Deep eutectic solvents (DES) are a new class of designer solvents. Type III DES are formed when a mixture of two high melting point compounds, usually a hydrogen bond donor and a quaternary ammonium salt, melt into a solution with a fusion temperature lower than either individual component. These solvents are considered ionic liquid analogues due to some shared properties, such as low vapor pressure and conductivity.[1-3] However, DES have many advantages over ionic liquids; e.g., easy preparation, low cost, low toxicity, and biodegradability.[3-4] The advantages of DES have created a wide field of potential applications in electrochemistry,[5-6] catalysis,[7] metal oxide dissolution,[8] and carbon dioxide capture[9] and separation.[10]

The DES structure can be simply tailored by modifying the chemical identity of the hydrogen bond donor or the ratio of components.[3] This is in contrast with ionic liquids for which a synthetic procedure is required to alter their structure.[11] However, the binary composition of DES also results in a more complex molecular arrangement which is not observed in regular molecular solvents or pure ionic liquids.[12] Hence, the connection between properties and structure of a DES is non-trivial. In particular, the different types of molecular interactions with similar energetics that contribute to DES physicochemical properties arise from the large variety of chemical

Reproduced by the permission of the PCCP Owner Societies
Cui, Y., K. D. Fulfer, J. Ma, T. K. Weldeghiorghis, and D. G. Kuroda. *Physical Chemistry Chemical Physics* **2016**, 18, 31471-31479.
DOI: 10.1039/C6CP06318G
http://pubs.rsc.org/en/content/articlelanding/2016/cp/c6cp06318g#!divAbstract

structures of the hydrogen bond donor and acceptor. The presence of spatial heterogeneities in the DES structure is a good example of this intricate energetic balance.[13]

Both ionic and polar compounds have been found to be soluble in DESs.[3] Interestingly, DES have much better dissolution power for organic compounds than water, in some cases reaching four orders of magnitude larger;[14] even though the polarities of DES and water are very similar.[15] However, the molecular property defining the solubility of DES has yet to be determined.

The solvation structure and dynamics of various solutes in DES have been investigated in previous years. Some of the first examples involved time-resolved fluorescence spectroscopy and molecular dynamics simulations.[16-17] To date, most experimental studies have relied on incorporating molecular dyes in order to gain insights into the solvation and its dynamics in the DES;[15-16, 18-19] however, dielectric relaxation spectroscopy has also been used to investigate ionic DES.[20] Here, we have studied the solvent–solute interactions and its dynamics via steady state and time-resolved vibrational spectroscopy using a small ionic probe. Compared to the use of molecular dyes, the use of a vibrational probe has many advantages. First, it relies on vibrational transitions which can be localized to a specific covalent bond.[21-30] Second, vibrational modes of ions have been shown to be very sensitive to the local environment and as such have been successfully applied in a wide variety of problems.[31-38] In addition, nonlinear vibrational spectroscopic experiments can be performed with energies that only change the temperature of the sample by a few Kelvin, making it possible to investigate the system under thermal equilibrium.[39-40] Thus, vibrational probes in conjunction with vibrational photon-echo spectroscopy are ideal for studying solvent–solute interactions as well as the DES solvent dynamics sensed by the solute under thermal conditions from which one can infer the location of the probe. It should be noted

that the window of measurable dynamics via 2DIR is limited by the vibrational lifetime of the probe used, which in the case of SeCN ion is ~300 ps.[41]

In this study, Fourier Transform Infrared spectroscopy (FTIR) and Two-Dimensional Infrared spectroscopy (2DIR) were used to investigate the solvation dynamics and structure of the thiocyanate ion in three different DES composed of choline chloride with either ethylene glycol, glycerol, or urea (Scheme 3.1). Furthermore, the experimental results are compared with Molecular Dynamics (MD) simulations to verify the assigned structure and dynamics.

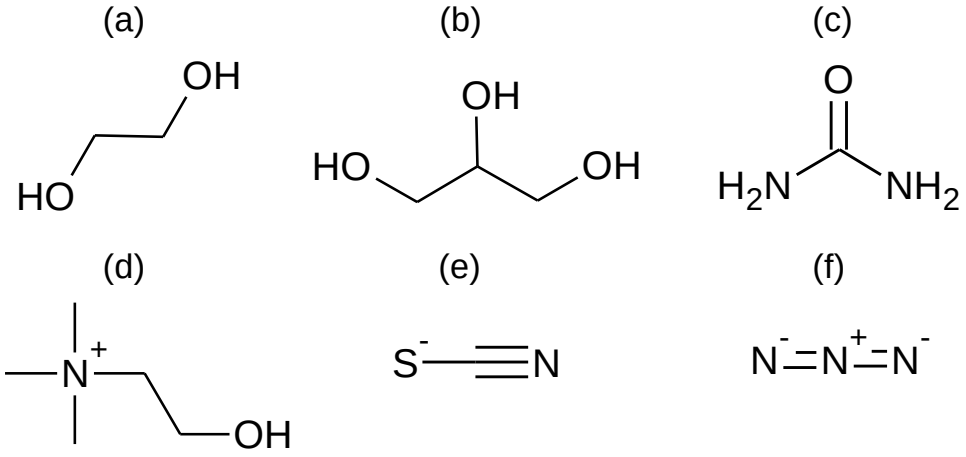

Scheme 3.1. Structures of (a) ethylene glycol (EG), (b) glycerol (G), (c) urea (U), (d) choline ion, (e) thiocyanate ion, and (f) azide ion.

3.2. Experimental and theoretical methodologies

3.2.1. Experimental methods

1. Sample preparation. Ethylene glycol (Sigma Aldrich, 99.8%), glycerol (Fisher) and urea (Acros Organics, 99.5%) were used without further purification. Choline chloride (Sigma Aldrich, 98%) was dried in a vacuum oven at 100 ˚C and -1.0 bar for 24 hours and then stored in a N2-filled glovebox. All of the deep eutectic solvents were prepared in a glovebox with a molar

ratio of choline chloride to hydrogen bond donor of 1 : 2 unless otherwise noted. Each DES was prepared without heating. DES EG (choline chloride–ethylene glycol) and DES G (choline chloride–glycerol) were prepared directly by stirring. DES U (choline chloride and urea) was prepared by sonicating the components in a room temperature bath. Ammonium thiocyanate (Baker Analyzed Reagent 99.1%) or tetrabutylammonium azide (Santa Cruz Biotech, 490%) were added to the DES solutions at a concentration of 100 mM. All of the DES were stored in a moisture-free environment.

2. Linear IR spectroscopy. Linear IR measurements were performed using a Bruker Tensor 27. All of the samples were measured with 0.5 cm^{-1} resolution at room temperature, using an O-ring sealed sample cell composed of CaF_2 windows and a 25 mm spacer, which was prepared in a N_2-filled glovebox in order to minimize exposure to water.

3. Two dimensional IR spectroscopy. 2DIR spectroscopy experiments were performed in a setup similar to that previously described in the literature.[42] In short, a Spectra Physics Spitfire Ace Ti:Sapphire amplifier with a 5 kHz repetition rate and OPA-800C were used to produce broadband IR pulses with a temporal width of ~60 fs. Three replicas were produced from the IR pulses and focused onto the sample in a boxcar configuration.[43] The time intervals between the first and second pulses (t), between the second and third pulses (T_w), which generates the photon echo, and between the fourth pulse and the photon echo (t) were controlled with four motorized translation stages (PI Micos). Photon echo in the $k_1 + k_2 + k_3$ phase matching direction was detected interferometrically using a fourth infrared pulse (local oscillator). The interferogram was dispersed by a Triax monochromator (75 grooves per mm) and detected using a liquid nitrogen cooled MCT array with 64 elements (Infrared Systems Development). All of the 2DIR spectra were collected by sampling t, from 3.5 ps to 3.5 ps every 4 fs. For each sample, the waiting time

was scanned from 0 ps to 100 ps with steps which increased exponentially starting at 0.5 ps. The 2DIR spectra were obtained by double Fourier Transformation along t and t from the signal in the (t, T_w, t) domain, keeping T_w as a parameter. The sample cell for 2DIR was prepared in the same manner as that for FTIR. Furthermore, the 2DIR optical setup is encased in an air-dried box; all experiments were performed at o1% humidity.

4. NMR. Pulse field gradient (PFG) diffusion experiments were performed on a 400 MHz Bruker AV spectrometer with a wide bore magnet using a Diff60 diffusion probe and Great 1/60 gradient amplifier. The diffusion probe has a gradient sensitivity of 600 mT A^{-1} m^{-1} (60 G A^{-1} cm^{-1}). Diffusion data were collected at 25 °C, and the sample temperature was controlled using a Bruker BVT 3000 digital variable temperature controller. The probe gradient coil temperature was controlled using Neslab Merlin M33 (Thermo Scientific) recirculating chiller.

Diffusion experiments were done using pulse gradient stimulated echo (diffSTE) sequence that uses the same sequences as described in ref. 44. In brief, the diffusion data were collected with constant gradient pulse duration (δ) and diffusion time (Δ). A 2 ms homospoil gradient pulse was used to remove unwanted signal. For all three samples, gradient pulse duration of 1–2 ms and diffusion times between 75–100 ms were used. The maximum gradient strength (g) used was 360 G cm1 for DES EG, 1000 G cm1 for DES U, and 760 G cm^{-1} for DES G. The gradient strength (g) was varied between the maximum value and 5% of the maximum value linearly in 32 increments. The diffusion constant (D), was determined by fitting experimental data to the Stejskal–Tanner-equation,[45]

$$\frac{S}{S_0} = e^{-\gamma^2 g^2 \delta^2 (\Delta - \frac{\delta}{3}) D}$$

where S is signal attenuated by gradient pulses, S_0 is the reference signal (with no gradient attenuation), γ is the gyromagnetic ratio of the observed nucleus (^{1}H), and the other variables are from the pulse sequence.

3.2.2. Theoretical methods

1. Molecular dynamics. The molecular dynamics simulations were performed using the SANDER module of the AMBER 12 program package.[46] A quantum mechanics/molecular mechanics method was used to model the system. The thiocyanate ion was parameterized according to parameterized model number 3 (PM3) semi-empirical formalism while the DES components were modeled classically with the GAFF force field. The system consisted of an SCN ion embedded in a 40 Å cube containing a variable number of choline chloride and hydrogen bond donors at a molar ratio of 1 : 2, respectively. The concentration of thiocyanate was kept at B0.1 M assuming that the densities of the solutions are the same as the pure DES.[2] Periodic boundary conditions were imposed in the simulation. Particle mesh Ewald methodology was used for long-range electrostatic interactions with a cutoff of 10 Å. The SHAKE algorithm was used to fix the bonds involving hydrogen. The simulation was initiated using an initial geometry for the SCN ion obtained from ab initio calculations. The system was energy-minimized for 200 steps using the steepest descent method followed by 300 steps of the conjugate gradient method. Subsequently, the system was equilibrated at normal temperature and pressure (298 K and 1 bar, denoted NTP) for 10 ns with a 2 fs step. Finally, a production run at NTP was recorded for 5 ns extracting snapshots every 20 fs. All simulations used a Langevin thermostat for temperature control.

2. *Ab initio* calculation. DFT calculations were performed at the B3LYP level with the 6-311++G** basis set using the GAUSSIAN 09 software package.[47]

3.3. Result

3.3.1. Linear IR spectra

Solvation of the thiocyanate ion in three DES (DES G, DES EG, and DES U) and their parental molecular solvents (ethylene glycol and glycerol) was first investigated by FTIR spectroscopy. FTIR spectra of the bands corresponding to the nitrile stretch mode of the thiocyanate ion in each sample after background subtraction and normalization are shown in Figure 3.1. All of the samples present a single band, though for some of the solutions this band is asymmetric; i.e., the band cannot be modeled with a single Voigt profile (Figure 3.2). Notably, the nitrile stretch band is asymmetric only in the two molecular solvents; i.e., G and EG. The major difference between the nitrile bands of DES and the molecular solvents is the full width at half maximum (FWHM) which is largest (~54 cm^{-1}) in each of the molecular solvents. In contrast, the FWHMs of the thiocyanate nitrile bands in DES EG, DES G, and DES U are 40 cm^{-1}, 42 cm^{-1}, and 32 cm^{-1}, respectively. Contrary to the FWHM, the frequency of the maximum (ν_{max}) of the nitrile peaks does not show a significant variation with solvents. The nitrile stretch bands are located at ~2057 cm^{-1} in EG, DES EG, and DES G; while in glycerol and in DES U the bands are positioned at 2059 cm^{-1} and 2056 cm^{-1}, respectively.

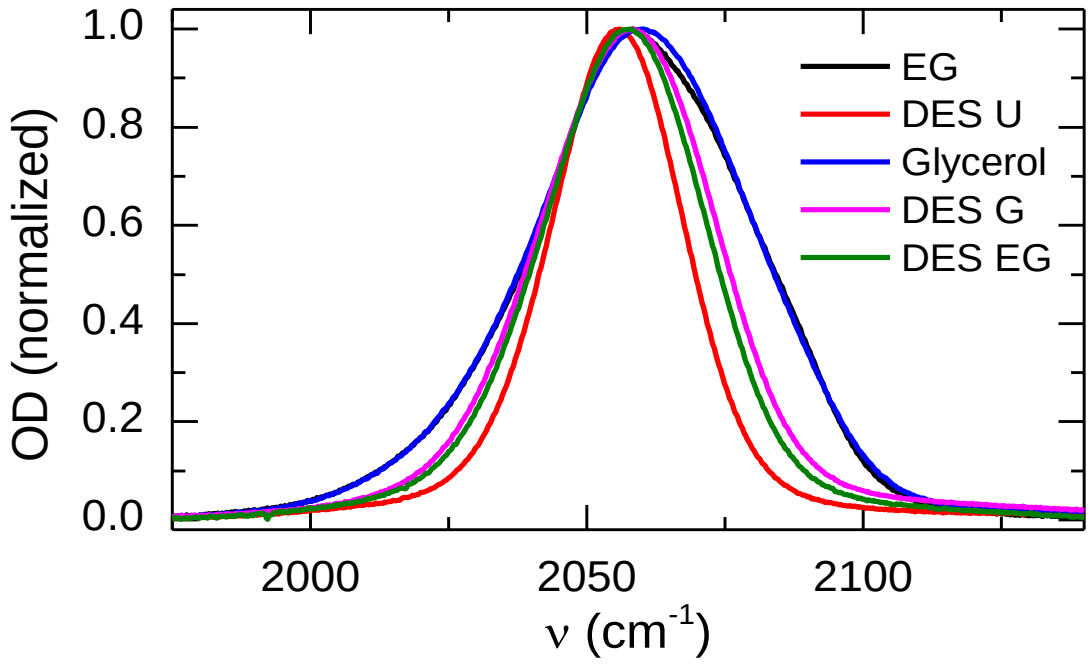

Figure 3.1. FTIR spectra of thiocyanate ion as a probe in EG, G, DES EG, DES G, and DES U.

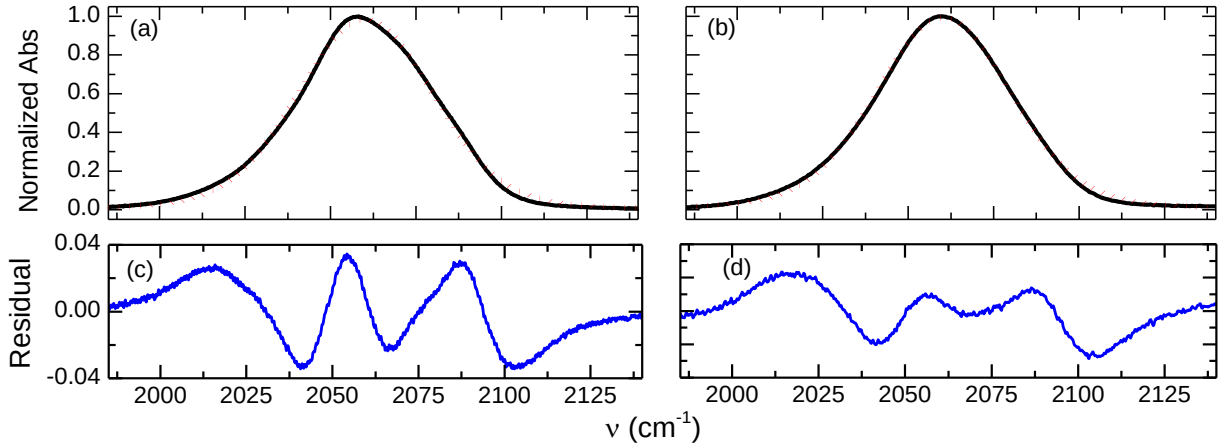

Figure 3.2. Modelling of the thiocyanate nitrile stretch band in (a) ethylene glycol and (b) glycerol with a single Voigt profile. Data is shown as black solid lines and modeling is represented by red dashed lines. The model line does not correctly model the measured data, as can be seen by the residuals from the fit shown in (c) and (d) for ethylene glycol and glycerol, respectively. This indicates that the thiocyanate stretch of the probe ion in the ethylene glycol and glycerol cannot be modeled with a single Voigt profile.

3.3.2. Two dimensional IR spectroscopy

Figure 3.3 shows the 2DIR spectra for the nitrile stretch region of thiocyanate in the three different DES. The 2DIR spectra, represented as a function of the pump (ω_τ) and probe (ω_t) frequencies, show two peaks. Overlapped with the diagonal of the 2DIR spectrum (i.e., $\omega_\tau = \omega_t$; the black solid line in Figure 3.3), the red (positive) peak corresponds to the signal arising from the n = 1 to n = 0 transitions (i.e., stimulated emission and bleach signals). Conversely, the blue peak (negative) arises from the n = 1 to n = 2 transition due to the photoinduced absorption signal. The separation of ~20 cm1 between the positive and negative peaks of the 2DIR spectra evidences the anharmonicity of the vibrational potential of the thiocyanate nitrile stretch. The observed anharmonicity is in agreement with previously measured values in other solvents.[48-49]

The time evolution of the 2DIR spectra shows that the 2DIR peaks are elongated and tilted along the diagonal at T_w = 0 ps. In contrast, as T_w increases the peaks acquire a rounder and less tilted shape. The time evolution of the 2DIR peak shapes indicates the occurrence of spectral diffusion.[43] Interestingly, none of the measured spectra acquire a completely upright shape within the longest measured T_w of 100 ps. While the nitrile peaks of DES EG exhibit an almost upright position at T_w = 100 ps, the corresponding peaks in DES G and DES U remain significantly tilted at the same waiting time. It is important to note that no obvious cross peaks appear in the 2DIR spectra within 100 ps of waiting time.

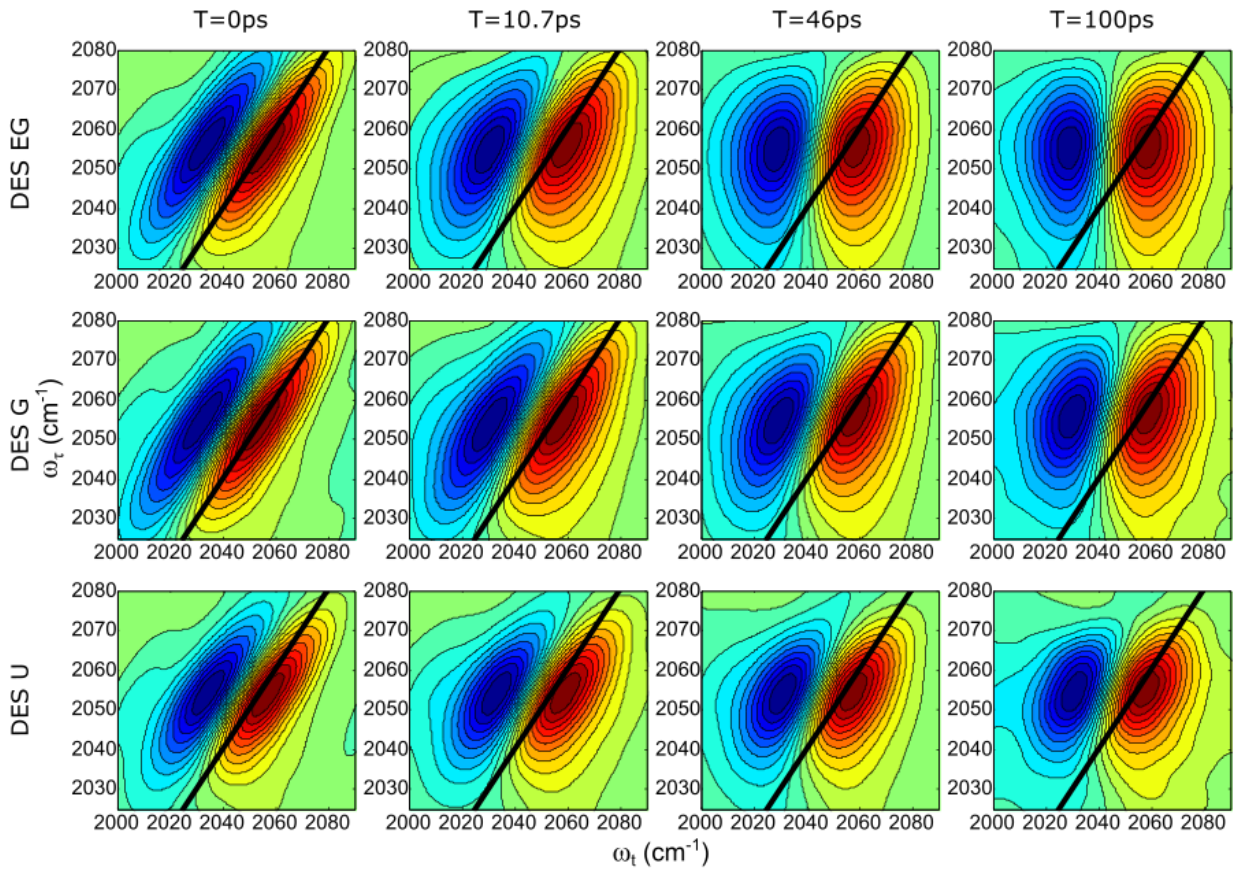

Figure 3.3. 2DIR spectra of DES EG, DES G, and DES U at T_w=0 ps, 10.7 ps, 46 ps, and 100 ps.

3.4. Discussion

The linear IR spectra of the thiocyanate nitrile stretch in the different DES show very similar bands located at ~2057 cm^{-1}. It has been previously demonstrated that the thiocyanate nitrile stretch transition frequency increases when thiocyanate is hydrogen bonded to other molecules through its nitrogen atom.[50] In particular, the experimental and theoretical evidence demonstrates that thiocyanate in methanol exhibits two bands in the IR spectrum corresponding to the nitrile group with and without a hydrogen bond located at ~2070 cm^{-1} and ~2057 cm^{-1}, respectively.[50-51] Similar transition frequencies of the thiocyanate nitrile stretch in methanol and in DES suggest that the anion is not forming hydrogen bonds through its nitrile group in the three

DES. Moreover, the linear spectra of the nitrile stretch do not present an obvious symmetry or shoulder in any of the DES samples indicating that the population of thiocyanate ions having a hydrogen bond through the nitrogen atom is negligible. In addition, the lack of a significant difference in the ν_{max} of the CN stretch transition demonstrates that the molecular environment around the anion is very similar in all three DES. This last result is in agreement with a previous work where it was shown that the polarities of DES U, DES G, and DES EG are very similar.[15]

To confirm the lack of hydrogen bonds through the nitrile end of the thiocyanate ion in the DES, the changes in the nitrile stretch of thiocyanate in an EG solution were evaluated as a function the concentration of choline chloride (Figure 3.4). In pure EG, the existence of the nitrile hydrogen bonded band is evident on the high-frequency side of the peak where a strong shoulder is observed. As the concentration of choline chloride is increased the band shape of the nitrile stretch becomes more symmetric and narrow, and shifts to lower frequencies. These changes in the nitrile bandwidth and location indicate that addition of the hydrogen bond acceptor decreases the ability of the DES environment to form hydrogen bonds through the nitrile end of the anion. This result agrees with previous experimental work that demonstrated that the chloride ion forms a strong complex with the hydrogen bond donor.[3,52] It is expected that the thiocyanate ion incorporates into the DES molecular structure. In particular, thiocyanate is expected to occupy the same places as the chloride ion, which inevitably leads to the formation of hydrogen bonds.

Linear IR spectroscopy shows no evidence of hydrogen bonding through the nitrile group of SCN, but it is very likely that the probe forms hydrogen bonds through its sulphur atom where the negative charge is localized.[53] In contrast to the nitrile hydrogen bond, the spectroscopic signature of the hydrogen bond through the sulphur atom is not seen in the FTIR because the sulphur atom does not participate significantly in the nitrile stretch mode (figure 3.5 and table 3.1).

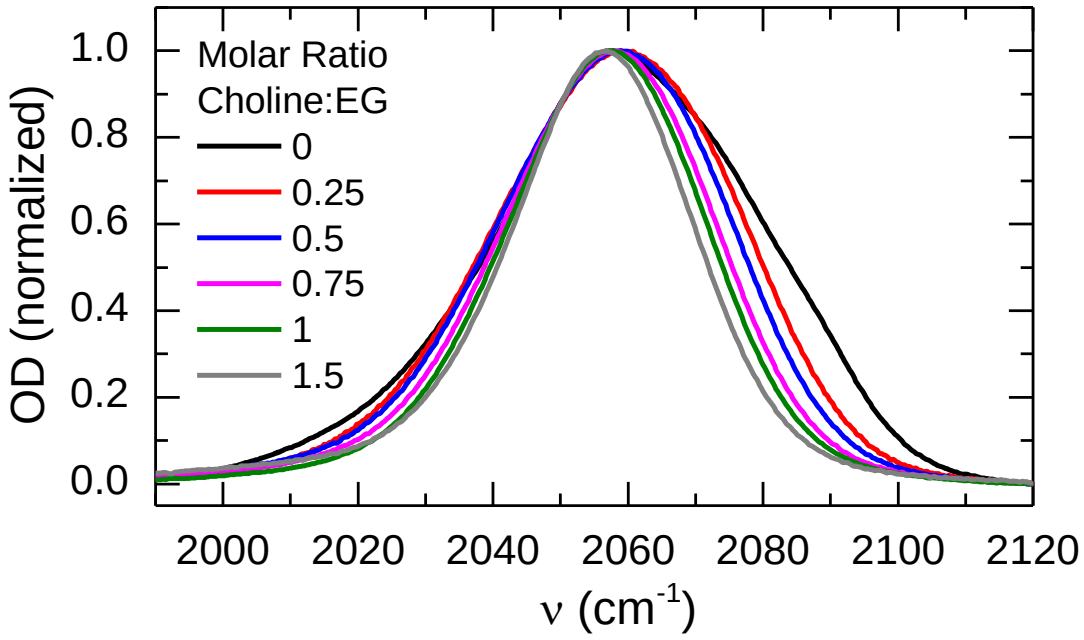

Figure 3.4. FTIR spectra of thiocyanate ion probe in EG solutions with varying concentrations of choline chloride.

Figure 3.5. The nitrile stretch mode of the thiocyanate ion is localized mainly on the carbon (grey) and nitrogen (blue).

Table 3.1. Displacement vectors for the nitrile stretch of the thiocyanate ion.

	X	Y	Z
C	0.00	0.00	0.80
N	0.00	0.00	-0.61
S	0.00	0.00	-0.03

To further support the indication that the thiocyanate ion is in an environment where hydrogen bonds are formed, the same samples were probed using the azide ion. The azide ion is symmetric and has N_3^- asymmetric stretch mode which is comprised of all three atoms of the anion. As a result, the formation of the hydrogen bond from either end of the molecule is directly observed in its linear IR spectrum. FTIR spectra of the azide ion in the three DES and their parental solvents are presented in Figure 3.6. The spectra show that the asymmetric stretch band of azide has approximately the same FWHM for all of the samples (see Figure 3.6 and Table 3.2) which demonstrates that the DES and their parental solvents form hydrogen bonds with anionic solutes. Moreover, the ν_{max} of the band for the three DES are very similar (within ~2 cm^{-1}) which reinforces the idea that anions observe a very similar environment in all of the DES. Additionally, 2DIR spectroscopy of the azide samples in DES, and molecular solvents show that the ion has the same dynamics irrespective of the environment (table 3.3). These results strongly support the idea that the azide or thiocyanate ions occupy the same places as chloride ions.

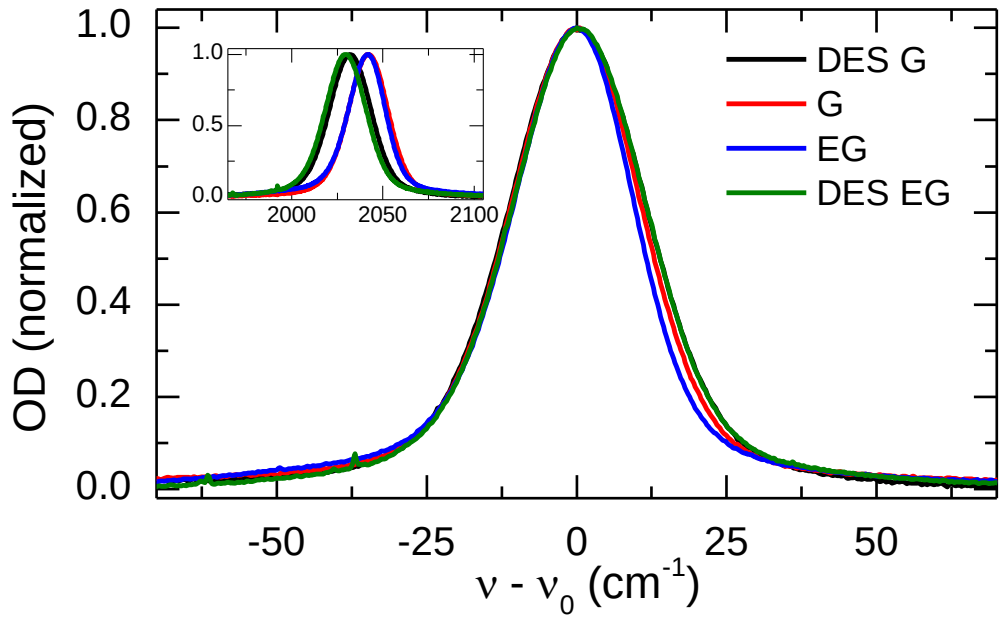

Figure 3.6. Centralized FTIR spectra of tetrabutylammmonium azide in EG, G, DES G and DES EG. Inset shows the non-centralized FTIR spectra.

Table 3.2. Fitting parameters used to model the FFCF of the azide ion stretch mode in DES EG, EG, DES G, and G. The decorrelation times are very similar for the azide probe in each environment.

	A	τ / ps	y_0
DES EG	0.16±0.01	1.6±0.3	0.66±0.01
EG	0.29±0.01	1.9±0.3	0.44±0.01
DES G	0.10±0.01	1.5±0.3	0.75±0.01
G	0.10±0.01	1.4±0.4	0.73±0.01

Table 3.3. Vibrational population relaxation times, T_{10}, for the thiocyanate probe in both molecular solvents and in each DES. The T_{10} times are very similar for all three DES.

	T_{10} / ps
EG	6.6±0.1
G	8.4±0.1
DES EG	16.2±0.8
DES G	17.6±0.9
DES U	17.4±0.2

The experimental results presented here were further investigated using MD simulations. Radial distribution functions (RDFs) of the thiocyanate atoms with different atoms of the DES components are presented in Figure 3.7. In the case of the thiocyanate nitrogen atom, the RDFs shows that the thiocyanate nitrogen points towards the choline nitrogen with only a small percentage of the thiocyanate nitrogen atoms forming hydrogen bonds with the hydrogen bond donor in all three DES. Moreover, the RDFs of the thiocyanate sulphur atom reveal that the

hydrogen bonds occur primarily through this end of the anion in all of the DES, as previously deduced from our experiments. In addition, a comparison between the radial distributions of the chloride and thiocyanate ions reveals a strong similarity (Figure 3.8), which confirms that both ions occupy the same locations within the DES structure. The IR experiments show that the lineshape of the nitrile stretch is not significantly dependent on the molecular structure of the hydrogen bond donor forming the DES. However, a close inspection of the FWHM reveals the following trend:

FWHM(DES G) > FWHM(DES EG) > FWHM(DES U).

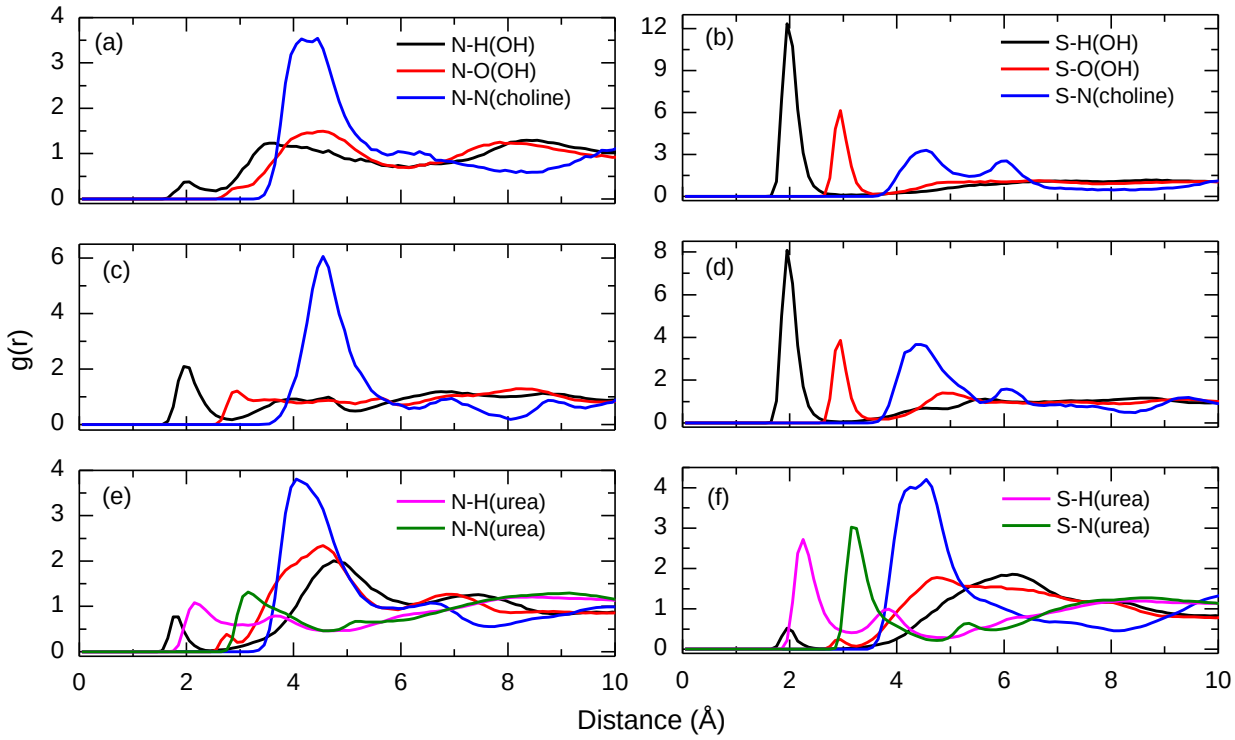

Figure 3.7. Radial distribution functions of the thiocyanate ion in (a and b) DES EG, (c and d) DES G, and (e and f) DES U.

According to semi-classical theory, the IR lineshape is described by,[43]

$$I(\omega) = 2Re\int_0^\infty \mu^2 \exp(i(\omega - \langle\omega_{10}\rangle)t)\exp(-g(t) - \frac{t}{2T_{10}} - 2Dt)dt,$$

where μ is the transition dipole magnitude for the v = 0 to v = 1 transition, $\langle\omega_{10}\rangle$ is the transition frequency, g(t) is the double time integral of the frequency–frequency correlation function (FFCF),[43]

$$g(t) = \int_0^t d\tau_1 \int_0^{\tau_1} \langle\delta\omega_{10}(\tau_2)\delta\omega_{10}(0)\rangle d\tau_2,$$

T_{10} is the vibrational population relaxation time, and D is the rotational diffusion coefficient. The

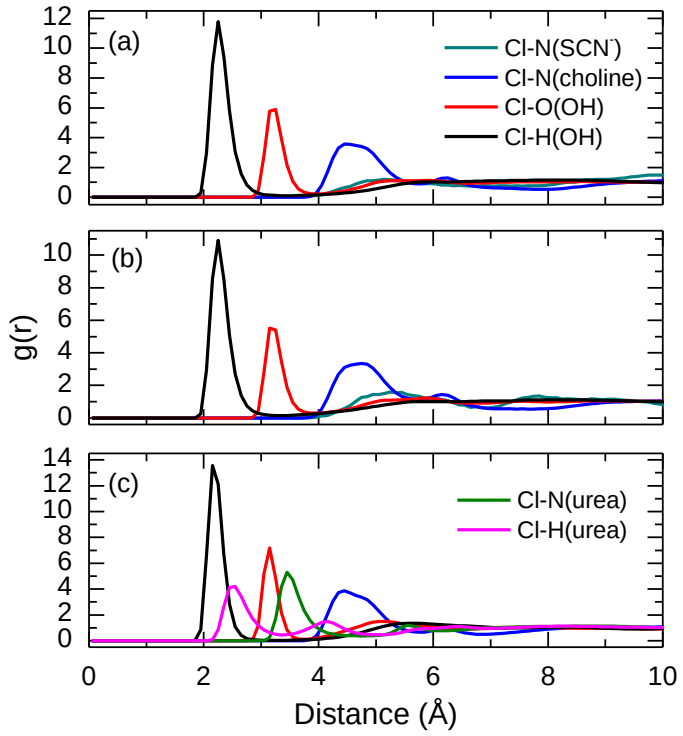

Figure 3.8. Radial distribution functions (RDFs) of the chloride ion in (a) DES EG, (b) DES G, and (c) DES U. RDFs of the chloride ion show that SCN^- and Cl^- occupy approximately the same space in the DES solutions.

expression of the lineshape shows that the width of the band is defined by the FFCF (g(t)), the vibrational lifetime (T_{10}), and rotational diffusion (D). However, the effect of rotational diffusion

is neglected here due to the high viscosity of the DES solvents.[2] Moreover, the vibrational lifetimes of the thiocyanate nitrile stretch in the three DES are found to be nearly identical (table 3.3), and so the differences in FWHM for the different DES must arise from the FFCF.

Over waiting time, T_w, the pump and probe frequencies lose correlation due to various processes occurring in the system, such as the motions of the components of the solvation shell.[43] This loss of correlation is described by the FFCF. The FFCF dynamics, evaluated from the inverse slope of the zeroth contour line of the 2DIR spectra,[54] shows a significant difference among the three DES samples (Figure 3.9). In the case of DES EG, the FFCF decays almost to zero within the 100 ps window investigated. In contrast, neither DES G nor DES U shows such a ‘‘fast’’ decay of the FFCF. The FFCF dynamics of each sample is well modeled with a biexponential function of the form: $A_1\exp(-t/\tau_{1c}) + A_2\exp(-t/\tau_{2c})$; but only the FFCF of DES EG and DES G are well modelled with a stretched exponential. Fitting parameters for each solvent (Table 3.4) show that the FFCF of thiocyanate in DES has two characteristic times, one short (~10 ps) and one long ($\gg$10 ps), which should correspond to two different molecular motions of the solvent components.

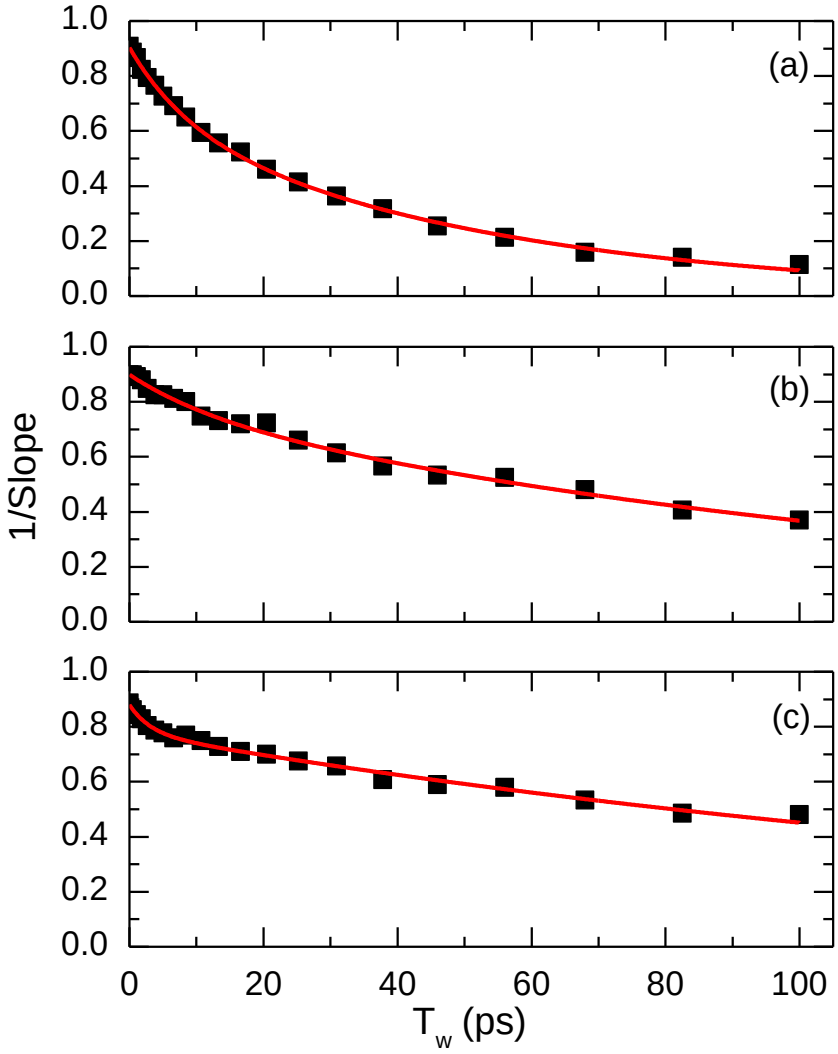

Figure 3.9. FFCF of (a) DES EG, (b) DES G, and (c) DES U.

Table 3.4. FFCF fitting parameters. Δ values were obtained from a fitting procedure similar to methods described previously.[54]

	A_1	Δ^2/cm^{-2}	τ_1/ps	A_2	Δ^2/cm^{-2}	τ_2/ps
DES EG	0.26±0.06	62.2	9±1	0.65±0.06	162.0	52±3
DES G	0.13±0.08	33.9	13±5	0.77±0.08	224.7	136±30
DES U	0.10±0.02	19.1	3±1	0.78±0.02	132.9	184±30

It has been previously demonstrated that the solvent dynamics in a two-omponent system can be described by a frequency correlation function of the form:[55-56]

$$FFCF(t) = A_{solv} \exp\left(-\frac{t}{\tau_{solv}}\right) + A_{exch} \exp\left(-\frac{t}{\tau_{exch}}\right),$$

where A_i is the amplitude and τ_i is the corresponding decay constant for the *i*th term. According to this model, the correlation decays are affected by the in-place motions of the solvent as well as by the exchange of molecular components in and out of the solvation shell. The model also assumes that the in-place solvent motions are those involving rotations and translations which do not significantly change the position of the centre of mass of the molecule. In contrast, the exchange dynamics originate from diffusion motions in which the centre of mass of the molecules involved is significantly varied. Consequently, the time scale of exchange is expected to have a significantly slower dynamics than the dynamics of the solvent motions. Thus, the fast and slow components of the FFCF dynamics of thiocyanate ion in the three different DES are assigned to in-place molecular motions and exchange diffusion processes, respectively.

DES have a structure similar to that of ionic liquids where the positional correlation is well defined for many solvation shells; i.e., a pseudo lattice.[57] As previously shown, the thiocyanate ion is hydrogen bonded to the hydrogen bond donor through its sulphur atom, while its nitrogen points toward the choline cation. It is important to note that the highest perturbation to the frequency of the thiocyanate nitrile stretch will be produced by motions of the choline cation since the Coulomb interaction is the strongest possible molecular interaction among the DES components. Hence, it is likely that the nitrile group mainly senses the motions of the choline cation within its solvation shell. Moreover, the motions causing different interactions with the thiocyanate ion through its sulphur atom will not be probed due to the small participation of this atom in the nitrile stretch mode.[50] Within this pseudo lattice model, the fast FFCF component should correspond to

‘‘oscillations’’ of the lattice, and the slow component should be assigned to motions of the DES molecular constituents diffusing in and out of the solvation shell.

Previously, it was shown that the diffusional motions in and out of the solvation shell have a close relationship with the molecular mechanism of viscosity.[49] Interestingly, this is also true in the case of DES where the slow FFCF correlation decay shows a strong correlation with the viscosity (Figure 3.10a). The correlation reveals that the two quantities are related, but does not provide a clear molecular mechanism. Pulsed Field Gradient Nuclear Magnetic Resonance (PFG-NMR) experiments show that the diffusion constant of the choline cations in different DES is inversely correlated to the slow FFCF component (Figure 3.10b) which supports the hypothesis that the longer decay time might arise from the motions of the choline cations diffusing in and out of the solvation shell. It should be noted that another mechanism might appear in the FFCF dynamics, which arises from the rotational dynamics of the thiocyanate ion;[41] the 2DIR experiments presented in this work are not able to distinguish between the two possible mechanisms. However, the approximate MD FFCF calculated from the carbon–nitrogen distance of the thiocyanate ions from MD simulations (Figure 3.11 and table 3.5) shows not only that the slow decay time from our experimentally obtained FFCF have the same time scale, but also that they are highly correlated to the time scales of the choline diffusion in and out of the solvation shell. These results further support the picture of the slow FFCF component arising due to translational diffusion of choline ions from the solvation shell of the thiocyanate ion.

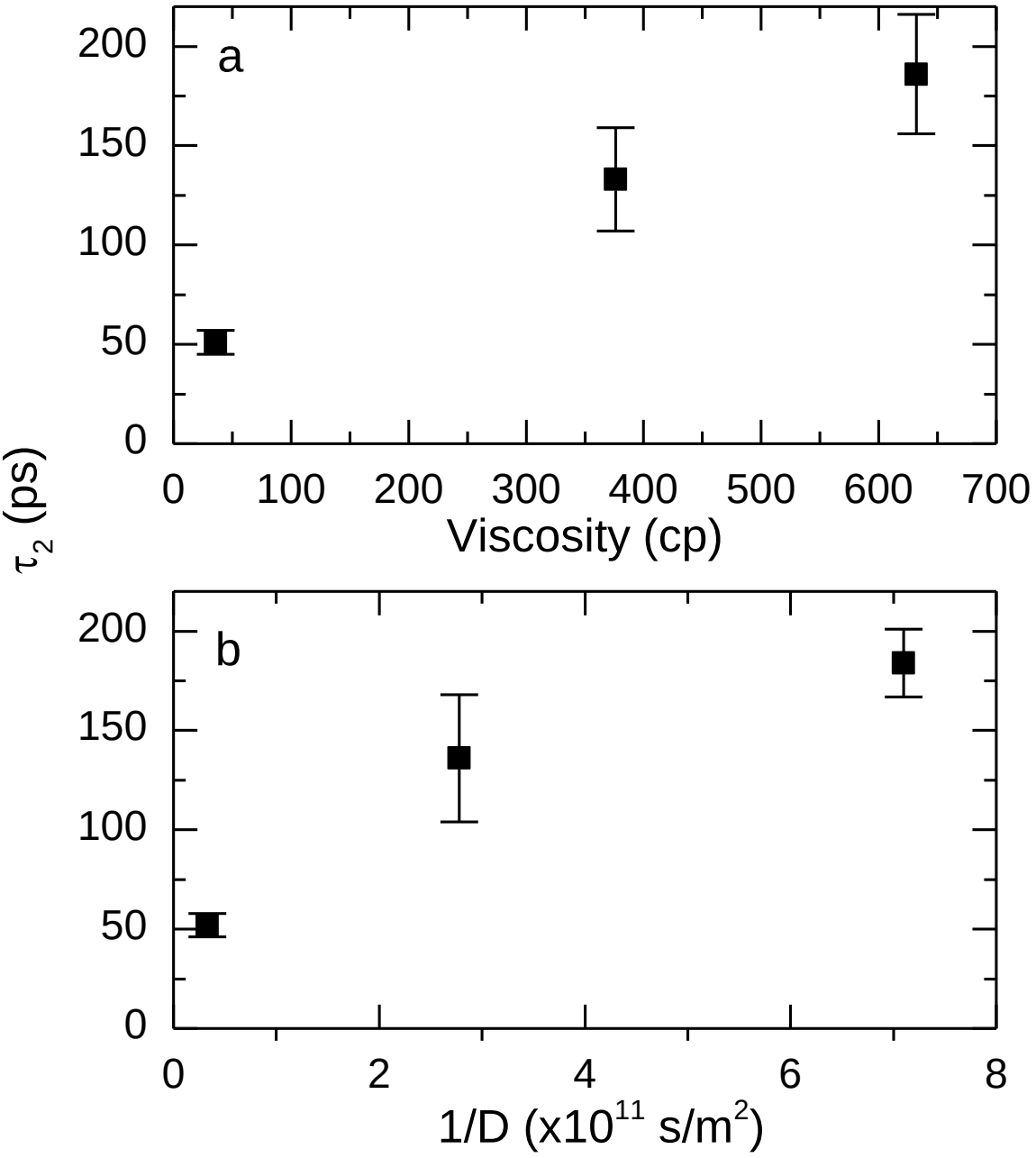

Figure 3.10. (a) DES viscosity (from ref. 2) versus slow correlation decay time ($R^2 = 0.998$) and (b) choline cation diffusion constant in each DES versus slow correlation decay time ($R^2 = 0.96$).

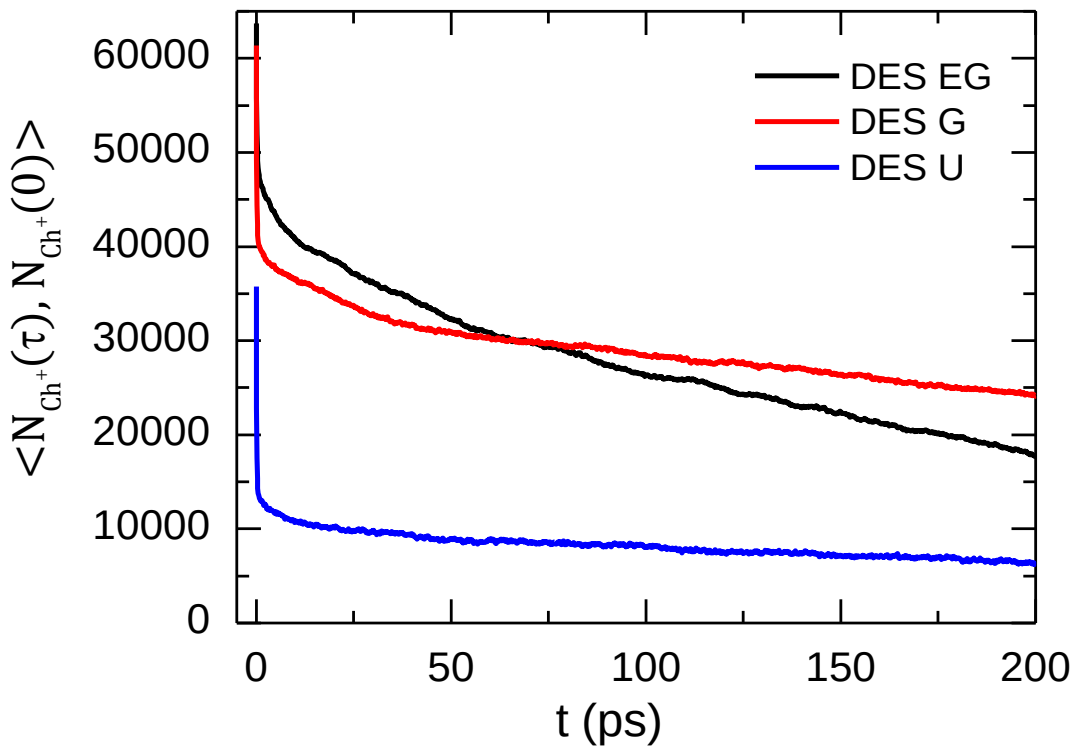

Figure 3.11. Time autocorrelation functions of the number of choline ions (N_{Ch^+}) in the first solvation shell of the thiocyanate ion, $C(t) = \langle N_{Ch^+}(\tau), N_{Ch^+}(0)\rangle$, obtained from MD simulations for DES EG, DES G, and DES U.

Table 3.5. Amplitude and time constants from modeling the time autocorrelation function of the frequency fluctuations as a tri-exponential decay.

	$A_1 \times 10^4$	τ_1 / ps	$A_2 \times 10^3$	τ_2 / ps	$A_3 \times 10^4$	τ_3 / ps
DES EG	1.64±0.03	0.24±0.01	7.44±0.05	17.5±0.3	3.864±0.005	268±1
DES G	2.12±0.02	0.13±0.01	6.90±0.04	17.2±0.2	3.310±0.003	657±2
DES U	2.25±0.02	0.12±0.01	3.14±0.03	10.0±0.2	1.001±0.001	458±2

Conversely, the fast component of the FFCF is assigned to the motions of the molecular components within the solvation shell of the thiocyanate ion. These in-place motions of the DES

components are likely related to the strength of the pseudo lattice which is directly related to the interaction between the hydrogen bond donor and the anion of the DES.[3] DFT calculations of the period of harmonic oscillation computed from the potential energy as a function of anion–hydrogen bond donor distance (Table 3.6) show a linear relationship with the fast correlation decay time (Figure 3.12). This observed correlation further supports the idea that the oscillatory motions are related to the strength of the pseudo-lattice or, equivalently, to the strength of the hydrogen bond between the donor and the anion.

Table 3.6. Harmonic period (in fs) calculated from the force constant of the interaction between the hydrogen bond donors and the chloride ion from DFT calculations.

	Harmonic period (fs)
EG-Cl	325
G-Cl	490
U-Cl	245

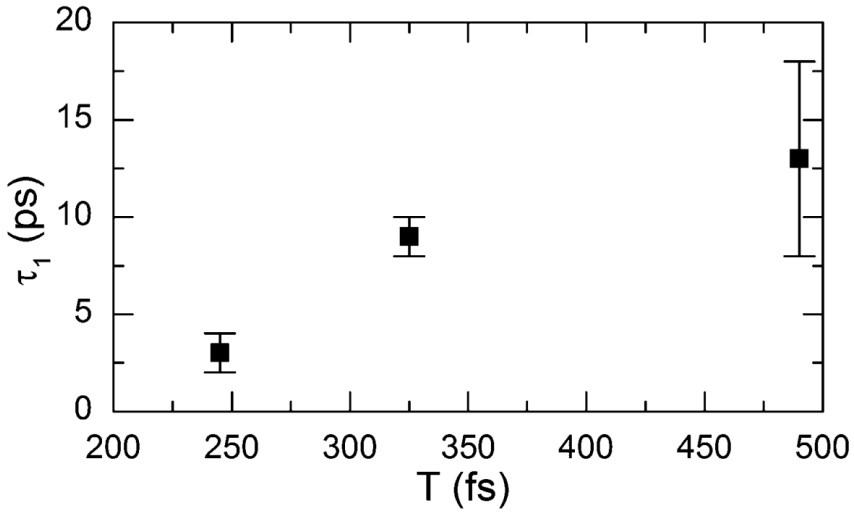

Figure 3.12. Period, *T*, of the harmonic oscillatory motions of the hydrogen bond donor–chloride ion interaction versus the fast correlation decay time (R2 = 0.82).

MD simulations were used to further test the proposed molecular model for the motions observed by the thiocyanate ion in the different DES. First, the autocorrelation of the average carbon–nitrogen distance, as a measure of the FFCF, shows that the time scales are similar to that observed experimentally (Figure 3.13 and Table 3.7). Second, the time autocorrelation function for the number of choline ions in the solvation shell of thiocyanate shows that the DES samples have motions on the same time scales as the experimentally measured FFCF characteristic times (Table 3.7). However, the characteristic times computed from the autocorrelation function of the number of the choline ions do not match the observed experimental trends which is likely due to the off-the-self models used to parametrize the components of the DES in the MD simulation and the arbitrary definition of the first solvation shell cut-off. Thus, the time scale agreement between the experimental FFCF and the autocorrelation of the motions of the choline cations, or the approximate MD FFCF (Figure 3.14), supports our proposed molecular mechanism for the FFCF. Moreover, the simulation results reveal that the fast dynamical component of the autocorrelation function corresponds to those choline ions oscillating within or near the solvation shell, while the slow component relates to those ions diffusing fully in and out of the solvation shell. However, the contributions from the hydrogen bond donor are clearly non-negligible as seen by the difference between the autocorrelation timescales of the number of choline ions in the thiocyanate solvation shell and of the approximate MD FFCF.

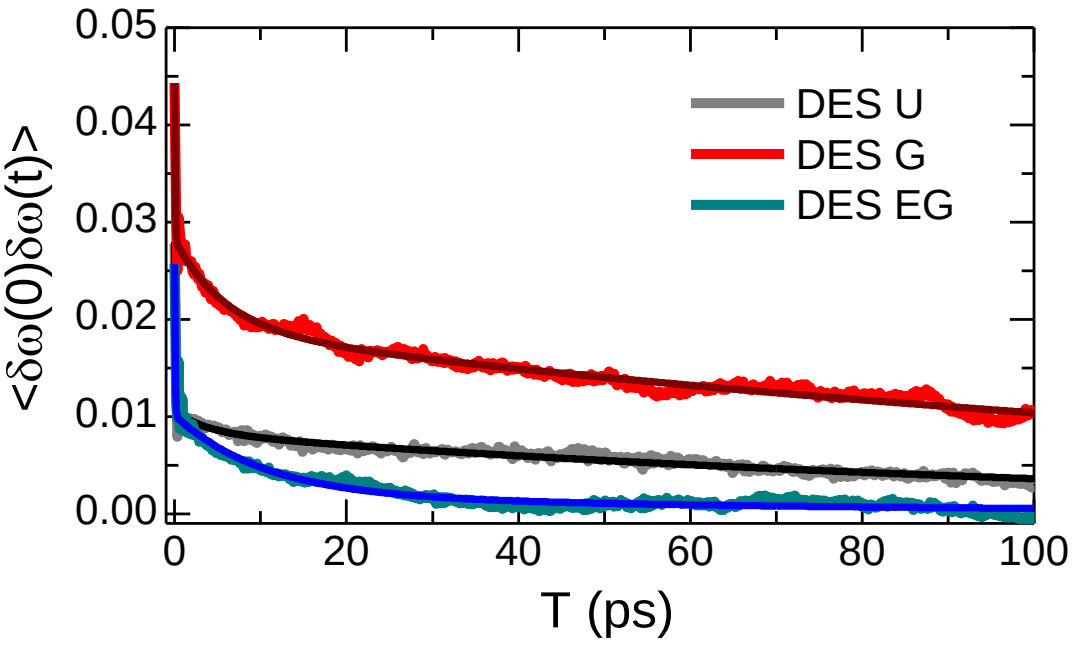

Figure 3.13. Time autocorrelation function of the frequency fluctuations ($\langle \delta\omega(0), \delta\omega(t) \rangle$) obtained from CN distance averaged over 150 fs steps of MD simulations for DES U, DES G, and DES EG.

Table 3.7. Amplitude and time constants from modeling the time autocorrelation function of the frequency fluctuations as a tri-exponential decay.

	A_1	τ_1 / ps	A_2	τ_2 / ps	A_3	τ_3 / ps
DES EG	0.016±0.001	0.06±0.01	0.0083±0.0002	10.3±0.6	0.0019±0.0002	80±13
DES G	0.016±0.001	0.06±0.01	0.0092±0.0002	5.8±0.3	0.0190±0.0001	166±3
DES U	0.017±0.001	0.10±0.01	0.0022±0.0002	3.8±0.6	0.0083±0.0001	119±2

The FFCF dynamics provides a suitable framework for explaining the molecular motions that the anionic probe observes in the DES. However, it does not explain the FWHM of the IR lineshape of the thiocyanate ion (Figure 3.1). In DES, the IR lineshape is clearly dominated by the inhomogeneous distribution of frequencies since the vibrational lifetime is relatively long and only

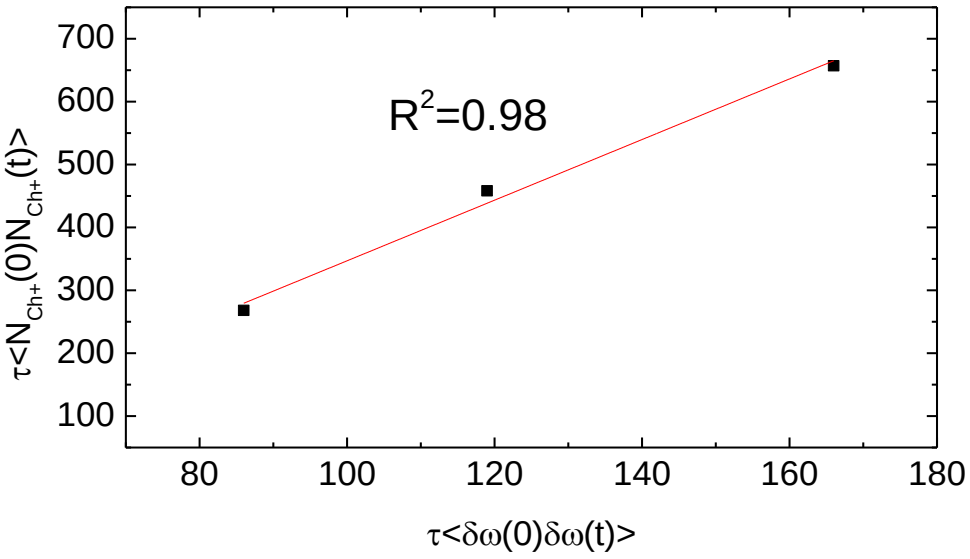

Figure 3.14. Correlation between time scales of diffusion of choline ion and FFCF from the average distance between nitrogen and carbon of SCN^- ion.

accounts for ~2 cm^{-1} of the total bandwidth and the FFCF dynamics is relatively slow. In the case of thiocyanate where two dynamics have been observed, the width of the line is described only by $\delta^2 = \Delta_1^2 + \Delta_2^2$ in the inhomogeneous limit,[43] and corresponds to a FWHM of 35.3 cm^{-1}, 37.9 cm^{-1}, and 28.9 cm^{-1} for DES EG, DES G, and DES U, respectively. Note the FWHM values present the same trend as the FWHM of the IR lineshape indicating that the system can be well modelled within the inhomogeneous limit. In this case, the inhomogeneous width also provides insights of the molecular environment since it shows how many different environments the probe is observing. DES G and DES EG do not present a large difference in the number of environments, but DES U has a lower number of possible environments. In other words, DES G and DES EG have more disorganized molecular structures than DES U.

It has been proposed that the density and other properties of DES can be described by hole theory.[58-59] In this theory, holes (defect sites) arising from the disorder of the DES structure are responsible for defining the DES properties. Notably, the inhomogeneous widths show good

agreement with the inverse molar volumes of each DES. In the case of DES U and DES EG, which have nearly identical molar mass, this may represent a meaningful correlation. However, in the case of DES G, which has a much higher molar mass, the correlation may simply be fortuitous. Aside from the apparent agreement of solution organization with inverse molar volume, the DES organization does not appear to obviously correlate with either the free volume or the average hole size as predicted by hole theory for these DES.[44] This lack of agreement indicates that hole theory alone might not provide the predictors required for linking microscopic and macroscopic properties of DES as previously suggested in ref. 44.

3.5. Summary

The nitrile stretch transition of the thiocyanate ion in three different DES was study by IR spectroscopies. These studies show that the thiocyanate anion is hydrogen bonded through its sulphur atom in all DES and it observes two solvation processes with different dynamics, both on a picosecond time scale. The two dynamical processes are assigned to in-place and diffusional motions of the solvation shell components. Molecular dynamics simulations and *ab initio* computations confirm the molecular interpretation of our experimental findings. Finally, modelling of the IR lineshape of the thiocyanate nitrile stretch demonstrates that DES are disorganized solvents. However, the level of organization observed for the different DES might not be sufficient for explaining the macroscopic properties of DES, such as density.

3.6. References

1. Abbott, A. P.; Capper, G.; Davies, D. L.; Rasheed, R. K.; Tambyrajah, V., Novel Solvent Properties of Choline Chloride/Urea Mixtures. *Chemical Communications* **2003**, 70-71.

2. Smith, E. L.; Abbott, A. P.; Ryder, K. S., Deep Eutectic Solvents (Dess) and Their Applications. *Chemical reviews* **2014**, *114*, 11060-11082.

3. Zhang, Q.; Vigier, K. D. O.; Royer, S.; Jérôme, F., Deep Eutectic Solvents: Syntheses, Properties and Applications. *Chemical Society Reviews* **2012**, *41*, 7108-7146.

4. Welton, T., Room-Temperature Ionic Liquids. Solvents for Synthesis and Catalysis. *Chemical reviews* **1999**, *99*, 2071-2084.

5. Yang, H.; Guo, X.; Birbilis, N.; Wu, G.; Ding, W., Tailoring Nickel Coatings Via Electrodeposition from a Eutectic-Based Ionic Liquid Doped with Nicotinic Acid. *Applied Surface Science* **2011**, *257*, 9094-9102.

6. Gómez, E.; Cojocaru, P.; Magagnin, L.; Valles, E., Electrodeposition of Co, Sm and Smco from a Deep Eutectic Solvent. *Journal of electroanalytical chemistry* **2011**, *658*, 18-24.

7. Phadtare, S. B.; Shankarling, G. S., Halogenation Reactions in Biodegradable Solvent: Efficient Bromination of Substituted 1-Aminoanthra-9, 10-Quinone in Deep Eutectic Solvent (Choline Chloride: Urea). *Green Chemistry* **2010**, *12*, 458-462.

8. Abbott, A. P.; Capper, G.; Davies, D. L.; McKenzie, K. J.; Obi, S. U., Solubility of Metal Oxides in Deep Eutectic Solvents Based on Choline Chloride. *Journal of Chemical & Engineering Data* **2006**, *51*, 1280-1282.

9. Li, X.; Hou, M.; Han, B.; Wang, X.; Zou, L., Solubility of Co2 in a Choline Chloride+ Urea Eutectic Mixture. *Journal of Chemical & Engineering Data* **2008**, *53*, 548-550.

10. Shahbaz, K.; Mjalli, F.; Hashim, M.; AlNashef, I., Using Deep Eutectic Solvents Based on Methyl Triphenyl Phosphunium Bromide for the Removal of Glycerol from Palm-Oil-Based Biodiesel. *Energy & Fuels* **2011**, *25*, 2671-2678.

11. Durand, E.; Lecomte, J.; Villeneuve, P., Deep Eutectic Solvents: Synthesis, Application, and Focus on Lipase-Catalyzed Reactions. *European Journal of Lipid Science and Technology* **2013**, *115*, 379-385.

12. Perkins, S. L.; Painter, P.; Colina, C. M., Molecular Dynamic Simulations and Vibrational Analysis of an Ionic Liquid Analogue. *The Journal of Physical Chemistry B* **2013**, *117*, 10250-10260.

13. Berchiesi, G.; Rafaiani, G.; Vitali, G.; Farhat, F., Cryoscopic and Dynamic Study of the Molten System Fluoroacetamide-Sodium Trifluoroacetate. *Journal of Thermal Analysis and Calorimetry* **1995**, *44*, 1313-1319.

14. Morrison, H. G.; Sun, C. C.; Neervannan, S., Characterization of Thermal Behavior of Deep Eutectic Solvents and Their Potential as Drug Solubilization Vehicles. *International journal of pharmaceutics* **2009**, *378*, 136-139.

15. Pandey, A.; Rai, R.; Pal, M.; Pandey, S., How Polar Are Choline Chloride-Based Deep Eutectic Solvents? *Physical Chemistry Chemical Physics* **2014**, *16*, 1559-1568.

16. Das, A.; Das, S.; Biswas, R., Density Relaxation and Particle Motion Characteristics in a Non-Ionic Deep Eutectic Solvent (Acetamide+ Urea): Time-Resolved Fluorescence Measurements and All-Atom Molecular Dynamics Simulations. *The Journal of chemical physics* **2015**, *142*, 034505.

17. Das, A.; Biswas, R., Dynamic Solvent Control of a Reaction in Ionic Deep Eutectic Solvents: Time-Resolved Fluorescence Measurements of Reactive and Nonreactive Dynamics in (Choline Chloride+ Urea) Melts. *The Journal of Physical Chemistry B* **2015**, *119*, 10102-10113.

18. Abbott, A. P.; Harris, R. C.; Ryder, K. S.; D'Agostino, C.; Gladden, L. F.; Mantle, M. D., Glycerol Eutectics as Sustainable Solvent Systems. *Green Chemistry* **2011**, *13*, 82-90.

19. Dai, Y.; Witkamp, G.-J.; Verpoorte, R.; Choi, Y. H., Tailoring Properties of Natural Deep Eutectic Solvents with Water to Facilitate Their Applications. *Food chemistry* **2015**, *187*, 14-19.

20. Mukherjee, K.; Das, A.; Choudhury, S.; Barman, A.; Biswas, R., Dielectric Relaxations of (Acetamide+ Electrolyte) Deep Eutectic Solvents in the Frequency Window, $0.2 \leq N/Ghz \leq 50$: Anion and Cation Dependence. *The Journal of Physical Chemistry B* **2015**, *119*, 8063-8071.

21. Reimers, J. R.; Hall, L. E., The Solvation of Acetonitrile. *Journal of the American Chemical Society* **1999**, *121*, 3730-3744.

22. Nyquist, R., Solvent-Induced Nitrile Frequency Shifts: Acetonitrile and Benzonitrile. *Applied spectroscopy* **1990**, *44*, 1405-1407.

23. Getahun, Z.; Huang, C.-Y.; Wang, T.; De León, B.; DeGrado, W. F.; Gai, F., Using Nitrile-Derivatized Amino Acids as Infrared Probes of Local Environment. *Journal of the American Chemical Society* **2003**, *125*, 405-411.

24. Maienschein-Cline, M. G.; Londergan, C. H., The Cn Stretching Band of Aliphatic Thiocyanate Is Sensitive to Solvent Dynamics and Specific Solvation. *The Journal of Physical Chemistry A* **2007**, *111*, 10020-10025.

25. Taskent-Sezgin, H.; Chung, J.; Banerjee, P. S.; Nagarajan, S.; Dyer, R. B.; Carrico, I.; Raleigh, D. P., Azidohomoalanine: A Conformationally Sensitive Ir Probe of Protein Folding, Protein Structure, and Electrostatics. *Angewandte Chemie International Edition* **2010**, *49*, 7473-7475.

26. Cremeens, M. E.; Fujisaki, H.; Zhang, Y.; Zimmermann, J.; Sagle, L. B.; Matsuda, S.; Dawson, P. E.; Straub, J. E.; Romesberg, F. E., Efforts toward Developing Direct Probes of Protein Dynamics. *Journal of the American Chemical Society* **2006**, *128*, 6028-6029.

27. Fayer, M. D., Fast Protein Dynamics Probed with Infrared Vibrational Echo Experiments. *Annual review of physical chemistry* **2001**, *52*, 315-356.

28. Maekawa, H.; Ge, N.-H., Picosecond Rotational Interconversion Adjacent to a C□ O Bond Studied by Two-Dimensional Infrared Spectroscopy. *The Journal of Physical Chemistry B* **2012**, *116*, 11292-11301.

29. Decatur, S. M., Ir Spectroscopy of Isotope-Labeled Helical Peptides: Probing the Effect of N-Acetylation on Helix Stability. *Biopolymers* **2000**, *54*, 180-185.

30. Kuroda, D. G.; Abdo, M.; Chuntonov, L.; Smith III, A. B.; Hochstrasser, R. M., Vibrational Dynamics of a Non-Degenerate Ultrafast Rotor: The (C12, C13)-Oxalate Ion. *The Journal of chemical physics* **2013**, *139*, 164514.

31. Ohta, K.; Maekawa, H.; Saito, S.; Tominaga, K., Probing the Spectral Diffusion of Vibrational Transitions of Ocn-and Scn-in Methanol by Three-Pulse Infrared Photon Echo Spectroscopy. *The Journal of Physical Chemistry A* **2003**, *107*, 5643-5649.

32. Thøgersen, J.; Réhault, J.; Odelius, M.; Ogden, T.; Jena, N. K.; Jensen, S. J. K.; Keiding, S. R.; Helbing, J., Hydration Dynamics of Aqueous Nitrate. *The Journal of Physical Chemistry B* **2013**, *117*, 3376-3388.

33. Kuroda, D. G.; Vorobyev, D. Y.; Hochstrasser, R. M., Ultrafast Relaxation and 2d Ir of the Aqueous Trifluorocarboxylate Ion. *The Journal of chemical physics* **2010**, *132*, 044501.

34. Singh, P. K.; Kuroda, D. G.; Hochstrasser, R. M., An Ion's Perspective on the Molecular Motions of Nanoconfined Water: A Two-Dimensional Infrared Spectroscopy Study. *The Journal of Physical Chemistry B* **2013**, *117*, 9775-9784.

35. Dahl, K.; Sando, G. M.; Fox, D. M.; Sutto, T. E.; Owrutsky, J. C., Vibrational Spectroscopy and Dynamics of Small Anions in Ionic Liquid Solutions. *The Journal of chemical physics* **2005**, *123*, 084504.

36. Mandal, A.; Ramasesha, K.; De Marco, L.; Tokmakoff, A., Collective Vibrations of Water-Solvated Hydroxide Ions Investigated with Broadband 2dir Spectroscopy. *The Journal of chemical physics* **2014**, *140*, 204508.

37. Moilanen, D. E.; Wong, D.; Rosenfeld, D. E.; Fenn, E. E.; Fayer, M., Ion–Water Hydrogen-Bond Switching Observed with 2d Ir Vibrational Echo Chemical Exchange Spectroscopy. *Proceedings of the National Academy of Sciences* **2009**, *106*, 375-380.

38. Park, K. H.; Choi, S. R.; Choi, J. H.; Park, S.; Cho, M., Real-Time Probing of Ion Pairing Dynamics with 2dir Spectroscopy. *ChemPhysChem* **2010**, *11*, 3632-3637.

39. Nienhuys, H.-K.; Woutersen, S.; Van Santen, R. A.; Bakker, H. J., Mechanism for Vibrational Relaxation in Water Investigated by Femtosecond Infrared Spectroscopy. *Journal of Chemical Physics* **1999**, *111*.

40. Chuntonov, L.; Kumar, R.; Kuroda, D. G., Non-Linear Infrared Spectroscopy of the Water Bending Mode: Direct Experimental Evidence of Hydration Shell Reorganization? *Physical Chemistry Chemical Physics* **2014**, *16*, 13172-13181.

41. Tamimi, A.; Bailey, H. E.; Fayer, M. D., Alkyl Chain Length Dependence of the Dynamics and Structure in the Ionic Regions of Room-Temperature Ionic Liquids. *The Journal of Physical Chemistry B* **2016**, *120*, 7488-7501.

42. Kim, Y. S.; Hochstrasser, R. M., Applications of 2d Ir Spectroscopy to Peptides, Proteins, and Hydrogen-Bond Dynamics†. *The Journal of Physical Chemistry B* **2009**, *113*, 8231-8251.

43. Hamm, P.; Zanni, M., *Concepts and Methods of 2d Infrared Spectroscopy*; Cambridge University Press, 2011.

44. D'Agostino, C.; Harris, R. C.; Abbott, A. P.; Gladden, L. F.; Mantle, M. D., Molecular Motion and Ion Diffusion in Choline Chloride Based Deep Eutectic Solvents Studied by 1 H Pulsed Field Gradient Nmr Spectroscopy. *Physical Chemistry Chemical Physics* **2011**, *13*, 21383-21391.

45. Stejskal, E. O.; Tanner, J. E., Spin Diffusion Measurements: Spin Echoes in the Presence of a Time-Dependent Field Gradient. *The journal of chemical physics* **1965**, *42*, 288-292.

46. Case, D.; Darden, T.; Cheatham III, T.; Simmerling, C.; Wang, J.; Duke, R.; Luo, R.; Walker, R.; Zhang, W.; Merz, K., Amber 12. *AMBER 12, University of California: San Francisco* **2012**.

47. Gaussian09, R. A., 1, Mj Frisch, Gw Trucks, Hb Schlegel, Ge Scuseria, Ma Robb, Jr Cheeseman, G. Scalmani, V. Barone, B. Mennucci, Ga Petersson Et Al., Gaussian. *Inc., Wallingford CT* **2009**.

48. van Wilderen, L. J.; Kern-Michler, D.; Müller-Werkmeister, H. M.; Bredenbeck, J., Vibrational Dynamics and Solvatochromism of the Label Scn in Various Solvents and Hemoglobin by Time Dependent Ir and 2d-Ir Spectroscopy. *Physical Chemistry Chemical Physics* **2014**, *16*, 19643-19653.

49. Ren, Z.; Ivanova, A. S.; Couchot-Vore, D.; Garrett-Roe, S., Ultrafast Structure and Dynamics in Ionic Liquids: 2d-Ir Spectroscopy Probes the Molecular Origin of Viscosity. *The journal of physical chemistry letters* **2014**, *5*, 1541-1546.

50. Schultz, P. W.; Leroi, G. E.; Popov, A. I., Solvation of Scn-and Secn-Anions in Hydrogen-Bonding Solvents. *Journal of the American Chemical Society* **1996**, *118*, 10617-10625.

51. Bachelin, M.; Gans, P.; Gill, J. B., Spectrochemistry of Solutions. Part 24.—Li, Na, K and Bu N4 N Thiocyanates in Methanol: Infrared Spectroscopic Evidence for Ion Pairing and Hydrogen Bonding. *Journal of the Chemical Society, Faraday Transactions* **1992**, *88*, 3327-3330.

52. Hammond, O. S.; Bowron, D. T.; Edler, K. J., Liquid Structure of the Choline Chloride-Urea Deep Eutectic Solvent (Reline) from Neutron Diffraction and Atomistic Modelling. *Green Chemistry* **2016**, *18*, 2736-2744.

53. Miessler, G. L.; Tarr, D. A., *Inorganic Chemistry*, 4th ed.; Pearson Prentice Hall: Upper Saddle River, NJ, 2011, p xiv, 754 p.

54. Kwac, K.; Cho, M., Molecular Dynamics Simulation Study of N-Methylacetamide in Water. Ii. Two-Dimensional Infrared Pump–Probe Spectra. *The Journal of chemical physics* **2003**, *119*, 2256-2263.

55. Dunbar, J. A.; Arthur, E. J.; White, A. M.; Kubarych, K. J., Ultrafast 2d-Ir and Simulation Investigations of Preferential Solvation and Cosolvent Exchange Dynamics. *The Journal of Physical Chemistry B* **2015**, *119*, 6271-6279.

56. Kwak, K.; Park, S.; Fayer, M., Dynamics around Solutes and Solute–Solvent Complexes in Mixed Solvents. *Proceedings of the National Academy of Sciences* **2007**, *104*, 14221-14226.

57. Kokorin, A. I. i., *Ionic Liquids: Theory, Properties, New Approaches*; InTech, 2011.

58. Abbott, A. P.; Barron, J. C.; Ryder, K. S.; Wilson, D., Eutectic-Based Ionic Liquids with Metal-Containing Anions and Cations. *Chemistry–A European Journal* **2007**, *13*, 6495-6501.

59. Abbott, A. P.; Capper, G.; Gray, S., Design of Improved Deep Eutectic Solvents Using Hole Theory. *ChemPhysChem* **2006**, *7*, 803-806.

CHAPTER 4
EVIDENCE OF MOLECULAR HETEROGENEITIES IN AMIDE BASED DEEP EUTECTIC SOLVENTS

4.1. Introduction

Deep Eutectic Solvents (DES) are a novel class of room temperature liquids based on the well-known eutectic phenomenon.[1] Thus, DES are formed when two compounds are mixed and the fusion temperature of the mixture is lower than that of either individual component.[2-4] DESs are typically made by mixing a quaternary ammonium salt and a Lewis or Brønstead acid.[4] Similar to other designer solvents, such as ionic liquids (ILs), DESs have low vapor pressures and high conductivities.[4-7] However, DESs present several advantages over other designer solvents. For example, they are easily prepared by mixing and can be made with low cost and environmentally friendly materials.[6, 8-9] In addition, DESs physicochemical properties can be tailored not only by changing their components, but also by changing the ratio between components.[4, 10] For these reasons, DESs have recently gained significant popularity in different areas of science and engineering such as: electrochemistry,[11-12] metal oxide dissolution,[13] catalysis,[14-15] carbon dioxide absorption,[16] separation process,[17] oil-recovery,[18] polymerization,[19] etc.

Currently, the most studied DESs are composed of choline chloride and various hydrogen bond donors, like urea or glycerol, due to the sustainable nature of all the components.[4, 9] While there are an increasingly large number of studies on the applications of DESs, experimental and theoretical studies concentrating on unraveling the complex structure of choline based DESs have only recently started to appear.[20-25] These investigations have shown that the hydrogen bond network formed among choline ions and, chlorine ions, and the hydrogen bond donors is

responsible for the melting point depression of the mixture.[5] Two recent papers using neutron scattering on choline chloride-urea DES confirmed that the hydroxyl group of the choline ion plays an important role in the hydrogen bond network of the DES.[22, 24] Additionally, it has been proposed that hydrogen bonds assist in the charge delocalization of chloride ion by weakening the electrostatic interaction between the choline and the chloride ions, which causes the depression of the melting point. However, work from Abbott and co-workers demonstrated that the difference in the melting point temperature between DESs formed with urea and either choline chloride or chlorocholine chloride is only 3 ºC,[5] indicating that the hydroxyl group and hydrogen bonding does not significantly affect the depression of the mixture. Instead, it has proposed that entropy might play a major role in the formation of DESs. Furthermore, a recent *ab-initio* molecular dynamics simulation study did not find any evidence of charge delocalization in three different choline chloride based DESs.[26] While many previous experimental studies have centered on the structure and dynamics of components in different acetamide type I DESs,[27-36] a few have concentrated on the type III DES,[20-22, 25] which is the motivation of this study. Importantly, the effects of the chemical structure of the HBA cation on the resulting structure of the DESs remains unexplored.

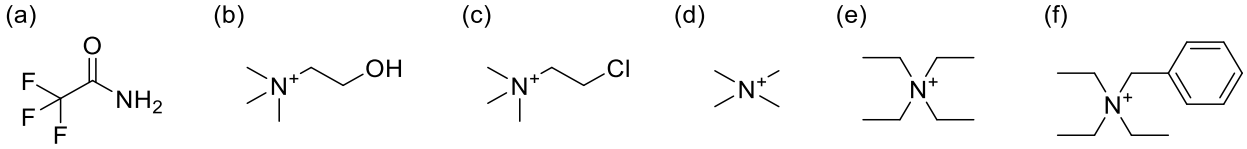

Scheme 4.1. Structure of (a) trifluoroacetamide (TFAm), (b) choline ion, (c) chlorocholine ion, (d) tetramethylammonium ion, (e) tetraethylammonium ion, (f) benzyltriethylammonium ion.

Table 4.1. Compositions and abbreviation of the Deep Eutectic Solvents

HBD (2.5 moles)	HBA (1 mol)	Abbreviation
Trifluoroacetamide	Choline chloride	DES1
	Chlorocholine chloride	DES2
	Tetramethylammonium chloride	DES3
	Tetraethylammonium chloride	DES4
	Benzyltriethylammonium chloride	DES5

This work focuses on shedding some light onto the effect of the "chemical structure" of the HBA cation on the microscopic structure and properties of the DES. We investigate DESs formed between trifluoroacetamide (TFAm) and various quaternary ammonium salts; i.e., choline chloride, chlorocholine chloride, tetramethylammonium chloride, tetraethylammonium chloride, or benzyltriethylammonium chloride (see scheme 4.1). TFAm is selected because it forms DESs that are liquids at room temperature.[37] In addition, TFAm can be used as a probe of the structure and dynamics of the DES molecular components because its amide vibrational mode is known to be sensitive to different molecular environments.[38-43] To this end, Fourier transform infrared spectroscopy (FTIR) and two dimensional infrared spectroscopy (2DIR) are used to characterize the vibrational dynamics of the amide mode including its frequency-frequency correlation function, which has encoded important information about the molecular motions in the system.[44-45] The selection of photon echo IR spectroscopy is based on its capability for measuring vibrational dynamics on ultrafast time scale; i.e., sub- and picoseconds.[44] 2DIR spectra have an enhanced frequency resolution, which allows one to discriminate different species,[44, 46-47] and measure transitions that are not clearly observed in the linear spectrum.[44, 48-49] Finally, a set of

complementary molecular dynamics simulations is used to help interpret and support the molecular process giving rise to the observed vibrational dynamics in the investigated DESs.

4.2. Experimental and theoretical methodologies

4.2.1. Experimental methods

1. **Sample preparation.** TFAm (2, 2, 2-trifluoroacetamide, Oakwood Chemical, 98%) was used as received, with no further purification. TFAm was determined to have 0.04% of water via Karl-Fisher titration. The hydrogen bond acceptors, choline chloride (Acros Organics, 99%), chlorocholine chloride (Alfa Aesar, 98%), and tetramethylammonium chloride (Sigma-Aldrich, 98%), tetraethylammonium chloride (Alfa Aesar), and benzyltriethylammonium chloride (Alfa Aesar, 99%) were dried at 90 oC in a vacuum oven for 24 hours. DESs were prepared by mixing the two components at a specific molar ratio of 1 HBA / 2.5 HBD in a vial by sonicating in a room temperature bath or by heating the solid mixture at the temperature lower than 70 oC until the clear liquid formed. All the chemical reagents and prepared solutions were stored and operated in a nitrogen flushed glove box.

2. **Linear IR spectroscopy.** The linear infrared measurements were performed on a Bruker Tensor 27 with a liquid nitrogen cooled narrow band MCT detector, with the resolution of 0.5 cm-1. The samples are measured in a sample cell composed of two CaF_2 windows without spacer (path length ~1 μm). Attenuated total reflectance FTIR (ATR-FTIR) spectra were measured on a Bruker Tensor 27 with a Pike diamond/ZnSe ATR crystal and a DTGS detector, with a resolution of 4 cm-1. All the linear IR measurements were performed at room temperature.

3. **Two Dimensional IR spectroscopy.** The 2DIR spectroscopy measurements were performed in a setup similar to that previously described in the literature.[50] Briefly, a broadband

IR pulse with a temporal width of ~60 fs was generated from a Spectra Physics Spitfire Ace Ti:Sapphire amplifier with 5 kHz repetition rate in combination with an optical parametric amplifier (Spectra Physics OPA-800C) and difference frequency generation crystal ($AgGaS_2$).

The photon echo signal was generated by focusing three replicas of the IR femtosecond pulses (each with a wavevector of either $\boldsymbol{k}_1$, $\boldsymbol{k}_2$, or $\boldsymbol{k}_3$) on the sample with a lens in a boxcar configuration.[44] The photon echo in the phase matching direction of $-\boldsymbol{k}_1 + \boldsymbol{k}_2 + \boldsymbol{k}_3$ was then heterodyned by a fourth pulse (local oscillator) and detected with a liquid nitrogen cooled MCT array detector (64 elements, Infrared Systems Development) after its dispersion via a monochromator (Triax Horiba). The time intervals between pulses, τ (between first and second pulses), T_w (between second and third pulses), and t (between third and the photon echo) were altered by four computer controlled translation stages (PI Micos). For each waiting time, the photon echo signals were collected by sampling τ from -4 ps to 4 ps with a step of 5 fs. In all cases, the local oscillator always preceded the signal by ~0.5 ps. A double Fourier transform along τ and t times was used to transform the signal in the time domain (i.e., $S[\tau, T_w, t]$) to the signal in the frequency domain (i.e., $S[\omega_\tau, T_w, \omega_t]$). The details of the FT analysis can be found in Ref. 51. Note that the data corresponding to $T_w = 0$ ps was not considered in the analysis of the slope because of distortions caused by pulse overlap and non-resonant signals from the materials of the sample cell.

The DES solutions in which the amide band was investigated were measured with a sample cell with a CaF_2 convex lens (focal length of 1 m and path lengths > 500 nm). The details of the lens sample cell can be found in Ref. 52. The $^{13}C{=}O$ centered sample was measured in a sample cell having two regular CaF_2 windows without spacer (path length ~1 μm). The 2DIR spectra of DES3 and DES4 were collected at 35 ^{0}C with a temperature controlled sample cell (Harrick

Scientific) to avoid the solidification of the sample, while the 2DIR spectra data of the other three DESs were collected at room temperature.

4. **Differential Scanning calorimetry.** The DSC measurements were performed on a DSC 2920 (TA instruments) using the empty pan as the reference. The solution sample (~10 mg) and reference were held on a hermetic alodined aluminum pan (TA instruments). The DSC cycle consisted of first cooling the DES and the reference solvent to -55 °C where they remained for 5 min to achieve equilibrium, followed by a heating step with a rate of 10 °C/min to achieve a final temperature of 40 °C.

4.2.2. Theoretical method

1. **Molecular dynamics.** The molecular dynamics simulations were performed using the SANDER module of the AMBER 12 program package.53 A quantum mechanics/molecular mechanics method was used to model the system. The DES components were modeled classically with the GAFF force field. The selection of the unmodified force field is due to its good matching with diffusion experiments.54 The system was embedded in a 50 Å cube of a variable number of TFAm and different hydrogen bond acceptors (see Scheme 1) at a molar ratio of 2.5:1 between hydrogen bond donor and acceptor. The initial box was built using the packmol software package.55 Periodic boundary conditions were imposed in the simulation. Particle mesh Ewald methodology was used for long-range electrostatic interactions with a cutoff of 10 Å. The SHAKE algorithm was used to fix the bonds involving hydrogen. The system was energy-minimized for 200 steps using the steepest descent method followed by 300 steps of the conjugate gradient method, then the system was equilibrated at 400 K and 1 bar (denoted normal temperature and pressure, NTP) for 1 ns with a 2 fs per step. This step was followed by another NTP step in which

the temperature was held at 300 K. In the two NTP steps, the simulation used a Langevin thermostat as temperature control. After 1 ns of NVT, a production run at NVE was recorded for 10 ns extracting snapshot every 500 fs.

4.3. Result

4.3.1. Linear IR spectra

Steady-state IR spectroscopy was first used to study the structural differences of DES having different HBA cations. The FTIR-ATR spectra of all the investigated DESs in the frequency range from 1650 to 1775 cm^{-1} are shown in Figure 4.1. The two observed bands in this IR region correspond unequivocally to the vibrational transitions of TFAm, since the different cations of the HBAs do not have vibrational transitions in this part of the spectrum (see Figures 4.2 and 4.3). Furthermore, the strong absorption at 1724 cm^{-1} and a weak band at 1625 cm^{-1} have been previously assigned to the amide mode and the scissoring mode of the amide hydrogens of TFAm, respectively.[56] Overall, the amide band of the different samples shows a similar and slightly asymmetric line shape, and it is not well modeled with a single Voight profile. Moreover, the line shape is significantly different when the TFAm molecule is isolated (Figure 4.4), which is consistent with the presence of a vibrational exciton. In addition, the frequency positions of the maxima, as well as their bandwidths, do not vary significantly. A similar trend is observed for the scissoring mode at 1622 cm^{-1} (inset of Figure 4.1), though the location of the maximum band is slightly different in the different DES samples.

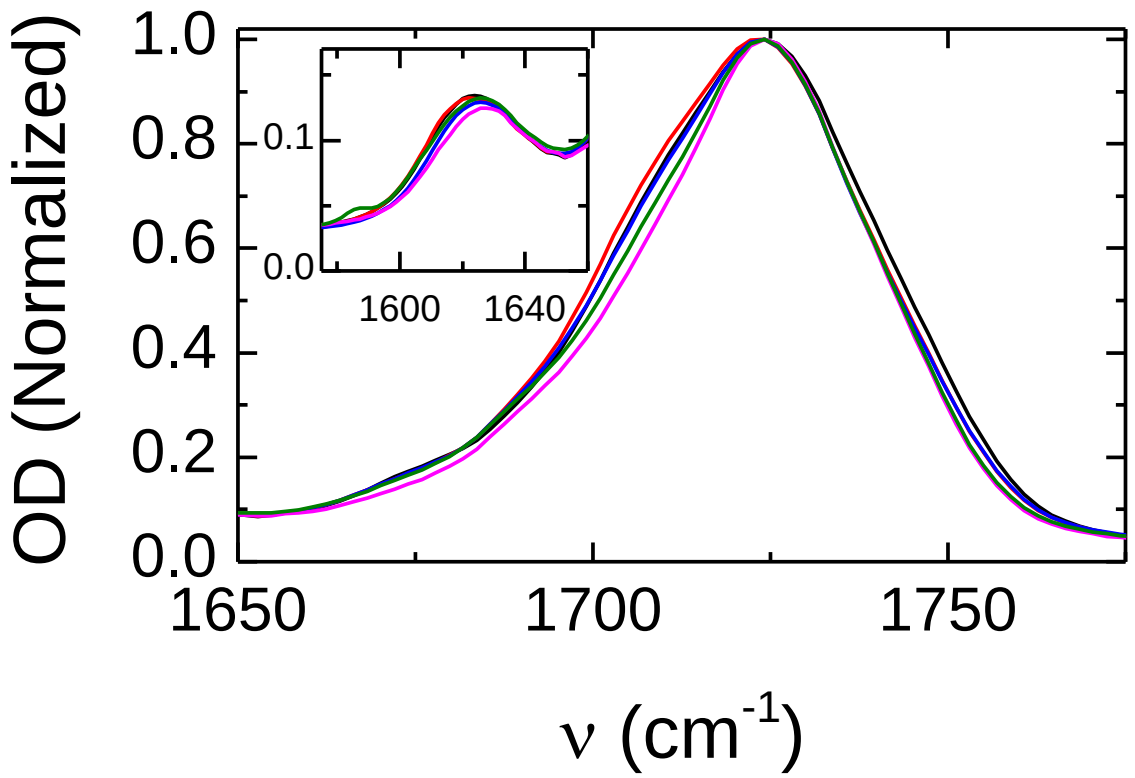

Figure 4.1. FTIR spectra of each TFAm based DES in the amide region. Inset shows the spectra of the $\delta(NH_2)$ scissoring mode.

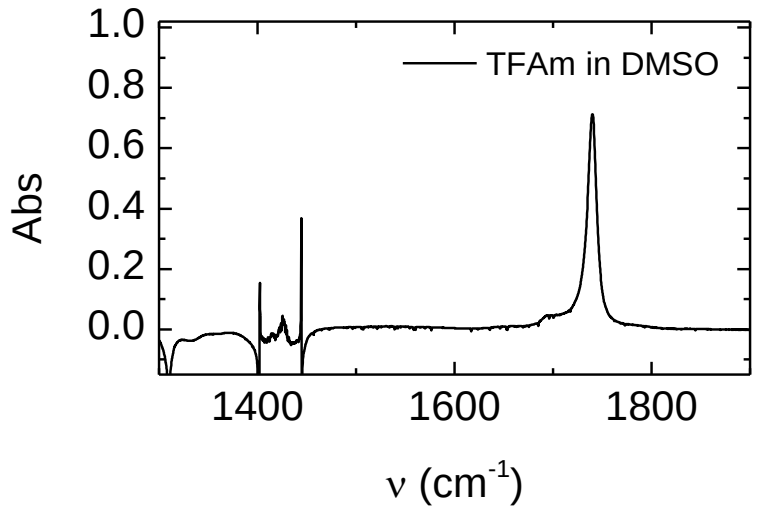

Figure 4.2. FTIR spectrum after background subtraction of 0.1 M TFA in DMSO. The sample was measured in a CaF_2 cell with a 25 μm path length.

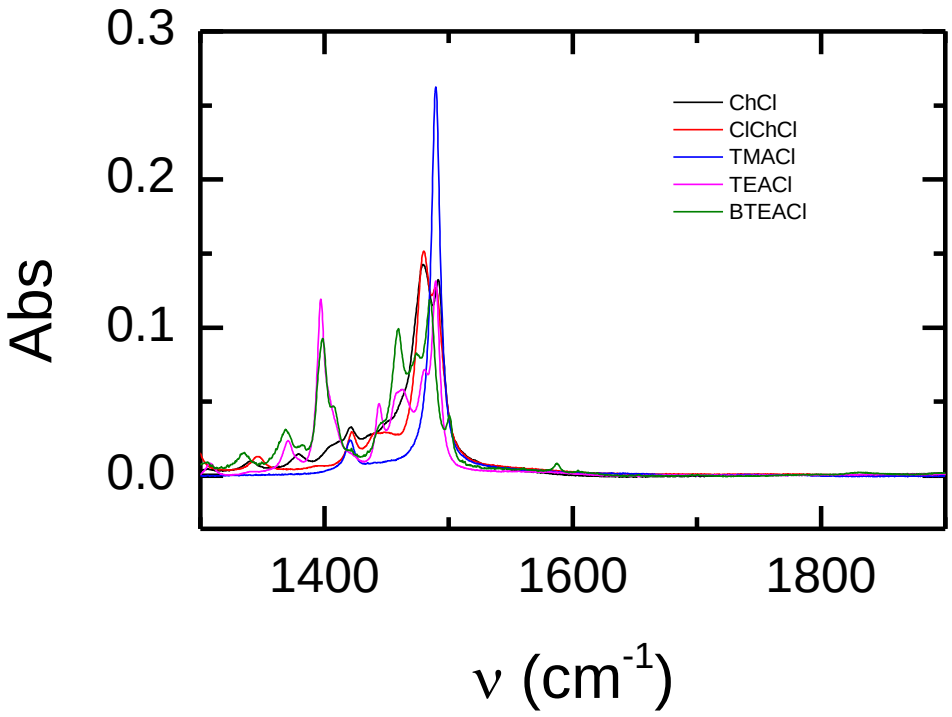

Figure 4.3. FTIR spectra after background subtraction (D_2O) of choline chloride (ChCl), chlorocholine chloride (ClChCl), tetramethylammonium chloride (TMACl), tetraethylammonium chloride (TEACl), and benzyltriethylammonium chloride (BTEACl) in D_2O. All samples have a concentration of 0.05 M. The samples were measured in a CaF_2 cell with a 25 μm path length.

4.3.2. Two dimensional IR spectra

The structure and dynamics of the TFAm-based DESs were further studied by 2DIR spectroscopy. Because of the excitonic nature of the amide band of TFAm (Figures 4.4 and 4.5), the main band was not used to investigate the dynamics and structure of the TFAm-based DES. In turn, our studies had focused on the ^{13}C amide band from the natural abundance of carbon-13 isotope in TFAm, which is ~1%.[57] The amide mode of the isotopically labeled TFAm has a transition frequency redshifted by ~50 cm^{-1} from ^{12}C amide vibrational mode. To our knowledge

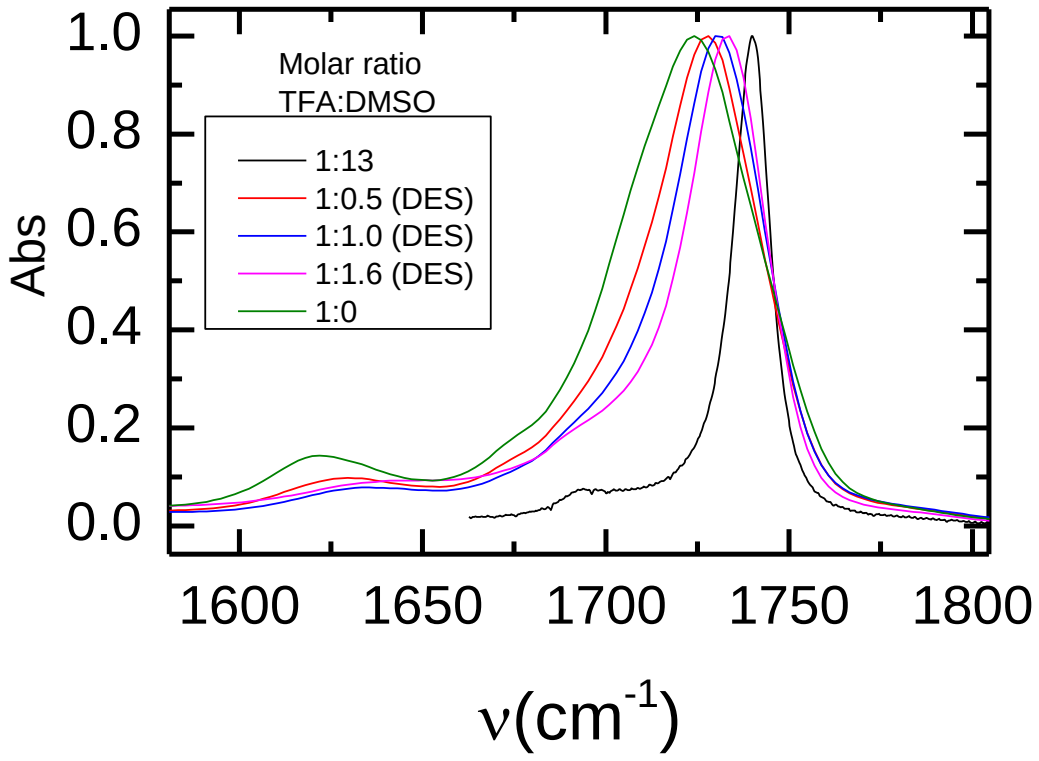

Figure 4.4. ATR-FTIR spectra of DES and DES in DMSO at different molar ratio as shown in the label. All the DES have a molar ratio of 2.5:1 between TFA and ChCl.

the vibrational frequency of the ^{13}C amide of TFAm has not been reported yet, but the observed value is in good agreement with the experimentally measured 40 cm^{-1} down shift of the amide I mode for different secondary amides, as reported in the literature.[58-60] Moreover, density functional theory (DFT) calculations predict a redshift of ~60 cm-1 for the vibrational transition of the ^{13}C-labeled molecule. Note that the observed differences between theory and experiments in the frequency shift of isolated transitions could arise from the formation of a vibrational exciton which defines the central frequency of the amide band. Finally, analysis of the volume of the peaks assigned here to ^{12}C and ^{13}C amide modes of TFAm predict an isotope ratio of 0.5-1.1%, which is in good agreement with the ~1% abundance of ^{13}C. The frequency shift due to the 13C amide is

sufficient to disrupt the strong coupling between the 13C and 12C amide band and allow us to monitor environment of the TFAm from a local mode, that is, vibrational uncoupled transition.[60]

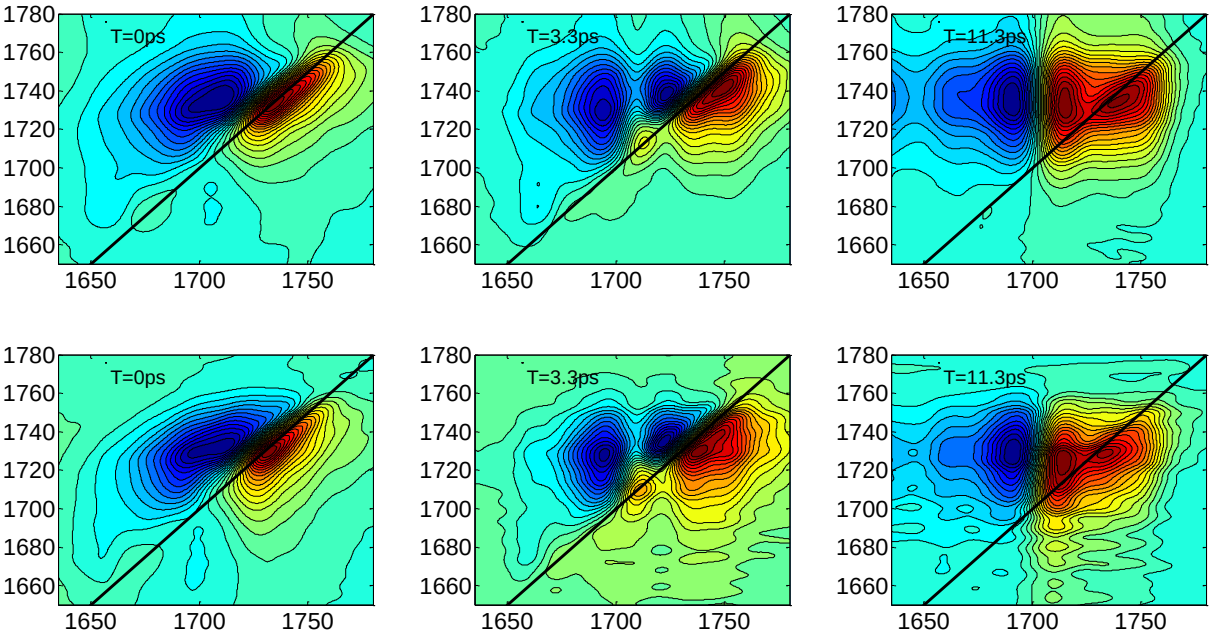

Figure 4.5. 2DIR spectra of DES1 (top) and DES2 (bottom) at the carbonyl region of TFA at T = 0 ps, 3.3 ps, and 11.3ps.

The 2DIR spectra of different DESs in the ^{13}C-amide region are shown in Figure 4.6. The 2DIR spectrum displays the absorptive third-order signal as a function of the pump (ω_τ) and probe (ω_t) frequencies for different waiting times (T_w). In each 2DIR spectrum a pair of peaks is observed. In each peak pair, the positive (red) peak overlaps with a diagonal line (black line, $\omega\tau = \omega_t$) and arises from the $\nu = 1$ to $\nu = 0$ amide vibrational transitions, while the negative (blue) peak is shifted to a lower frequency from the positive peak and corresponds to $\nu = 1$ to $\nu = 2$ amide vibrational transitions. The frequency difference of ~25 cm^{-1} between the maxima of the positive and the negative peaks observed in the 2DIR spectra exposes the anharmonic nature of the amide vibrational potential. The anharmonicity of ~13 cm^{-1}, obtained by fitting the trace passing through

the maximum on ω_τ (Figure 4.7 and table 4.2), is in agreement with previously studied amides.[61,62]

The waiting time (T_w) evolution of the 2DIR spectra shows that at T_w = 0 ps the positive and

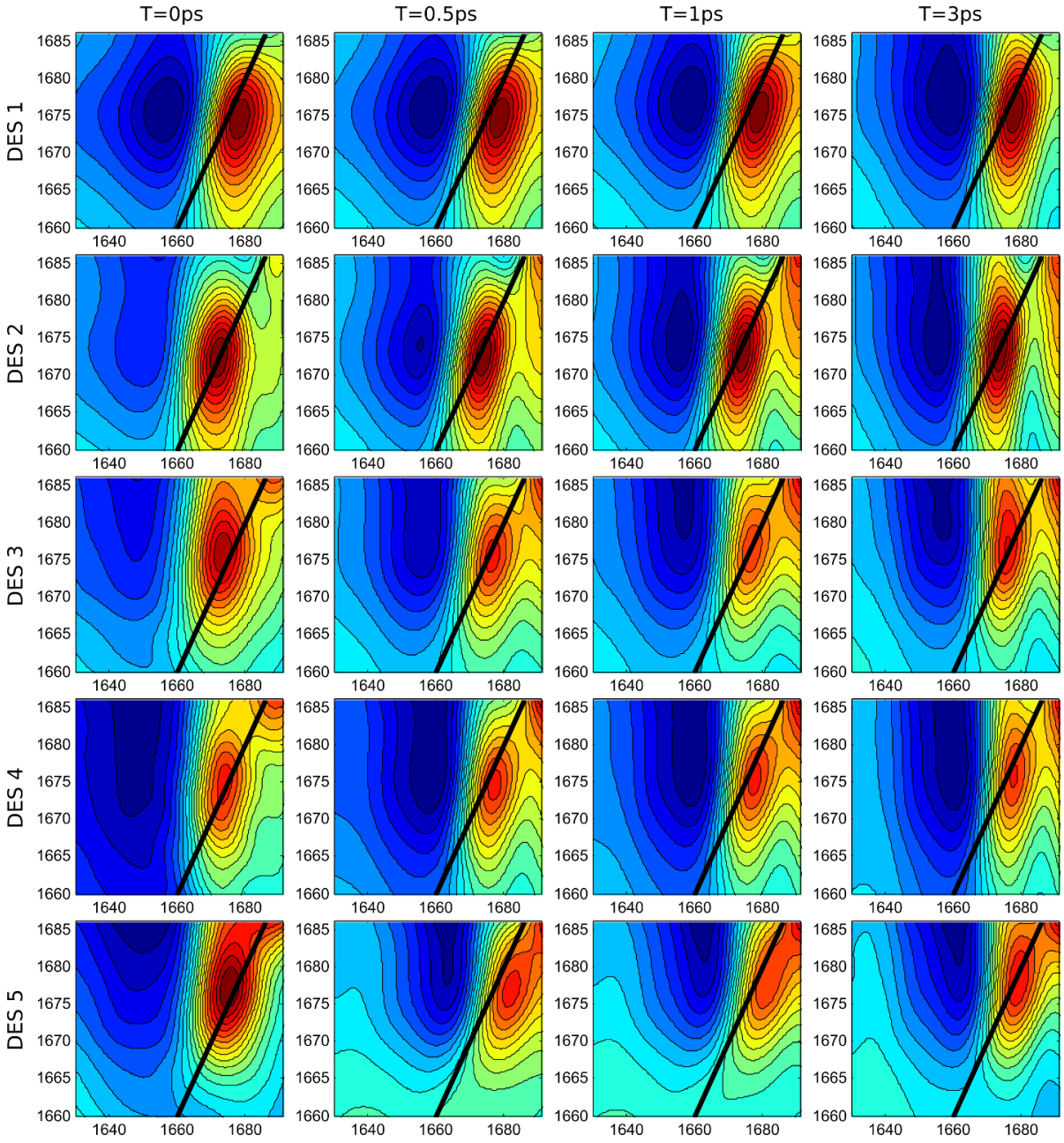

Figure 4.6. 2DIR spectra of DES at the ^{13}C=O vibrational frequency region. From top to bottom, DES1 to DES5. From left to right, the spectra at 0 ps, 0.5 ps, 1 ps, and 3 ps as waiting time.

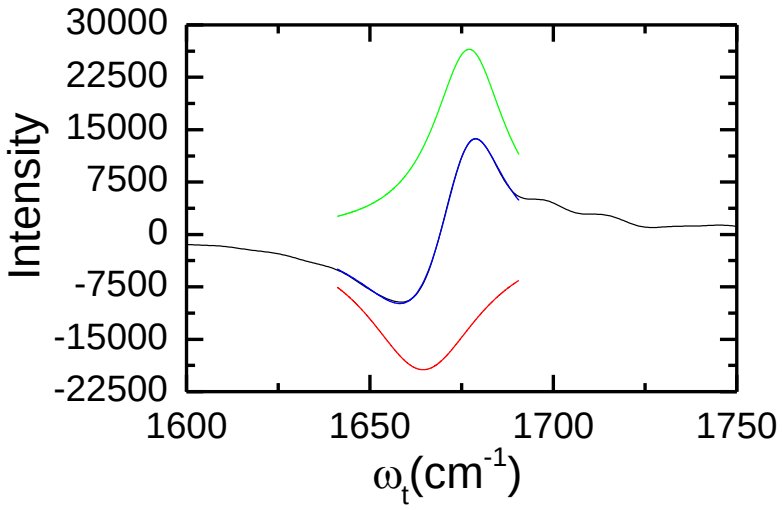

Figure 4.7. Trace of the 2DIR spectra (Figure 4.2 of main text) for DES1 at T= 0 ps. Black line is the experimental trace, and red, blue and green line are the modeling.

negative peaks are tilted along the diagonal, and as the waiting time increases, the peak pair loses its elongation along the diagonal and acquires a more upright shape. The evolution of the 2DIR peak shapes with T_w evidences the changes in the environment (spectral diffusion) sensed by the TFAm molecule.

Table 4.2. The trace passing through the maximum of the 2DIR for DES1 at T = 0 ps was fitted with two Lorentzian functions.

	Peak	
	Bleach/Stimulated emission (green line)	Photo-induced absorption (red line)
N (cm^{-1})	1677.0	1664.5
A (arb. units)	$0.99x10^6$	$1.14x10^6$
Γ (cm^{-1})	23.7	37.4
FWHM (cm^{-1})	23.7	37.4

4.4. Discussion

In the FTIR spectra of TFAm-based DESs, the amide band of TFAm does not serve as a direct reporter of the molecular environment due to its strong vibrational coupling among states) in nature[63] and sensitive to both environment and coupling (dipole orientation).[64,65] Thus, the entanglement between the location and orientation of the various TFAm molecules forming the exciton does not allow one to directly probe the motions of the molecular environment. However, any perturbation in the arrangement (coupling) of the vibrational oscillators (TFAm molecules) should produce a significant change in the exciton transition frequencies and transition dipoles due to the strong dependence of the magnitude and sign of the coupling constant with the geometrical arrangement of oscillators.[63] Thus, a difference in the molecular arrangement of TFAm molecules should be directly observed in the FTIR.

The FTIR spectra of amide band of TFAm show that the profiles are very similar irrespective of the HBA structure, indicating that the molecular arrangement of TFAm molecules in the investigated DES is not significantly altered by the different HBAs, even though the DES have different HBAs with various chemical moieties and symmetries. For example, the HBA cation of DES1 (choline ion) has a hydroxyl group capable of forming hydrogen bonds at a molar ratio of 1:2.5 with TFAm. While these results seems to be contradictory, it will be shown later that they are in agreement with a highly heterogeneous structure of the DES in which the majority of the TFAm are forming nanoscopic-sized clusters (or equivalent nanoheterogeneous structures) similar to those observed in ionic liquids. The interaction between the HBA and TFAm occurs mostly at the interface between the different nanodomains. Although the presence of heterogeneities in DES is not a new concept, since it has been proposed in previous studies,[34,36,66] here their presence is experimentally measured.

The strong coupling observed in the FTIR makes it hard to analyze the amide vibrational transition in terms of local modes. In addition, the naturally occurring ^{13}C amide band of TFAm is not observed directly in the linear IR spectra because of its low concentration and its overlap with the tail of the excitonic ^{12}C amide band as well as the NH_2 bending mode, as seen in Figure 4.1. Thus, the diagonal trace of the positive peak at zero waiting time for the ^{13}C amide mode is used to describe the distribution of uncoupled vibrational transitions in the amide band. Similar to the FTIR, the normalized diagonal trace (NDT) of 2DIR spectra at T = 0 ps can be used to model the amide line shape.[67] To this end, the NDT is fitted with one or two Gaussian functions, as shown in Figure 4.8, and the parameters of the fitting are in Table 4.3. Modeling of the NDT reveals that all the DES have very similar line shape parameters including central frequency and width, indicating that the TFAm environment is not significantly altered by the change in the HBA cation structure. In addition, the small shift observed in the central frequency could account for the small difference in the dielectric constant of the medium sense by the amide molecules. This result is in agreement with the similarity of the excitonic (^{12}C) amide band observed for the different DESs in the ATR-FTIR spectra and reinforces the idea that not all the TFAm-based DESs form homogeneous solutions at the molecular level.

The dynamics of the molecular motions of the environment perceived by the TFAm molecules was extracted from 2DIR spectra by analyzing the waiting time dependence of the ^{13}C amide peaks (Figure 4.6) with the inverse nodal line slope (referred to as slope through the rest of the manuscript). The slope is a metric directly related to the frequency-frequency correlation function (FFCF),[68] and so its waiting time evolution exposes the characteristic time of the molecular motions. The slope as a function of Tw for the different samples is shown in Figure 4.9.

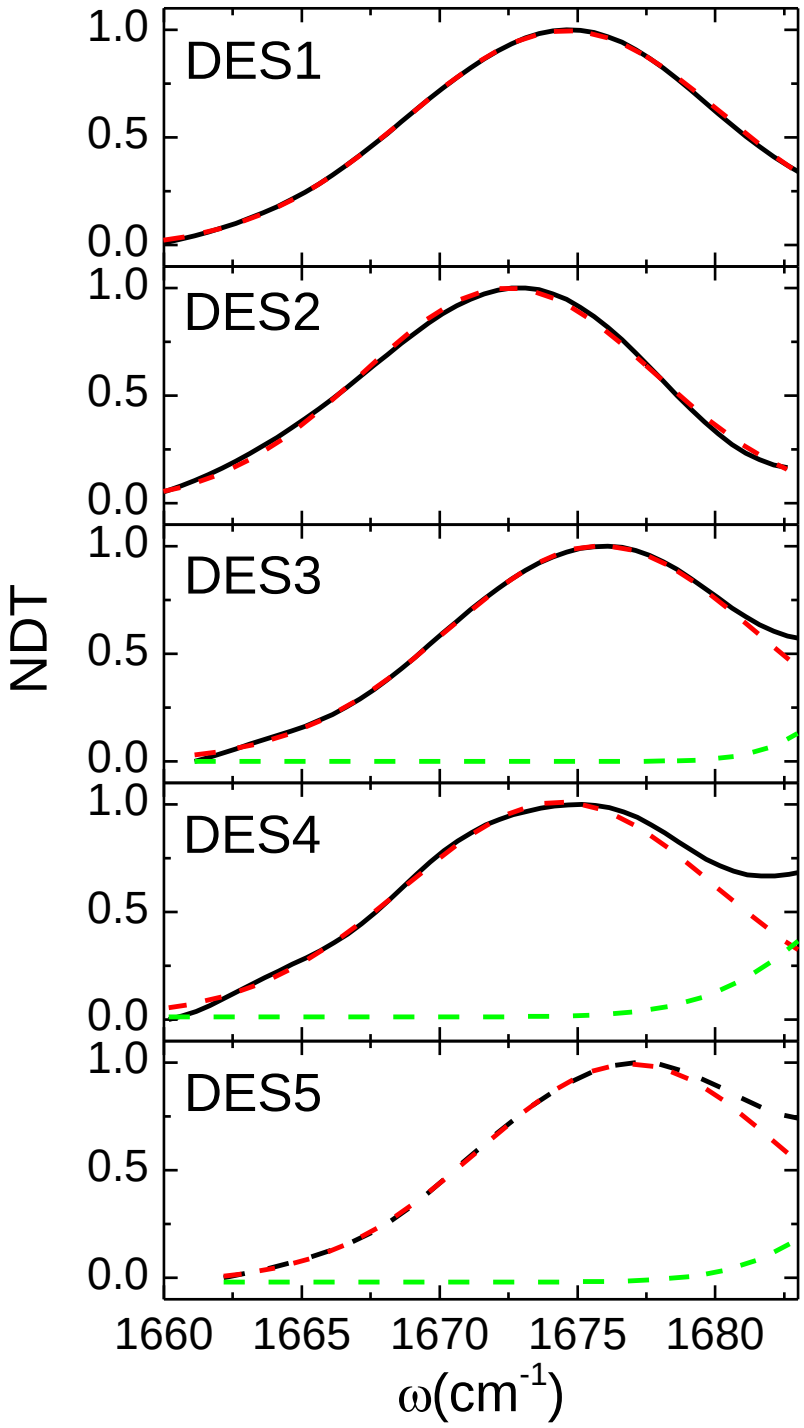

Figure 4.8. NDT of 2DIR of ^{13}C amide band at T_w = 0 ps for each DES. (black line) The experimental NDT. (dashed lines) The fitting with one or two Gaussian functions that correspond to the NDT (red) and tail of the ^{12}C amide band (green).

Table 4.3. Fitting parameters for the Gaussian modeling of normalized diagonal trace and the exponential modeling of slope with waiting time of $^{13}C=O$ band in their 2DIR spectra in the different DESs.

DES	NDT		Slope		
	$\nu\ (cm^{-1})$	$\sigma\ (cm^{-1})$	y_0	A	$\tau\ /\ ps$
1	1674.6 ± 0.1	5.8 ± 0.1	0.24 ± 0.01	0.21 ± 0.02	1.2 ± 0.2
2	1672.5 ± 0.1	5.3 ± 0.1	0.14 ± 0.01	0.26 ± 0.02	1.5 ± 0.3
3	1675.8 ± 0.1	5.3 ± 0.1	0.08 ± 0.01	0.29 ± 0.04	1.0 ± 0.2
4	1674.3 ± 0.2	5.6 ± 0.2	0.10 ± 0.01	0.24 ± 0.02	1.3 ± 0.2
5	1677.0 ± 0.1	5.5 ± 0.1	0.10 ± 0.02	0.34 ± 0.03	1.6 ± 0.4

It is evident that the loss of frequency correlation in all the samples occurs on a very fast time scale. To quantify the slope dynamics, the data was modeled with an exponential decay function of the form $f(t) = y_0 + A \exp(-T_w/\tau)$. The fitting parameters for the slope of each DES are listed in table 2. Interestingly, the ^{13}C amide peaks from TFAm have statistically the same correlation decay times ($\tau \approx 1$ ps) and amplitudes in different DESs, albeit the DES5, which has a slightly higher amplitude (A).

A characteristic time on the order of ~1-2 ps has been assigned to the thermal making and breaking of hydrogen bonds for water[69-72] and methanol.[73-75] Thus, it is not surprising that amides undergoing making and breaking of hydrogen bonds show a similar characteristic time as previously seen in N-methylacetamide.[76] In contrast, the offset (y_0) representing a slower component of the FFCF is not similar for all the DESs. Notably, the offset appears to be correlated to the asymmetry of the HBA cation, since the choline ion has the largest value, while the

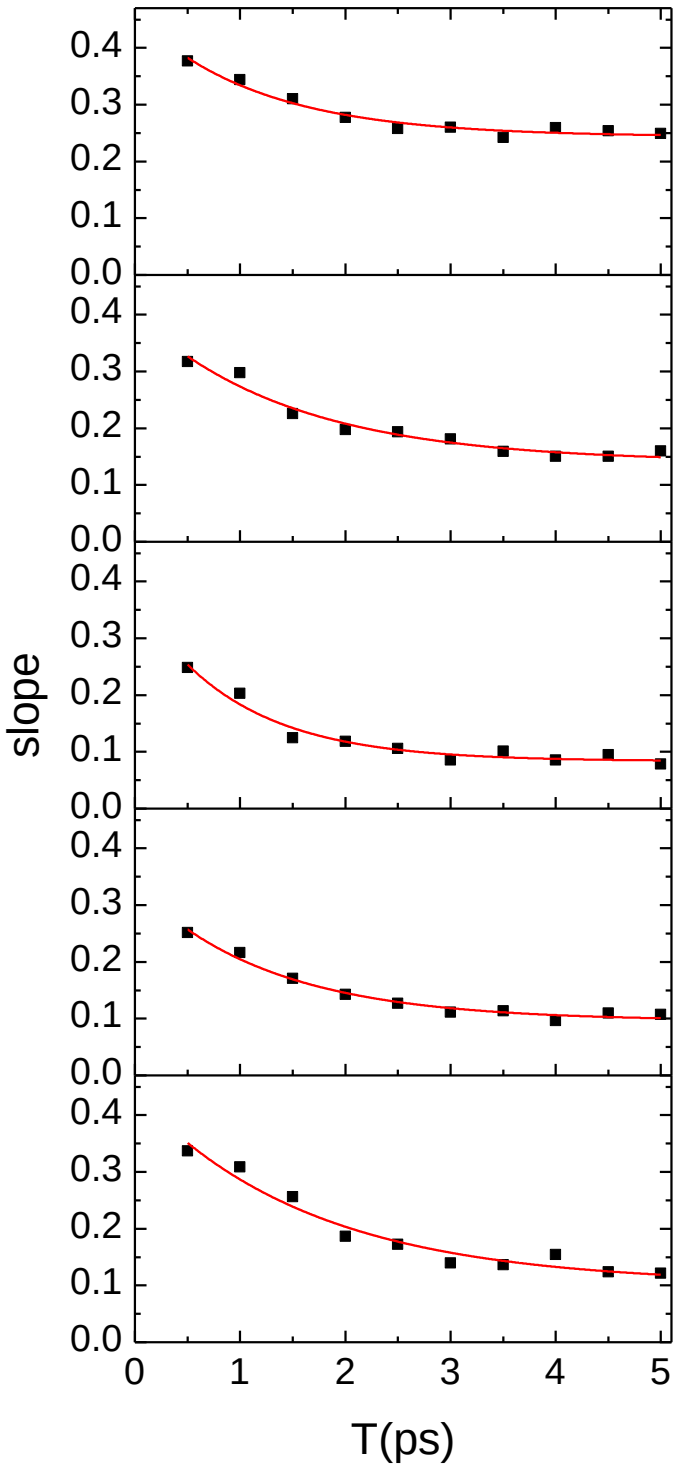

Figure 4.9. FFCFs of the DESs with different HBAs extracted from the 2DIR spectra of 13C amide obtained from the nodal line slope method. (■) Slope data. (red line) Slope data fitting with an exponential function as described in the text. Note that the slope at Tw = 0 ps was not taken into consideration due to the presence of nonresonance signals. Panels correspond to (a) DES 1, (b) DES 2, (c) DES 3, (d) DES 4, and (e) DES 5, respectively.

tetramethylammonium ion has the smallest offset. In addition, no correlation is observed with the viscosity of the solution (Table 4.4). The results indicate that the amide carbonyl group in the DESs with different HBAs have the same fast component of the solvation dynamics irrespective of the structure of the HBA cation, but the presence of a slower component is significantly altered by the cation structure. In addition, the lack of correlation with the viscosity indicates that the inhomogeneous term is not a slow dynamics component of the FFCF related to diffusional motions of amide solvation shell constituents.[25]

Table 4.4. Viscosity of selected DES measured as 298 K

	Viscosity (cp)
DES 1	128.1
DES 2	225.0
DES 4	202.9

This phenomenon further supports our interpretation of the FTIR and NDT where TFAm is located in heterogeneous domains where only those TFAm molecules located at the interface of the HBD domain are affected, since the asymmetric structure of the HBA cation favors their formation. In contrast, TFAm molecules in more homogeneous environments will see a smaller contribution of the slow dynamical component, because the probability of finding a TFAm molecule next to aggregates is smaller. The observed effect is similar to that seen in reverse micelles, where the number water at the interface is responsible for the observed slowdown in the dynamics of solvent.[77] In this molecular model, one will expect that highly

symmetric HBA cations will have the lowest interaction with themselves and the highest with the amide molecules, while highly asymmetric and functionalized HBA cations are more likely to interact with the same species through its functional groups and simultaneously will disorganize the solvent through its asymmetric structure.

The proposed heterogeneous model was supported by investigating the structure of DES1 (HBA choline chloride) and DES3 (HBA tetramethylammonium chloride) via molecular dynamics (MD) simulations. Only DES1 and DES3 were selected to be studied via MD, because experimentally they show the highest and lowest contribution of the slow dynamical component (y_0 of table 3) among all the investigated DESs. The local structure surrounding the HBA and HBD in the different DESs was obtained from the radial distribution function (RDF). RDFs of atoms of the components in the DES1 and DES3 are shown in Figure 4.10. The RDF between the oxygen and hydrogen atoms of TFAm reveals that TFAm is very likely to be hydrogen bonded to another TFAm as seen by the peak located at 1.95 Å (Figure 4.10a). Note that the two sharp peaks at 2.35 and 3.05 Å correspond to the two hydrogens of the same molecule hydrogen bonded to the oxygen atom. Moreover, the RDF between oxygens of TFAm also shows that the structure of the cation does not affect significantly the local structure of the amide (Figure 4.10b). Furthermore, the number of TFAm molecules in the first solvation shell derived from the RDF of the TFAm oxygen atoms shows that the number does not change in two DESs (1.41 for DES1 and 1.42 for DES3). The result is in agreement with the excitonic and invariant nature of the amide band of TFAm observed in the ATR-FTIR spectra of the different samples.

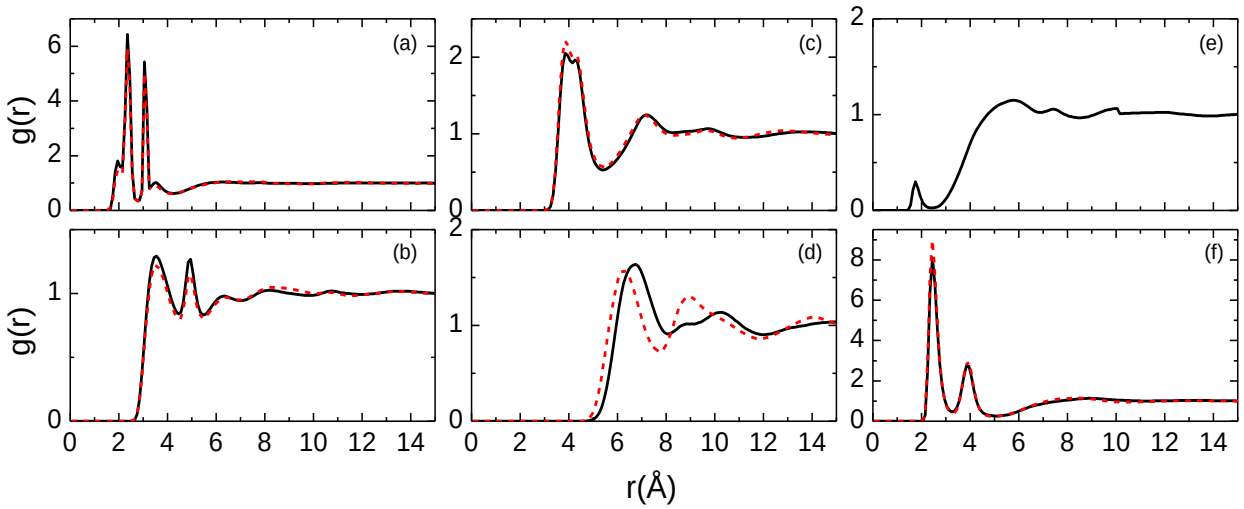

Figure 4.10. RDFs for various atoms for (a) O-H (both from TFAm), (b) O-O (both from TFAm), (c) O-N (oxygen from TFAm and N from quaternary ammonium group), (d) N-N (both from quaternary ammonium group), (e) O-O (one from TFAm and the other from choline ion), and (f) Cl-H (hydrogen from TFAm). Black and red lines correspond to DES1 and DES3, respectively.

The RDF between oxygen atoms of TFAm and choline ion (DES1) shows a tiny peak at 1.75 Å (Figure 4.10e) indicating that choline ion can form hydrogen bonds with TFAm, but their probability is low. As expected, the RDF of chloride ion with the hydrogen atom bonded to nitrogen (TFAm) or oxygen (choline ion) as seen in Figure 4.10f shows that chloride ions have hydrogen bond interactions with both HBD and HBA in DES1 but only with HBD in DES3. The result for DES1 is in agreement with a recent neutron scattering study, where it was demonstrated that the -OH···Cl- interaction is largely conserved in DES.[24] The predicted nanoscopic heterogeneity is observed in the RDF of the nitrogen atom of quaternary ammonium group (Figure 4.10d). In this case, the RDFs are significantly different between DES1 and DES3. For example, the first solvation shell (defined as the first minimum) is observed at 8.05 Å for DES1 and 7.75 Å for DES3. In addition, the coordination number is 3.64 and 3.13 for DES1 and DES3, respectively,

which indicates that the probability of finding a second HBA cation next to one another is higher for DES1 than for DES3.

This last result is in agreement with the higher degree of spatial nanoheterogeneity predicted from the IR experiments. Finally, the RDF between the oxygen atom of TFAm and the nitrogen atom of the quaternary ammonium group of either choline (DES1) or tetramethylammonium (DES3) as shown in Figure 4.10c agrees with a more heterogeneous environment for DES1, since the number of TFAm molecules in the solvation shell of the quaternary ammonium group is smaller for DES1 (1.24) than for DES3 (1.41). In other words, the results indicate that more TFAm molecules solvate the HBA cation in the latter than in the former, or equivalently, that HBA cations are more aggregated in DES1 than in DES3.

The proposed structural nanoscopic heterogeneity is strongly supported by DSC. DES1 is reported to have a melting point of -43 °C,[78] but its endotherm shows an endothermic peak at 23 °C (see Figure 4.11). The observed endotherm is not related to any observable phase transition,

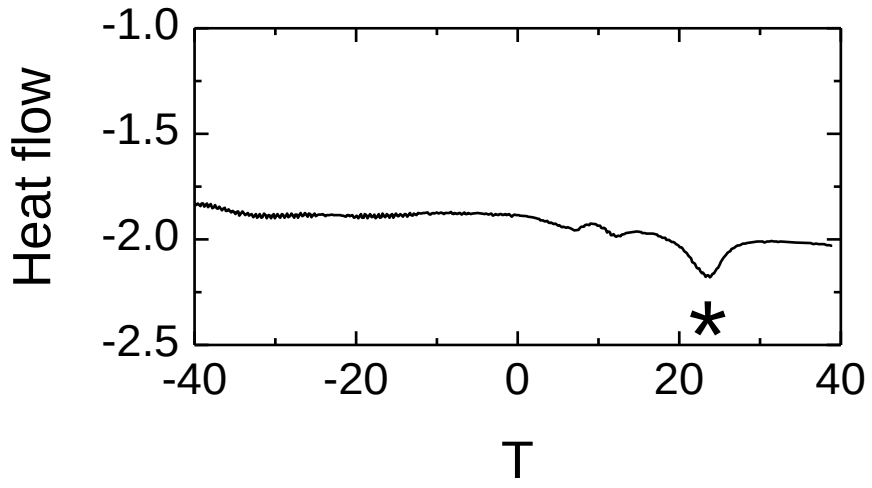

Figure 4.11. DSC thermogram of DES1. (★) The endotherm due to the nanometer-scale heterogeneities as described in the text.

since DES1 forms a clear liquid in the temperature range from -20 to 40 °C. The presence of an endothermic peak is not new, since it was previously observed in ionic liquids with nanometer scale heterogeneities.[79,80] Thus, the small endothermic peak observed in the DSC thermogram of DES1 further supports the existence of a nanoheterogeneous environment in DES1 as deduced from the time-resolved IR experiments.

4.5. Summary

The effect of the HBA cation chemical nature on the overall solution structure in a family of TFAm-based DESs is reported. Our results show that TFAm observes a fast dynamical component of ∼1 ps corresponding to the hydrogen bond making and breaking in all the investigated DESs, which is irrespective of the structure of the HBA cations. However, DESs with more symmetric HBA cations have lower contributions of a second slow molecular motion of the environment than those with asymmetric cations, which is caused by the interphase between HBA and HBD domains. In addition, a DES formed with an asymmetric HBA cation containing a hydroxyl group presents a similar contribution of the slow dynamical component compared with those where the hydroxyl group is replaced with a chloride atom. Finally, all the DES show very similar level of disorganization. The experimental results are interpreted in terms of a molecular model in which the HBA cation and the HBA are not homogeneously distributed in space. Furthermore, it was found that the level of heterogeneity in the molecular environment increases with the asymmetry in the geometry and the interactions of the HBA cations. The proposed heterogeneous molecular structure of the DESs is supported by molecular dynamics simulations. In addition, the presence of a nanoscopic heterogeneous environment is consistent with an endotherm observed in the DSC thermogram, which further supports the proposed DES structure.

4.6. References

1. Frederick, G., On Eutexia. *Proceedings of the Physical Society* **1884**, *6*, 124.

2. Abbott, A. P.; Barron, J. C.; Ryder, K. S.; Wilson, D., Eutectic-Based Ionic Liquids with Metal-Containing Anions and Cations. *Chem. Eur. J.* **2007**, *13*, 6495-6501.

3. Abbott, A. P.; Capper, G.; Davies, D. L.; Munro, H. L.; Rasheed, R. K.; Tambyrajah, V., Preparation of Novel, Moisture-Stable, Lewis-Acidic Ionic Liquids Containing Quaternary Ammonium Salts with Functional Side Chains. *Chem. Commun.* **2001**, 2010-2011.

4. Smith, E. L.; Abbott, A. P.; Ryder, K. S., Deep Eutectic Solvents (Dess) and Their Applications. *Chemical reviews* **2014**, *114*, 11060-11082.

5. Abbott, A. P.; Capper, G.; Davies, D. L.; Rasheed, R. K.; Tambyrajah, V., Novel Solvent Properties of Choline Chloride/Urea Mixtures. *Chemical Communications* **2003**, 70-71.

6. Zhang, Q.; Vigier, K. D. O.; Royer, S.; Jérôme, F., Deep Eutectic Solvents: Syntheses, Properties and Applications. *Chemical Society Reviews* **2012**, *41*, 7108-7146.

7. Tang, B.; Row, K. H., Recent Developments in Deep Eutectic Solvents in Chemical Sciences. *Monatsh. Chem.* **2013**, *144*, 1427-1454.

8. Welton, T., Room-Temperature Ionic Liquids. Solvents for Synthesis and Catalysis. *Chemical reviews* **1999**, *99*, 2071-2084.

9. Francisco, M.; van den Bruinhorst, A.; Kroon, M. C., Low-Transition-Temperature Mixtures (Lttms): A New Generation of Designer Solvents. *Angew. Chem. Int. Ed.* **2013**, *52*, 3074-3085.

10. Garcia, G.; Aparicio, S.; Ullah, R.; Atilhan, M., Deep Eutectic Solvents: Physicochemical Properties and Gas Separation Applications. *Energy Fuels* **2015**, *29*, 2616-2644.

11. Yang, H.; Guo, X.; Birbilis, N.; Wu, G.; Ding, W., Tailoring Nickel Coatings Via Electrodeposition from a Eutectic-Based Ionic Liquid Doped with Nicotinic Acid. *Applied Surface Science* **2011**, *257*, 9094-9102.

12. Gómez, E.; Cojocaru, P.; Magagnin, L.; Valles, E., Electrodeposition of Co, Sm and Smco from a Deep Eutectic Solvent. *Journal of electroanalytical chemistry* **2011**, *658*, 18-24.

13. Abbott, A. P.; Capper, G.; Davies, D. L.; McKenzie, K. J.; Obi, S. U., Solubility of Metal Oxides in Deep Eutectic Solvents Based on Choline Chloride. *J. Chem. Eng. Data* **2006**, *51*, 1280-1282.

14. Singh, B.; Lobo, H.; Shankarling, G., Selective N-Alkylation of Aromatic Primary Amines Catalyzed by Bio-Catalyst or Deep Eutectic Solvent. *Catal. Lett.* **2011**, *141*, 178-182.

15. Azizi, N.; Batebi, E., Highly Efficient Deep Eutectic Solvent Catalyzed Ring Opening of Epoxides. *Catal. Sci. Technol.* **2012**, *2*, 2445-2448.

16. Leron, R. B.; Li, M.-H., Solubility of Carbon Dioxide in a Choline Chloride–Ethylene Glycol Based Deep Eutectic Solvent. *Thermochim. Acta* **2013**, *551*, 14-19.

17. Shahbaz, K.; Mjalli, F.; Hashim, M.; AlNashef, I., Using Deep Eutectic Solvents Based on Methyl Triphenyl Phosphunium Bromide for the Removal of Glycerol from Palm-Oil-Based Biodiesel. *Energy Fuels* **2011**, *25*, 2671-2678.

18. Cui, Y.; Li, M.-C.; Wu, Q.; Pojman, J. A.; Kuroda, D. G., Synthesis-Free Phase-Selective Gelator for Oil-Spill Remediation. *ACS Applied Materials and Interfaces* **2017**, *9*, 33549-33553.

19. Mota-Morales, J. D.; Gutierrez, M. C.; Ferrer, M. L.; Sanchez, I. C.; Elizalde-Pena, E. A.; Pojman, J. A.; Del Monte, F.; Luna-Barcenas, G., Deep Eutectic Solvents as Both Active Fillers and Monomers for Frontal Polymerization. *J. Polym. Sci., Part A: Polym. Chem.* **2013**, *51*, 1767-1773.

20. Perkins, S. L.; Painter, P.; Colina, C. M., Experimental and Computational Studies of Choline Chloride-Based Deep Eutectic Solvents. *J. Chem. Eng. Data* **2014**, *59*, 3652-3662.

21. Perkins, S. L.; Painter, P.; Colina, C. M., Molecular Dynamic Simulations and Vibrational Analysis of an Ionic Liquid Analogue. *J. Phys. Chem. B* **2013**, *117*, 10250-10260.

22. Hammond, O. S.; Bowron, D. T.; Edler, K. J., Liquid Structure of the Choline Chloride-Urea Deep Eutectic Solvent (Reline) from Neutron Diffraction and Atomistic Modelling. *Green Chemistry* **2016**, *18*, 2736-2744.

23. Stefanovic, R.; Ludwig, M.; Webber, G. B.; Atkin, R.; Page, A. J., Nanostructure, Hydrogen Bonding and Rheology in Choline Chloride Deep Eutectic Solvents as a Function of the Hydrogen Bond Donor. *PCCP* **2017**, *19*, 3297-3306.

24. Araujo, C. F.; Coutinho, J. A. P.; Nolasco, M. M.; Parker, S. F.; Ribeiro-Claro, P. J. A.; Rudic, S.; Soares, B. I. G.; Vaz, P. D., Inelastic Neutron Scattering Study of Reline: Shedding Light on the Hydrogen Bonding Network of Deep Eutectic Solvents. *PCCP* **2017**, *19*, 17998-18009.

25. Cui, Y.; Fulfer, K. D.; Ma, J.; Weldeghiorghis, T. K.; Kuroda, D. G., Solvation Dynamics of an Ionic Probe in Choline Chloride-Based Deep Eutectic Solvents. *PCCP* **2016**, *18*, 31471-31479.

26. Zahn, S.; Kirchner, B.; Mollenhauer, D., Charge Spreading in Deep Eutectic Solvents. *ChemPhysChem* **2016**, *17*, 3354-3358.

27. Berchiesi, G.; Farhat, F.; de Angelis, M.; Barocci, S., High Dielectric Constant Supercooled Liquids, Tools in Energetic Problems. *J. Mol. Liq.* **1992**, *54*, 103-113.

28. Berchiesi, G.; Vitali, G.; Plowiec, R.; Barocci, S., Viscoelastic and Ultrasonic Relaxation in Molten Mixture of Acetamide and Calcium Nitrate. *J. Chem. Soc., Faraday Trans.* **1989**, *85*, 635-641.

29. Berchiesi, G.; De Angelis, M.; Rafaiani, G.; Vitali, G., Electrolyte-Acetamide Molten Mixtures. *J. Mol. Liq.* **1992**, *51*, 11-38.

30. Guchhait, B.; Al Rasid Gazi, H.; Kashyap, H. K.; Biswas, R., Fluorescence Spectroscopic Studies of (Acetamide+ Sodium/Potassium Thiocyanates) Molten Mixtures: Composition and Temperature Dependence. *J. Phys. Chem. B* **2010**, *114*, 5066-5081.

31. Guchhait, B.; Das, S.; Daschakraborty, S.; Biswas, R., Interaction and Dynamics of (Alkylamide+ Electrolyte) Deep Eutectics: Dependence on Alkyl Chain-Length, Temperature, and Anion Identity. *J. Chem. Phys.* **2014**, *140*, 104514.

32. Mukherjee, K.; Das, A.; Choudhury, S.; Barman, A.; Biswas, R., Dielectric Relaxations of (Acetamide+ Electrolyte) Deep Eutectic Solvents in the Frequency Window, $0.2 \leq N/Ghz \leq 50$: Anion and Cation Dependence. *J. Phys. Chem. B* **2015**, *119*, 8063-8071.

33. Tripathy, S. N.; Wojnarowska, Z.; Knapik, J.; Shirota, H.; Biswas, R.; Paluch, M., Glass Transition Dynamics and Conductivity Scaling in Ionic Deep Eutectic Solvents: The Case of (Acetamide+ Lithium Nitrate/Sodium Thiocyanate) Melts. *J. Chem. Phys.* **2015**, *142*, 184504.

34. Das, A.; Das, S.; Biswas, R., Fast Fluctuations in Deep Eutectic Melts: Multi-Probe Fluorescence Measurements and All-Atom Molecular Dynamics Simulation Study. *Chem. Phys. Lett.* **2013**, *581*, 47-51.

35. Das, S.; Biswas, R.; Mukherjee, B., Orientational Jumps in (Acetamide+ Electrolyte) Deep Eutectics: Anion Dependence. *J. Phys. Chem. B* **2015**, *119*, 11157-11168.

36. Kaur, S.; Gupta, A.; Kashyap, H. K., Nanoscale Spatial Heterogeneity in Deep Eutectic Solvents. *J. Phys. Chem. B* **2016**, *120*, 6712-6720.

37. Shahbaz, K.; Mjalli, F. S.; Hashim, M.; Al-Nashef, I. M., Using Deep Eutectic Solvents for the Removal of Glycerol from Palm Oil-Based Biodiesel. *J. Applied Sci.* **2010**, *10*, 3349-3354.

38. Ganim, Z.; Chung, H. S.; Smith, A. W.; DeFlores, L. P.; Jones, K. C.; Tokmakoff, A., Amide I Two-Dimensional Infrared Spectroscopy of Proteins. *Acc. Chem. Res.* **2008**, *41*, 432-441.

39. Wang, L.; Middleton, C. T.; Zanni, M. T.; Skinner, J. L., Development and Validation of Transferable Amide I Vibrational Frequency Maps for Peptides. *J. Phys. Chem. B* **2011**, *115*, 3713-3724.

40. DeFlores, L. P.; Ganim, Z.; Nicodemus, R. A.; Tokmakoff, A., Amide I′− Ii′ 2d Ir Spectroscopy Provides Enhanced Protein Secondary Structural Sensitivity. *J. Am. Chem. Soc.* **2009**, *131*, 3385-3391.

41. Smith, A. W.; Tokmakoff, A., Probing Local Structural Events in B-Hairpin Unfolding with Transient Nonlinear Infrared Spectroscopy. *Angew. Chem. Int. Ed.* **2007**, *46*, 7984-7987.

42. DeCamp, M.; DeFlores, L.; McCracken, J.; Tokmakoff, A.; Kwac, K.; Cho, M., Amide I Vibrational Dynamics of N-Methylacetamide in Polar Solvents: The Role of Electrostatic Interactions. *J. Phys. Chem. B* **2005**, *109*, 11016-11026.

43. DeCamp, M. F.; DeFlores, L.; McCracken, J. M.; Tokmakoff, A.; Kwac, K.; Cho, M., Amide I Vibrational Dynamics of N-Methylacetamide in Polar Solvents: The Role of Electrostatic Interactions. *J. Phys. Chem. B* **2005**, *109*, 11016-11026.

44. Hamm, P.; Zanni, M., *Concepts and Methods of 2d Infrared Spectroscopy*; Cambridge University Press, 2011.

45. Fayer, M. D., Dynamics of Liquids, Molecules, and Proteins Measured with Ultrafast 2d Ir Vibrational Echo Chemical Exchange Spectroscopy. *Annu. Rev. Phys. Chem.* **2009**, *60*, 21-38.

46. Zheng, J.; Kwak, K.; Fayer, M. D., Ultrafast 2d Ir Vibrational Echo Spectroscopy. *Acc. Chem. Res.* **2007**, *40*, 75-83.

47. Singh, P. K.; Kuroda, D. G.; Hochstrasser, R. M., An Ion's Perspective on the Molecular Motions of Nanoconfined Water: A Two-Dimensional Infrared Spectroscopy Study. *J. Phys. Chem. B* **2013**, *117*, 9775-9784.

48. Kuroda, D. G.; Hochstrasser, R. M., Dynamic Structures of Aqueous Oxalate and the Effects of Counterions Seen by 2d Ir. *PCCP* **2012**, *14*, 6219-6224.

49. Sokolowsky, K. P.; Payer, M. D., Dynamics in the Isotropic Phase of Nematogens Using 2d Ir Vibrational Echo Measurements on Natural-Abundance (Cn)-C-13 and Extended Lifetime Probes. *J. Phys. Chem. B* **2013**, *117*, 15060-15071.

50. Kim, Y. S.; Hochstrasser, R. M., Applications of 2d Ir Spectroscopy to Peptides, Proteins, and Hydrogen-Bond Dynamics. *J. Phys. Chem. B* **2009**, *113*, 8231.

51. Kim, Y. S.; Wang, J. P.; Hochstrasser, R. M., Two-Dimensional Infrared Spectroscopy of the Alanine Dipeptide in Aqueous Solution. *J. Phys. Chem. B* **2005**, *109*, 7511-7521.

52. Fulfer, K. D. A.; Kuroda, D. G., A Comparison of the Solvation Structure and Dynamics of the Lithium Ion in Linear Organic Carbonates with Different Alkyl Chain Lengths. *PCCP* **2017**.

53. Case, D.; Darden, T.; Cheatham III, T.; Simmerling, C.; Wang, J.; Duke, R.; Luo, R.; Walker, R.; Zhang, W.; Merz, K., Amber 12; University of California: San Francisco, 2012. 1-826.

54. Mainberger, S.; Kindlein, M.; Bezold, F.; Elts, E.; Minceva, M.; Briesen, H., Deep Eutectic Solvent Formation: A Structural View Using Molecular Dynamics Simulations with Classical Force Fields. *Mol. Phys.* **2017**, *115*, 1309-1321.

55. Martinez, L.; Andrade, R.; Birgin, E. G.; Martinez, J. M., Packmol: A Package for Building Initial Configurations for Molecular Dynamics Simulations. *J. Comput. Chem.* **2009**, *30*, 2157-2164.

56. Troitiño, D.; de la Blanca, E. S.; Garcia, M. V., Vibrational Spectra of Mono-, Di- and Trichloroacetamide and Mono- and Trifluoroacetamide. *Spectrochim. Acta, Part A* **1990**, *46*, 1281-1290.

57. Esler, M.; Griffith, D.; Wilson, S.; Steele, L., Precision Trace Gas Analysis by Ft-Ir Spectroscopy. 2. The 13c/12c Isotope Ratio of Co2. *Anal. Chem.* **2000**, *72*, 216-221.

58. Wang, J.; Zhuang, W.; Mukamel, S.; Hochstrasser, R., Two-Dimensional Infrared Spectroscopy as a Probe of the Solvent Electrostatic Field for a Twelve Residue Peptide. *J. Phys. Chem. B* **2008**, *112*, 5930-5937.

59. Maekawa, H.; Ballano, G.; Formaggio, F.; Toniolo, C.; Ge, N.-H., 13c□ 18o/15n Isotope Dependence of the Amide-I/Ii 2d Ir Cross Peaks for the Fully Extended Peptides. *Journal of Physical Chemistry C* **2014**, *118*, 29448-29457.

60. Zanni, M. T.; Hochstrasser, R. M., Two-Dimensional Infrared Spectroscopy: A Promising New Method for the Time Resolution of Structures. *Curr. Opin. Struct. Biol.* **2001**, *11*, 516-522.

61. Hamm, P.; Lim, M. H.; Hochstrasser, R. M., Structure of the Amide I Band of Peptides Measured by Femtosecond Nonlinear-Infrared Spectroscopy. *J. Phys. Chem. B* **1998**, *102*, 6123-6138.

62. DeFlores, L. P.; Ganim, Z.; Ackley, S. F.; Chung, H. S.; Tokmakoff, A., The Anharmonic Vibrational Potential and Relaxation Pathways of the Amide I and Ii Modes of N-Methylacetamide. *J. Phys. Chem. B* **2006**, *110*, 18973-18980.

63. Lesar, R.; Kopelman, R., Vibrational Excitons, Resonant Energy-Transfer, and Local Structure in Liquid Benzene. *J. Chem. Phys.* **1977**, *66*, 5035-5041.

64. Woutersen, S.; Hamm, P., Isotope-Edited Two-Dimensional Vibrational Spectroscopy of Trialanine in Aqueous Solution. *J. Chem. Phys.* **2001**, *114*, 2727-2737.

65. Kuroda, D. G.; Hochstrasser, R. M., Two-Dimensional Infrared Spectral Signature and Hydration of the Oxalate Dianion. *J. Chem. Phys.* **2011**, *135*, 204502.

66. Berchiesi, G.; Deangelis, M.; Rafaiani, G.; Vitali, G., Electrolyte-Acetamide Molten Mixtures. *J. Mol. Liq.* **1992**, *51*, 11-38.

67. Remorino, A.; Korendovych, I. V.; Wu, Y.; DeGrado, W. F.; Hochstrasser, R. M., Residue-Specific Vibrational Echoes Yield 3d Structures of a Transmembrane Helix Dimer. *Science* **2011**, *332*, 1206-1209.

68. Kwac, K.; Cho, M. H., Molecular Dynamics Simulation Study of N-Methylacetamide in Water. Ii. Two-Dimensional Infrared Pump-Probe Spectra. *J. Chem. Phys.* **2003**, *119*, 2256-2263.

69. Fecko, C. J.; Eaves, J. D.; Loparo, J. J.; Tokmakoff, A.; Geissler, P. L., Ultrafast Hydrogen-Bond Dynamics in the Infrared Spectroscopy of Water. *Science* **2003**, *301*, 1698-1702.

70. Woutersen, S.; Pfister, R.; Hamm, P.; Mu, Y. G.; Kosov, D. S.; Stock, G., Peptide Conformational Heterogeneity Revealed from Nonlinear Vibrational Spectroscopy and Molecular-Dynamics Simulations. *J. Chem. Phys.* **2002**, *117*, 6833-6840.

71. Ghosh, A.; Hochstrasser, R. M., A Peptide's Perspective of Water Dynamics. *Chem. Phys.* **2011**, *390*, 1-13.

72. Chung, J. K.; Thielges, M. C.; Fayer, M. D., Dynamics of the Folded and Unfolded Villin Headpiece (Hp35) Measured with Ultrafast 2d Ir Vibrational Echo Spectroscopy. *Proceedings of the National Academy of Sciences of the United States of America* **2011**, *108*, 3578-3583.

73. Woutersen, S.; Mu, Y.; Stock, G.; Hamm, P., Hydrogen-Bond Lifetime Measured by Time-Resolved 2d-Ir Spectroscopy: N-Methylacetamide in Methanol. *Chem. Phys.* **2001**, *266*, 137-147.

74. Ghosh, A.; Remorino, A.; Tucker, M. J.; Hochstrasser, R. M., 2d Ir Photon Echo Spectroscopy Reveals Hydrogen Bond Dynamics of Aromatic Nitriles. *Chem. Phys. Lett.* **2009**, *469*, 325-330.

75. Banno, M.; Ohta, K.; Yamaguchi, S.; Hirai, S.; Tominaga, K., Vibrational Dynamics of Hydrogen-Bonded Complexes in Solutions Studied with Ultrafast Infrared Pump-Probe Spectroscopy. *Acc. Chem. Res.* **2009**, *42*, 1259-1269.

76. Zanni, M. T.; Asplund, M. C.; Hochstrasser, R. M., Two-Dimensional Heterodyned and Stimulated Infrared Photon Echoes of N-Methylacetamide-D. *J. Chem. Phys.* **2001**, *114*, 4579-4590.

77. Piletic, I. R.; Tan, H. S.; Fayer, M. D., Dynamics of Nanoscopic Water: Vibrational Echo and Infrared Pump-Probe Studies of Reverse Micelles. *J. Phys. Chem. B* **2005**, *109*, 21273-21284.

78. Shahbaz, K.; Mjalli, F.; Hashim, M.; AlNashef, I., Using Deep Eutectic Solvents Based on Methyl Triphenyl Phosphunium Bromide for the Removal of Glycerol from Palm-Oil-Based Biodiesel. *Energy & Fuels* **2011**, *25*, 2671-2678.

79. Triolo, A.; Russina, O.; Bleif, H.-J.; Di Cola, E., Nanoscale Segregation in Room Temperature Ionic Liquids. *J. Phys. Chem. B* **2007**, *111*, 4641-4644.

80. Kabo, G. J.; Blokhin, A. V.; Paulechka, Y. U.; Kabo, A. G.; Shymanovich, M. P.; Magee, J. W., Thermodynamic Properties of 1-Butyl-3-Methylimidazolium Hexafluorophosphate in the Condensed State. *J. Chem. Eng. Data* **2004**, *49*, 453-461.

CHAPTER 5
SOLVENT STRUCTURE OF NON-IONIC DEEP EUTECTIC SOLVENT COMPOSED OF N-METHYLACETAMIDE AND LAURIC ACID

5.1. Introduction

Deep Eutectic Solvents (DES) are liquids composed of two or more solid components. Based on the eutectic phenomenon, the fusion point of the DES is lower than the melting points of the individual components of the mixture.[1] The selection of solids as individual components leads to DES with negligible vapor pressure.[2-3] Moreover, the physical or chemical properties can be tailored by the various components employed based on the different purpose of applications.[4-7] Because of those properties, DES are considered as designer solvents, similar to ionic liquids.[8] However, DES have some advantages compared with ionic liquids. The materials for preparing DES are usually cheap, safe, and easy to produce. In addition, the DES preparation process consists of a simple mixing.[6,8,9] The properties of DES are tailorable not only by varying the components identity, like ionic liquids but also the molar ratio of components.[5,10] Due to these advantages, DESs are widely studied and applied in scientific and engineering fields, such as: organic synthesis,[6,11] electrochemistry,[12,13] metal oxide dissolution,[14] carbon dioxide absorption,[15] separation processes,[16] polymerizations,[17,18] and lately in oil-spill remediation.[19]

The most studied DES have been those composed of quaternary ammonium chloride or metal chloride (hydrate), which are "ionic" DESs.[2] The dynamics, and structure of choline-based DESs are already well studied by either experimental or theoretical.[20-24] Based on the ionic nature of most DES, it is not surprising that most of the resulting DES are hydrophilic. We have reported that N-methylacetamide and lauric acid, a fatty acid, can form a hydrophobic DES at room temperature, which is the first of its kind.[5,19] Hydrophobic DESs have been reported by Maaike C. Kroon as immiscible water extractants.[25] They produced DESs with fatty acid and various

quaternary ammonium salts having three or four carbon alkyl chains. The authors reported that those DESs have low solubility of water in the DES and low leaching of quaternary ammonium salt into water. The above results indicate the strong interaction between chloride ion and HBDs, which is similar to other choline chloride-based DES. While in the system of NMA-LA, the components separate when mixed with water, which is probably due to the relatively weak interaction between NMA and LA molecules. However, the investigation of the interaction in non-ionic DES between components is to be addressed yet. Moreover, Biswas and coworkers studied the non-ionic DES of acetamide-urea and showed that the system has both structural and dynamical homogeneity.[26] Since the structures of acetamide and urea are similar, in the DES, the two components can evenly mix and form a homogeneous solvent. However, in the NMA-LA system, the two molecules are different in size, water solubility, and polarity. Thus, the system is expected to have a different structure from reported acetamide/urea. Moreover, the fusion point of the systems of NMA-LA at the molar ratios from 2:1 to 6:1 are below room temperature,[19] which provides a big window to study the interaction between components with different molar fractions.

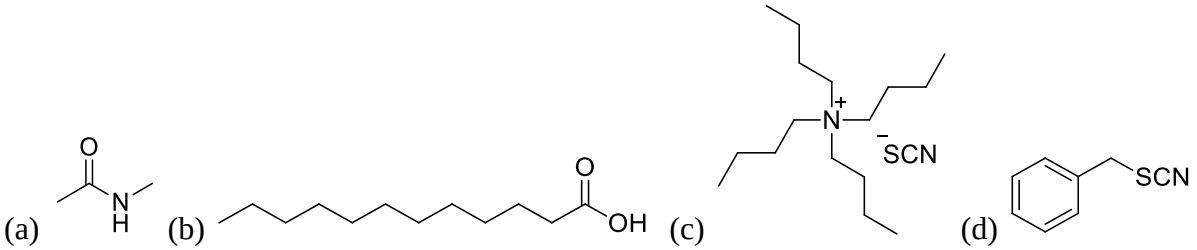

Scheme 5.1. Structure of (a) N-methylacetamide (NMA), (b) lauric acid (LA), (c)tetrabutylammonium thiocyanate (TBA SCN), (d) benzyl thiocyanate (BSCN)

Table 5.1. Compositions and abbreviation of the Deep Eutectic Solvents

Component 1	Component 2	Molar ratio of NMA: LA	Abbreviation
N-methylacetamide	Lauric acid	2:1	DES2
		4:1	DES4
		6:1	DES6

In this work, we focused on investigating the structure and interaction between components in the DES and the molar ratio's effect on the structure. We studied the DES composed of NMA and LA with molar ratio 2:1, 4:1, and 6:1. The carbonyl stretch of NMA and LA are used as a probe to report the interaction because the carbonyl stretch is already well studied and proven sensitive to the environment change.[27-29] The frequency difference of the non-hydrogen bonded carbonyl stretching mode of NMA and LA is ~50 cm^{-1}.[30-35] The separated bands ensured we analyzed each component individually. Moreover, we used both polar and non-polar probed to study structure or dynamics to extract the effect from the molar ratio of components. To this end, Fourier Transform Infrared (FTIR) and two-dimensional Infrared spectroscopy (2DIR) are used to study the vibration of each probe to decode the structure and dynamics in a solution environment. The photon echo signal from 2DIR delivers the information, including chemical exchange and spectral diffusion, which are important to describe the molecular interaction and motions in sub- or picosecond timescale.[36,37]

5.2. Experimental methodologies

5.2.1. Sample preparation

Lauric acid (Alfa Aesar, 99.5%), N-methylacetamide (Alfa Aesar, 99%) used for preparing DES were used as received. The two components were mixed at varied ratios. The DESs were prepared by mixing the two components in a vial, then operating the vial with vortex mixer and sonicator until a clear liquid formed. Heating was not applied during the DES preparation process. Infrared probe tetrabutylammonium thiocyanate (TCI, 95%), and benzyl thiocyanate (TCI, 99%) were used without further purification and added to the DESs. All the DESs and solutions were stored and prepared in a nitrogen flushed glove box.

5.2.2. Linear IR spectroscopy

Linear IR measurements were performed using a Bruker Tensor 27 with a liquid nitrogen cooled narrow band MCT detector. All of the samples were measured with 0.5 cm^{-1} resolution, and all the spectra were averaged from 40 scans at room temperature, using an O-ring sealed sample cell composed of CaF_2 windows and different thickness Teflon spacers, depending on the requirement of absorbance. All the sample cells were prepared in a nitrogen-filled glovebox to minimize exposure to moisture.

5.2.3. Two-dimensional IR spectroscopy

The 2DIR spectroscopy measurements were performed in the similar setup which described in the literature previously.[32] In short, the broadband infrared pulse was generated from a Spectra Physics Spitfire Ace Ti: Sapphire amplifier with 5 kHz repetition rate and an optical parametric amplifier (Spectra Physics OPA-800C). The photon echo of different samples was

generated by three replica IR pulses, with wave vectors of $\boldsymbol{k}_1$, $\boldsymbol{k}_2$, and $\boldsymbol{k}_3$ respectively, through the sample cell in a boxcar configuration.[36] The photon echo at the phase matching direction of $-\boldsymbol{k}_1 + \boldsymbol{k}_2 + \boldsymbol{k}_3$ or $\boldsymbol{k}_1 - \boldsymbol{k}_2 + \boldsymbol{k}_3$ depending on rephasing or non-rephasing signal, was overlapped with a fourth pulse, the local oscillator, as heterodyne detection. The interference of photon echo and local oscillator was detected by a liquid nitrogen cooled MCT 64 elements array detector with a monochromator. The time intervals between pulses τ (between first and second pulses), T_w (between second and third pulses), and t (between third and the photon echo) were controlled by translation stages. For the experimental measurements, the τ was scanned from -4 ps to 4 ps with a step 5 fs for each waiting time, and the local oscillator always preceded the signal by ~0.5 ps. To analyze the data, the signal in the time domain ($S(\tau, T_w, t)$), was transformed to the signal in the frequency domain by double Fourier Transforming with the two coherence times (τ and t) at different waiting times (T).[38] For the 2DIR measurement of pure DES, no spacer was used. The spacer used for DESs with probes in 2DIR measurements were the same as FTIR mentioned previously. A lens sample cell was used to reduce the absorbance when acquiring the 2DIR signal of amide I band in DES, using the same procedure our group reported previously.[39]

5.3. Result

5.3.1. Linear IR spectra

The normalized FTIR spectra of NMA-LA DES with varied molar ratios appear as two groups of peaks corresponding to the vibrational transitions of NMA (in the frequency range 1600 cm^{-1} - 1700 cm^{-1}) and lauric acid (in the frequency range 1700 cm^{-1} - 1775 cm^{-1}) according to the assignment done previously.[19] The band centered at 1566 cm-1 indicates the amide II band of NMA.[40] In figure 5.1, the amide band in the NMA has an asymmetric profile with shoulder bands

on both sides of the peak and is centered at 1656 cm^{-1}. With increasing concentration of NMA (DES2 to DES6), the ratio of area red-side band (at ~1630 cm^{-1}) to the center band increases. In contrast, it appears that the blue-side shoulder band of NMA does not show a significant change with the different DESs. The spectra of acid have two bands, which are at ~1710 cm^{-1} and ~1730 cm^{-1}. The ratio of two bands area varies with concentrations of LA. From DES2 to DES6, the total absorbance of acid bands decrease with the decreasing concentration of LA in the DES, and the absorbance of the low-frequency band decreases more than the other acid band.

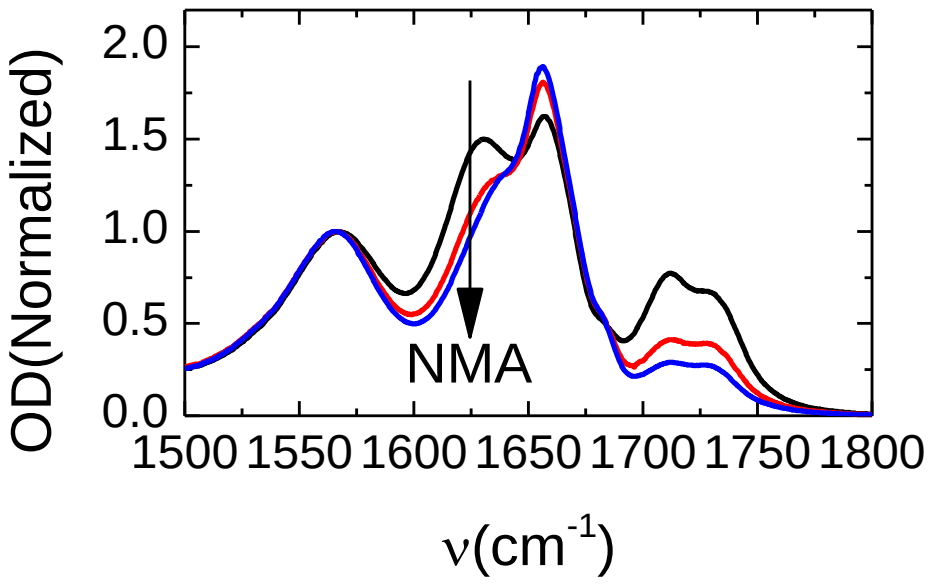

Figure 5.1. (a)Normalized FTIR spectra of acid carbonyl band of NMA-LA with a molar ratio of 2:1 (black line), 4:1 (red line), and 6:1 (blue line).

To study the vibrational modes of the NMA-LA system, the FTIR spectra of DES diluted with THF, as well as NMA dissolved in THF, were measured for comparison. From the normalized spectra in figure 5.2, the NMA bands are asymmetric in THF, and it is clear that there are bands at lower and higher frequencies than the central band. Compared with the central band of the sample in the spectra, the absorbance of the low-frequency band rises with increased concentration of

NMA. The opposite trend occurs for the band at ~1730 cm^{-1}, the absorbance drops with increased concentration. The two-band profiles of the acid carbonyl region also affected by the NMA concentration in THF solution. The high-frequency band increases and low-frequency band decreases as the concentration of NMA is increased. Comparing the spectra of the DES-THF mixture with pure NMA in THF, the acid band is absent, and the amide band of NMA also presents a two-band profile as seen in DES with THF. At a similar ratio of NMA: THF, the absorbance of the low-frequency band at ~1630 cm^{-1} of DES sample is significantly lower than for NMA in THF.

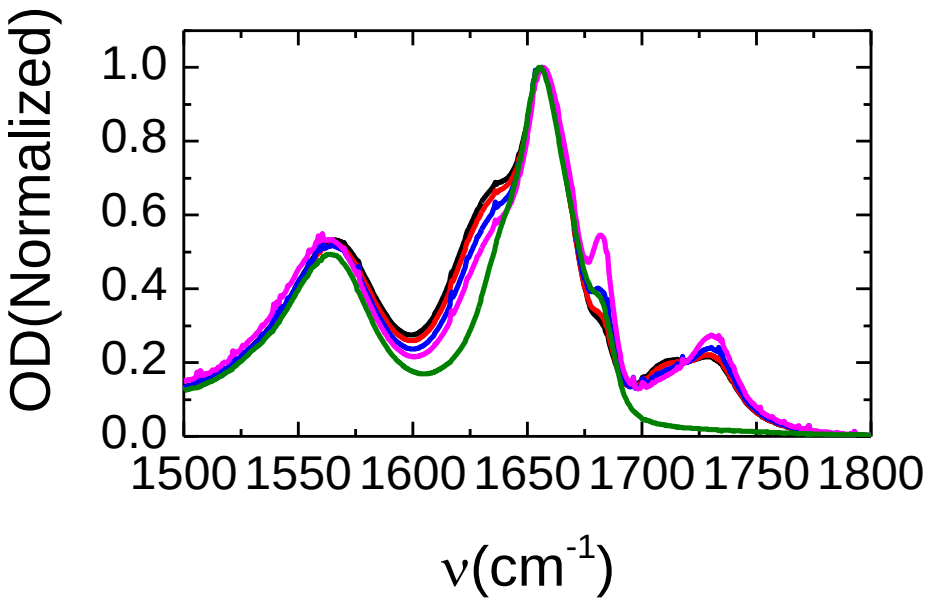

Figure 5.2. The concentration-dependent experiment of NMA-LA in THF as well as NMA in THF. The sample molar ratios of NMA-LA-THF mixture are 4:1:1 (black), 4:1:2 (red), 4:1:4 (blue), 4:1:8 (pink), and NMA in THF at a molar ratio of 4:1 (green).

The temperature dependent FTIR spectra were also measured, in order to investigate the thermodynamics of interactions in the DES with different molar ratios. The FTIR spectra of DESs were measured at the temperatures from 10 °C to 50 °C with 10 °C per step, which is in figure 5.3.

In their spectra, the two bands of amide I band in the spectra of different DES present different trends with temperature change. When the temperature increases, the band centered at ~ 1630 cm^{-1} decreases, and the band at ~1656 cm^{-1} increases. For the two-band profiles of acid vibrational transitions, the spectra present similar changes as the amide band with varied temperature.

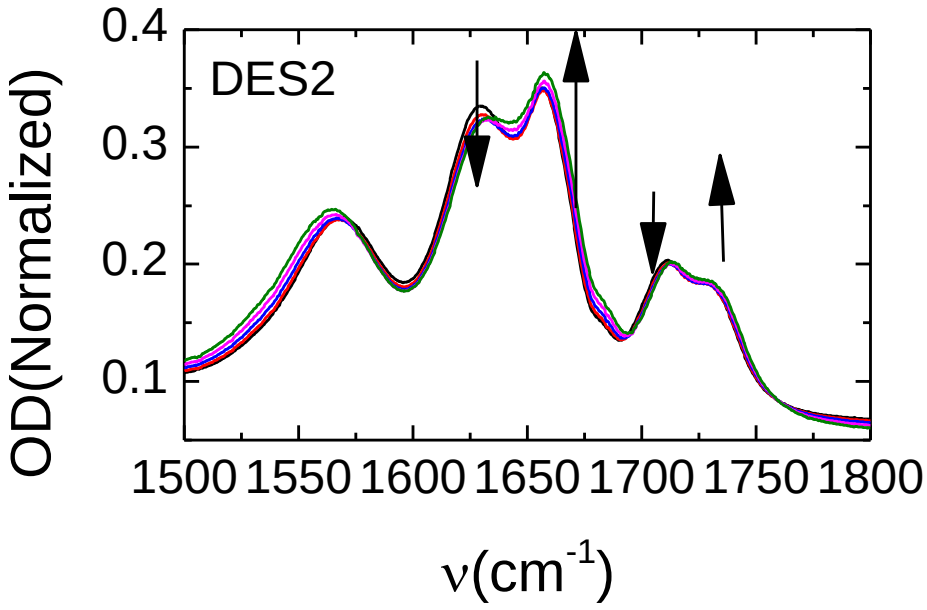

Figure 5.3 FTIR spectra of DES2, DES4, and DES6 with different temperatures at the carbonyl stretching the range of both NMA and lauric acid. The arrow denotes the temperature increasing.

(Figure 5.3. continued)

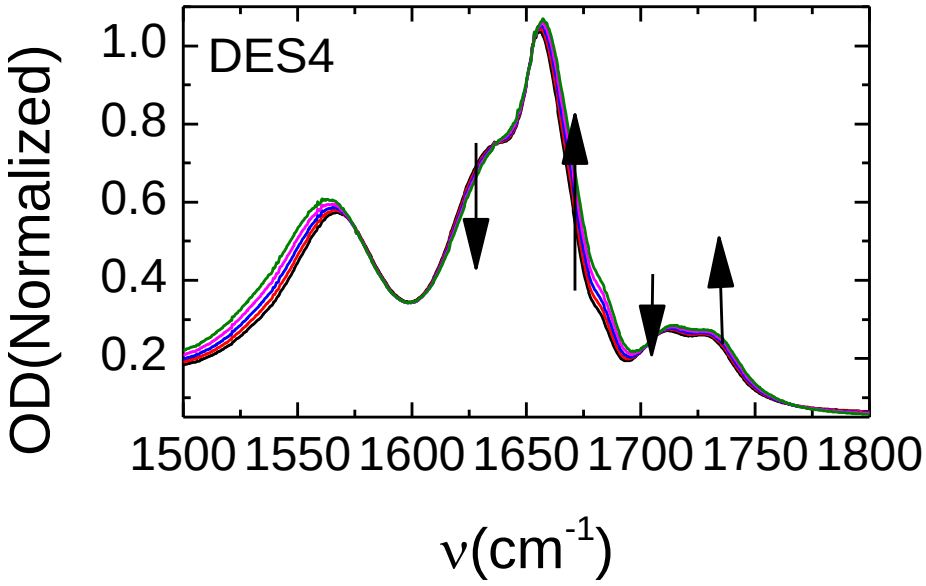
DES4
OD(Normalized)
1.0
0.8
0.6
0.4
0.2
1500 1550 1600 1650 1700 1750 1800
ν(cm-1)

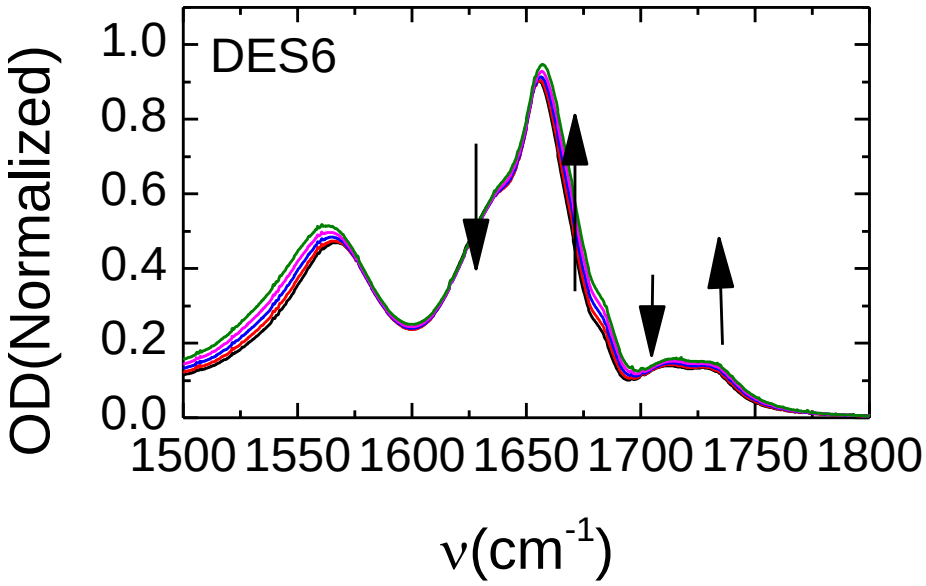
DES6
OD(Normalized)
1.0
0.8
0.6
0.4
0.2
0.0
1500 1550 1600 1650 1700 1750 1800
ν(cm-1)

5.3.2. Two dimensional IR spectra

The 2DIR spectra centered at amide band region of NMA-LA systems with different molar ratios were measured (figure 5.4). The red peaks (positive) at high probe frequency along the diagonal line indicate vibrational transitions from $\nu = 1$ to ground state ($\nu = 0$). The blue peaks (negative) refer to the transitions from $\nu = 1$ to $\nu = 2$. There are six pairs of peaks located along the diagonal line at short waiting time. The two pairs of peaks at ~1710 cm^{-1} and ~1730 cm^{-1} indicate the carbonyl stretching modes of lauric acid, which are also present in their FTIR spectra. The other four pairs of peaks are amide bands of the NMA molecule. The peaks at ~1556 cm^{-1} are amide II bands, and the three peaks at ~1615 cm^{-1}, ~1649 cm^{-1}, and ~1674 cm^{-1} are amide I bands of NMA molecule.[41] At early waiting times, all the diagonal peaks are tilted and elongated along the diagonal line. The cross peak between middle amide I band and the other two peaks of amide I band of NMA are observed at short waiting times. Moreover, the cross peak between middle amide I band and amide II band of NMA molecule are identifiable. There are no cross peaks observed between amide band and acid carbonyl peaks at short waiting times. With increased waiting time, the cross peaks between two positive peaks amide I bands at ~1649 cm^{-1} and ~1674 cm^{-1} overlapped with the negative peaks, making the negative peaks less intense. The other cross peaks present at short times also grow with time at different rates, and the cross peak between the amide II band and amide I band with the lowest frequency become evidenced. It is worth noting that the cross peaks between the acid carbonyl band and amide are present even at the short time and grow with increasing waiting time.

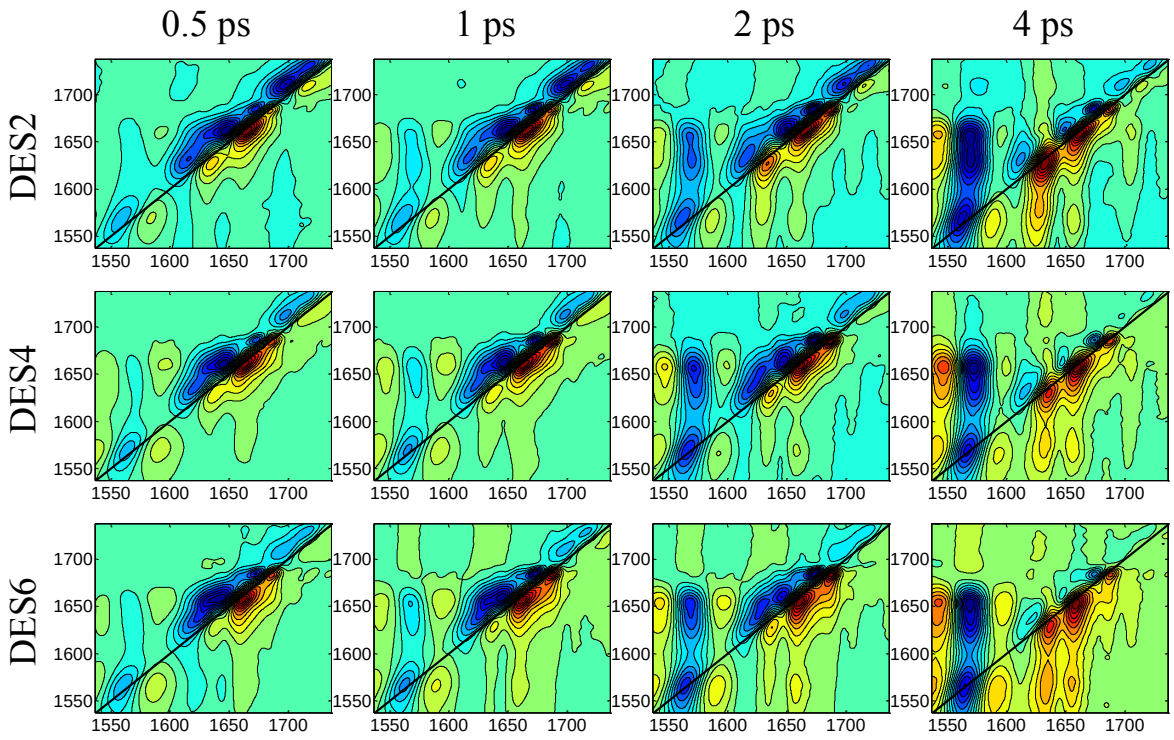

Figure 5.4. 2DIR spectra centered at the frequency of amide band of NMA in DES2, DES4, and DES6 from top to bottom. From left to right, the waiting times are 0.5 ps, 1 ps, 2 ps, and 4 ps.

The structure and dynamics of the DESs of NMA-LA were further studied by 2DIR spectroscopy in the acid bands region (figure 5.5). In each 2DIR spectrum, two pairs of peaks are observed. The anharmonicity of the two bands is both ~16 cm^{-1}, which agrees with the previous study.[30] For all the samples, at T_w = 0 ps, the peaks are tilted and elongated along the diagonal line. While the waiting time evolves, the shapes of peaks have no apparent change within 3 ps. Moreover, in the spectra of DES6, the positive cross peak can be observed, while the cross peaks of other samples are not obvious. For the samples of DES4 and DES6, an extra peak grows at ω_t = ~1710 cm^{-1} at later waiting time, which disappears at T_w = 0 ps.

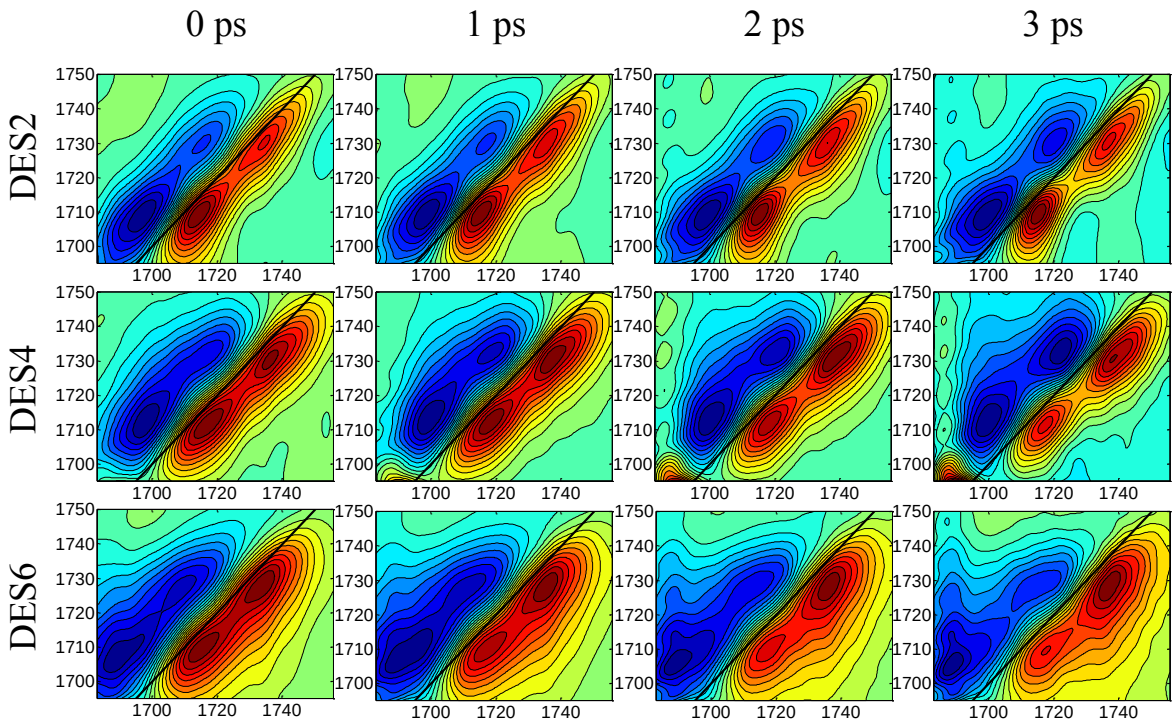

Figure 5.5. 2DIR spectra centered at the frequency of carbonyl band of LA in DES2, DES4, and DES6 from top to bottom. From left to right, the waiting times are 0 ps, 1 ps, 2 ps, and 3 ps.

5.4. Discussion

The amide I band of N-methylacetamide in various solutions has been extensively studied by experimental and theoretical methods.[27,41-45] Depending on the different interactions with solvent molecules around the NMA, the amide I band (carbonyl stretching transition) of NMA molecule was assigned as one hydrogen-bond, two hydrogen-bonds or free of the hydrogen-bond.[33,35,41] Also, the vibrational coupling between these amide I bands is confirmed. Our amide I band of NMA in THF (molar fraction of 0.8 of NMA) is similar to the spectra of neat NMA reported by Cunha et al..[41] According to their assignment, the amide I band with hydrogen bond (main band), and free band (high-frequency shoulder band) configurations are coupled and presented as the profile in figure 5.1. There is a shoulder band at the low frequency of the main

band mentioned by the author. They have assigned the low-frequency shoulder band at ~1630 cm^{-1}as the bending mode of water contained in the sample. In our case, a similar low-frequency shoulder is present in all the samples in figure 5.1. With the concentration of NMA decreasing, the shoulder band decreases. Considering the hydrogen bond acceptor nature of THF, the shoulder band should relate to hydrogen bond forming with amide I band. Tokmakoff's work has shown that the amide I band can form multiple hydrogen bonds through oxygen.[33] It is reasonable to assign the shoulder band as two hydrogen-bonds of amide I band. Therefore, the asymmetric profile of FTIR spectra of DES at the amide 1 band region are assigned as free, one hydrogen-bond (1HB), and two hydrogen bond (2HB) of the NMA carbonyl. Interestingly, in the spectra of NMA-LA DESs with different molar ratios, the two hydrogen-bonded band increases with increasing LA added to the mixtures, indicating that hydroxyl group of LA acts as a hydrogen bond donor, forming a hydrogen bond with NMA. The significant change of the profile in the FTIR spectra of DES at the lowest frequency amide I band from that profile of NMA in THF indicates that the existence of LA influences the hydrogen bond network of NMA, that LA can interact with NMA by forming extra hydrogen bond, such as a second hydrogen bond with oxygen atom of NMA.

The spectra of acetic acid in the solvent was reported by Hochstrasser.[30] By studying acetic acid and deuterated acetic acid in carbon tetrachloride, they assigned the vibration modes of a carbonyl group as a free band, one hydrogen-bond and cyclic dimer of acetic acid. In our NMA-LA systems, the carbonyl stretching modes of LA in each DESs of the FTIR spectra present two-band profile. The frequencies of the two bands are determined as ~1710 cm^{-1} and ~1730 cm^{-1} by Voigt function fitting, respectively. We assign the two-band profile of acid peaks in the NMA-LA as a hydrogen-bonded at low frequency and free band at high frequency. The frequencies red-shift

due to different dielectric constants of the solutions and the frequency difference between two bands agrees with the reported result.[30] This assignment also can explain the acid carbonyl peaks' behavior in the spectra of diluted DES4 with THF in figure 5.1, where dilution leads the free band to grow and hydrogen-bond band to drop. Further evidence to verify the low-frequency band as the free band is the spectra of LA in THF with 0.05 M of concentration shown in figure 5.6. At low concentration of LA in THF, the spectrum presents as a single symmetric peak, indicating a free band of the carbonyl stretching mode. The overlapping of the spectra of DES2 and LA in THF shows good agreement, so the blue-side band is assigned as a free band.

Because the acid bands are overlapped with amide I band, the explicit way to study the acid carbonyl stretching mode is by fitting with Voigt profiles. In this case, the two bands profile of carbonyl in each DES were fitted with three Voigt functions, where the first band accounts for the neighboring amide I band. The ratio of fitted band area of HB band over free band has a linear

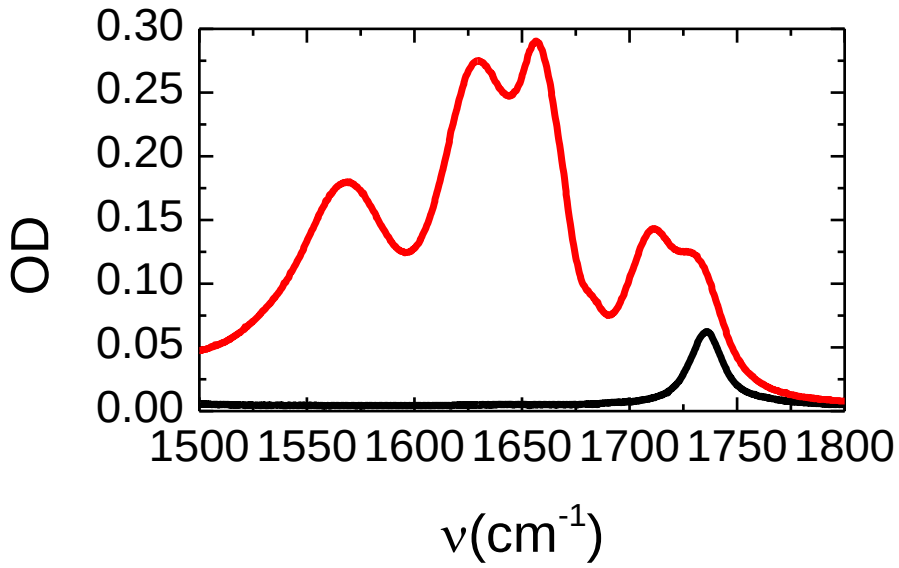

Figure 5.6. FTIR spectra of lauric acid in THF at a concentration of 0.05 M (black) and spectra of DES2 (red).

relation with the concentration of LA in the DESs (figure 5.7). Moreover, the similar trend of two bands ratio can be observed from the normalized diagonal trace (NDT) of each 2DIR spectra at T_w = 0 ps, which is proportional to the square of FTIR signal.[36] After normalized according to the hydrogen-bonded band, the NDT of each sample is presented in figure 5.8. The blue-side band increases with the lowered molar ratio of LA in DESs. The ratio change of acid band area with the concentration of LA provides evidence of the interaction between LA and NMA in the DES.

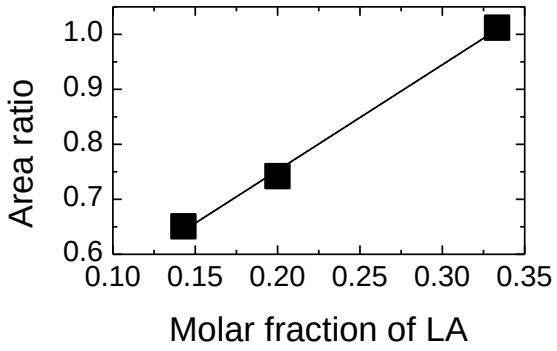

Figure 5.7. Area ratios of the HB band over a free band of acid carbonyl in NMA-LA of varied molar ratio, the solid line is linear fitting.

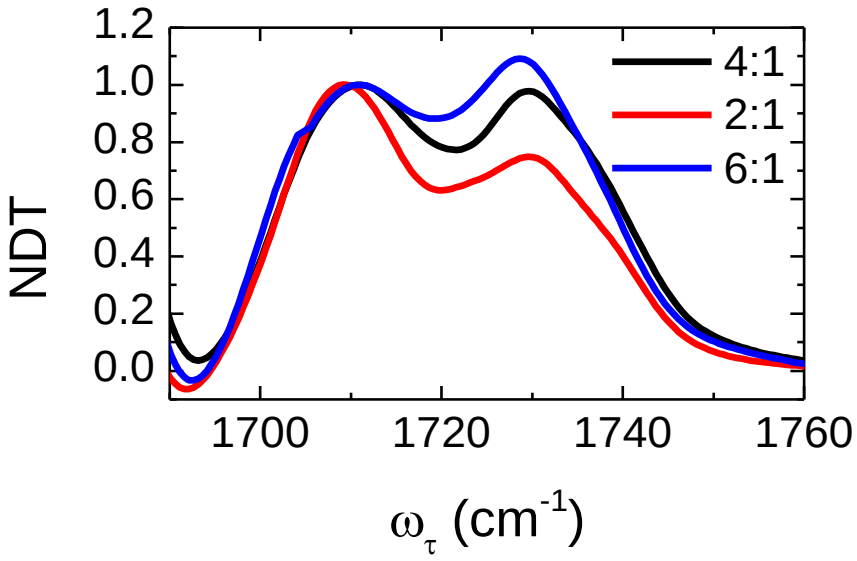

Figure 5.8. The NDT of acid bands in 2DIR spectra of DESs

The thermodynamics of hydrogen-bond in DESs can be extracted from the temperature-dependent FTIR spectra.[46] The FTIR spectra of a 2HB and 1HB band of amide I band in all the DESs with varied temperature were fitted with three-band Lorentzian functions, where the first peak represents neighboring amide II band. The area ratio of NMA amide I band with the reverse of temperature is shown in figure 5.9a. The linear fitting data are listed in table 5.2. Even the vibrational coupling between each configuration of amide I band in their spectra is reported,[35,41] and we have confirmed that with our 2DIR spectra of our DESs previously, the linear relations in each DES show that the thermodynamics is not significantly affected by coupling. We can still extract thermodynamics from the temperature-dependent experiments. Enthalpy of the two vibration states of amide I band in DES2, DES4, and DES6 were statistically the same, showing that the process of two bands of amide I band in all the DESs are not affected by the changing concentration of LA. On the other hand, the entropy is affected by the molar ratio of LA, which suggests the interaction between LA and NMA. The similar analysis to temperature-dependent acid carbonyl peaks in DESs are conducted (figure 5.9b). The enthalpy of the two acid bands in all the DES are similar, indicating the hydrogen bond formed with acid carbonyl is similar. The entropy of acid bands is similar in all the DESs, which is different with the entropy of NMA bands. For the acid bands, the change in molar ratio cannot influence the thermodynamics significantly.

The 2DIR spectra of DESs are composed with NMA peaks (amide I band and amide II bands), and acid peaks (carbonyl stretch) as described previously in this work. The amide I bands in the 2DIR spectra of each DES are similar to the 2DIR spectra of neat NMA reported by Cunha et al.,[41] which suggests that the amide I band in DESs has a similar local environment to neat NMA. In other words, NMA molecules are very likely to be aggregated in the DES. In addition to considering the long carbon non-polar side chain of LA, the highly heterogeneous structure of DES

can be drawn as a polar domain composed of NMA molecules, and a non-polar domain formed by side-chain of acid. The carboxylic group of LA interacts with NMA as the interface to connect polar and non-polar domains.

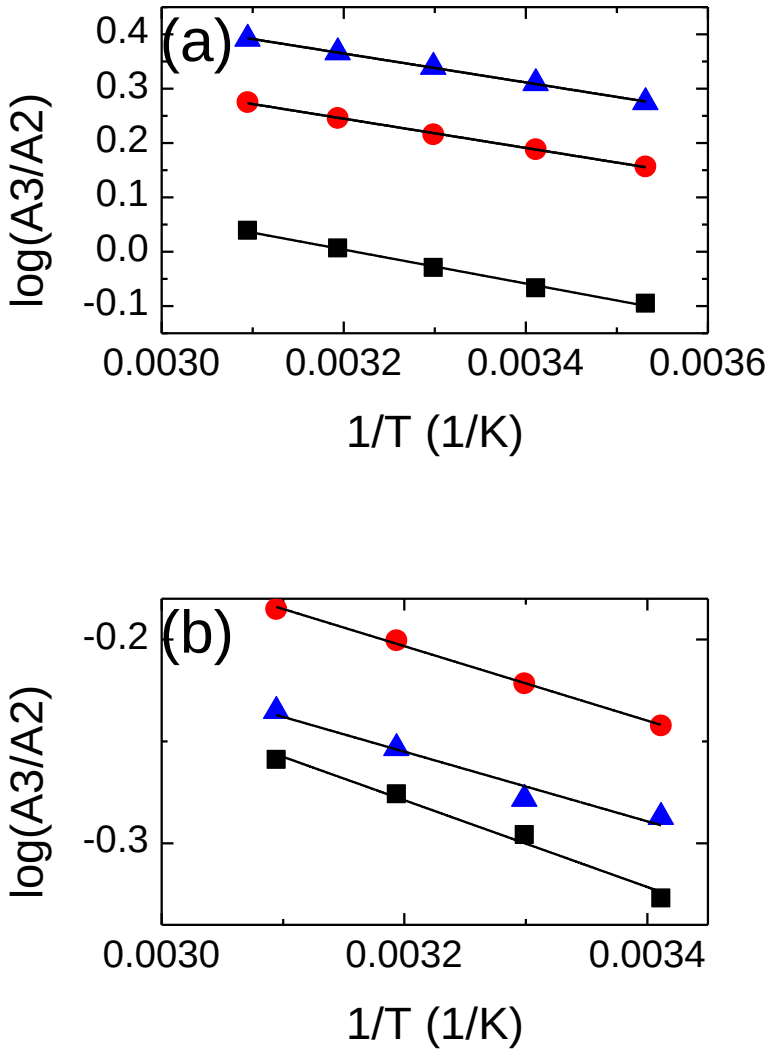

Figure 5.9. Natural logarithm of the area ratio of the 2HB band and 1HB band of amide band of NMA (a) and acid carbonyl band (b) in DES2 (black), DES4 (red), and DES6 (blue). The solid line indicates linear fitting.

Table 5.2. Linear fitting parameters of band area ratio vs. reverse of temperature, amide bands (top) and acid bands (bottom)

DES	Amide bands				Acid bands			
	slope	intercept	ΔH/ kJ/mol	ΔS/ J/molK	slope	intercept	ΔH/ kJ/mol	ΔS/ J/molK
2	-312±12	1.00±0.04	2.6±0.1	8.3±0.3	-213±18	0.40±0.06	1.8±0.1	3.3±0.5
4	-269±6	1.11±0.02	2.24±0.05	9.2±0.2	-183±6	0.38±0.02	1.5±0.1	3.2±0.2
6	-266±4	1.22±0.01	2.21±0.03	10.1±0.1	-171±23	0.29±0.08	1.4±0.2	2.4±0.7

The dynamics of the 2DIR spectra of free amide I band in each DES was also analyzed with the CLS method. The CLSs of free amide I band in each DES are shown in figure 5.10, and exponential fitting parameters are listed in table 5.3. All the characteristic times are ~1-2 ps, indicating the hydrogen bond making and breaking of the solvation shell, as previously seen.[27,42,47-51] In the case of NMA-LA systems, we use the model of confinement in reverse micelles to connect the dynamics observed and the heterogeneous structure we proposed. The water dynamics inside the reverse micelle has been described by many works.[52-55] Fayer and co-workers have used the O-D stretch as a probe to study the water dynamics inside reverse micelles relating to the size of water pool (reverse micelle) by linear and time-resolved infrared spectroscopy.[54,55] In the case of large reverse micelles, the dynamics is decoupled into core region, behaving like bulk water, and interface observed confinement according to the size of reverse micelle. In the case of small reverse micelles, the slowed spectral diffusion was observed with decreasing the size of reverse micelle. The size of the polar domain will change with a different ratio between components in the system. The identical dynamics of free amide band match well with the core region in Fayer's model, since they are not affected by the pool size. The difference of the offset (y_0) refers to a slower motion,

and y_0 increases with the concentration of NMA decreasing, causing the pool size of the polar domain to shrink. This phenomenon agrees with the water confined dynamics reported. Therefore, our assignment of the heterogeneous structure is well explained with the model of confined dynamics in a reverse micelle.

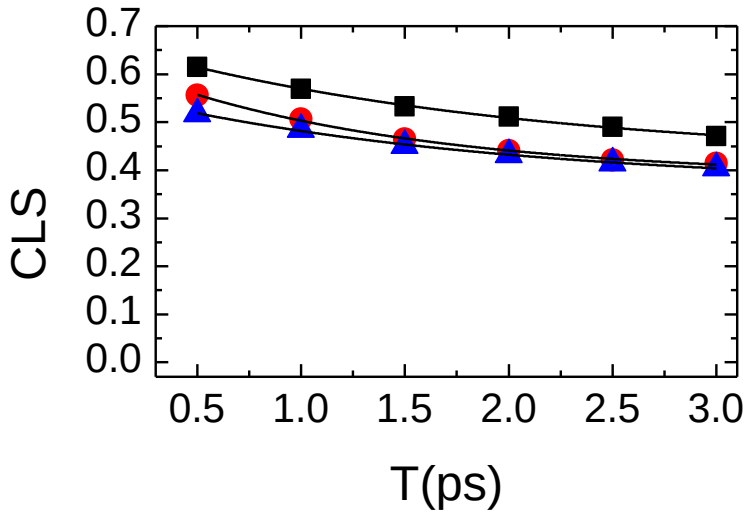

Figure 5.10. Spectral diffusion of free amide I band in 2DIR of DES2 (black), DES4 (red), and DES6 (blue). The solid black line is single exponential fitting to CLS of each DES.

Table 5.3. Parameters of exponential fitting to CLS in 2DIR spectra of DESs

	y_0	A	T / ps
DES2	0.42±0.01	0.25±0.01	1.9±0.2
DES4	0.39±0.01	0.25±0.01	1.3±0.1
DES6	0.36±0.01	0.20±0.01	1.8±0.3

The dynamics of each DESs at acid carbonyl region was extracted from their 2DIR spectra with Central Line Slope method (CLS).[43] The CLS was learned as a metric to describe the correlation change within picosecond time scale, and since the time constants of frequency-

frequency correlation function can be extracted from the CLS change with waiting time, then the dynamics can be learned. The CLSs of the free band and HB band at different T_w are presented in figure 5.11. The CLS of DESs at both acid carbonyl bands decay slowly, and the CLSs of each sample exhibit similar slow dynamics. Thus, changing the ratio of the two components does not influence the interaction with a carbonyl group.

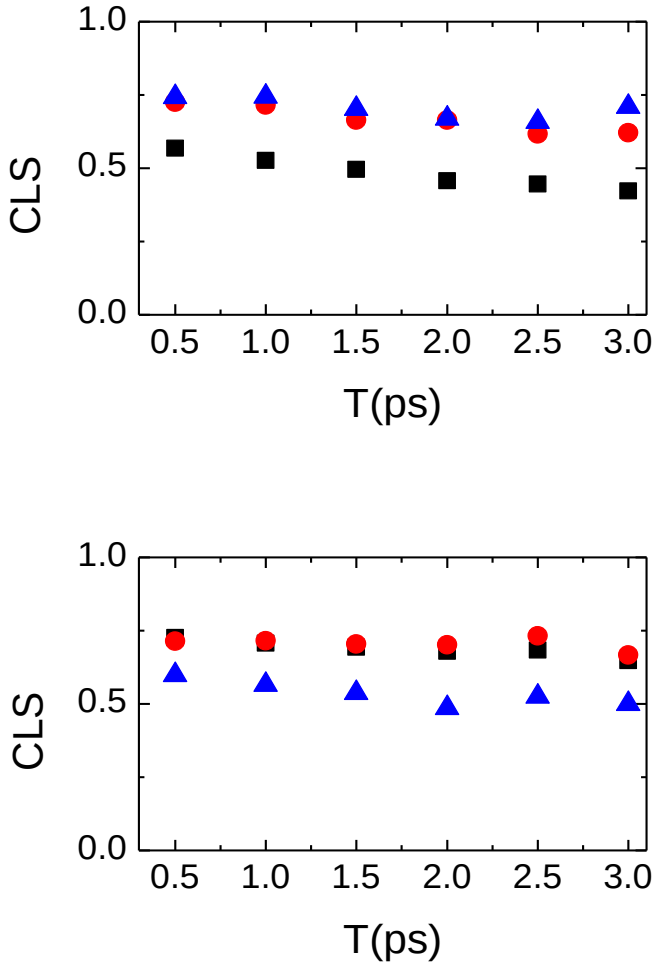

Figure 5.11. CLS of HB band (top) and free band (bottom) of the acid carbonyl group in the DES2 (black), DES4 (red), and DES6 (blue) from 2DIR spectra.

One interesting fact with the 2DIR spectra of DESs in the acid carbonyl frequency region is that the cross peak grows with time only in DES6, while the other DESs have no sign that the

cross peak exists within 3 ps. The cross peak intensity between free and HB bands of each DES in their 2DIR at various waiting times is shown in figure 5.12. From the cross peak intensity change with time, it is clear that compared with DES6, the cross peak in the other DESs is negligible. The similar low cross peak intensity of DES2 and DES4 show that the breaking and forming of a hydrogen bond with the carbonyl group of acid are not observed during 3 ps by 2DIR spectra. Usually, hydrogen bond exchange is expected to be observed in 2DIR spectra of hydrogen bond related bands, like the appearance in DES6. The fact of no hydrogen bond exchange with the acid carbonyl group in DES2 and DES4 2DIR spectra is probably due to the higher concentration of LA confining the hydrogen bond forming and breaking when the polar domain is becoming smaller, resulting from the concentration of non-polar group, the side chain of LA, increasing.

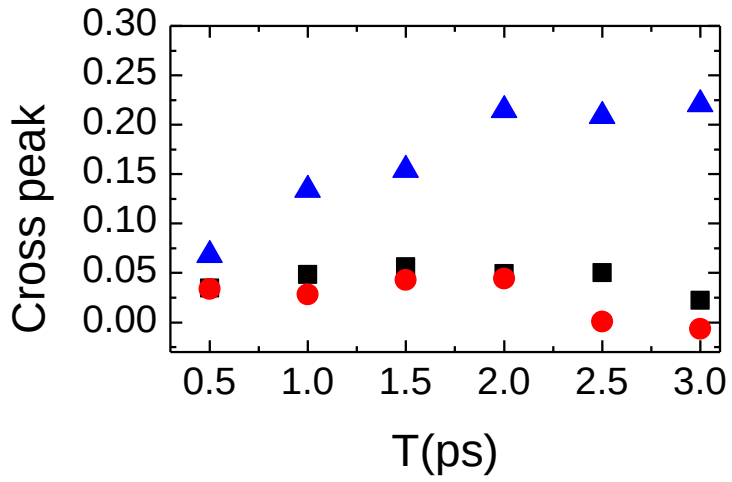

Figure 5.12. Cross peak is growing with waiting time for DESs. DES2 (black), DES4 (red), and DES6 (blue).

We further test the confinement effect with ionic and molecular thiocyanate probes to confirm our model of the DES systems. For comparison, the probes in NMA were also measured.

Because of their polarity, we expect the probes will reside in the polar domain. The FTIR spectra of these two probes are shown in figure 5.13. For the ionic probe, all the spectra have asymmetric

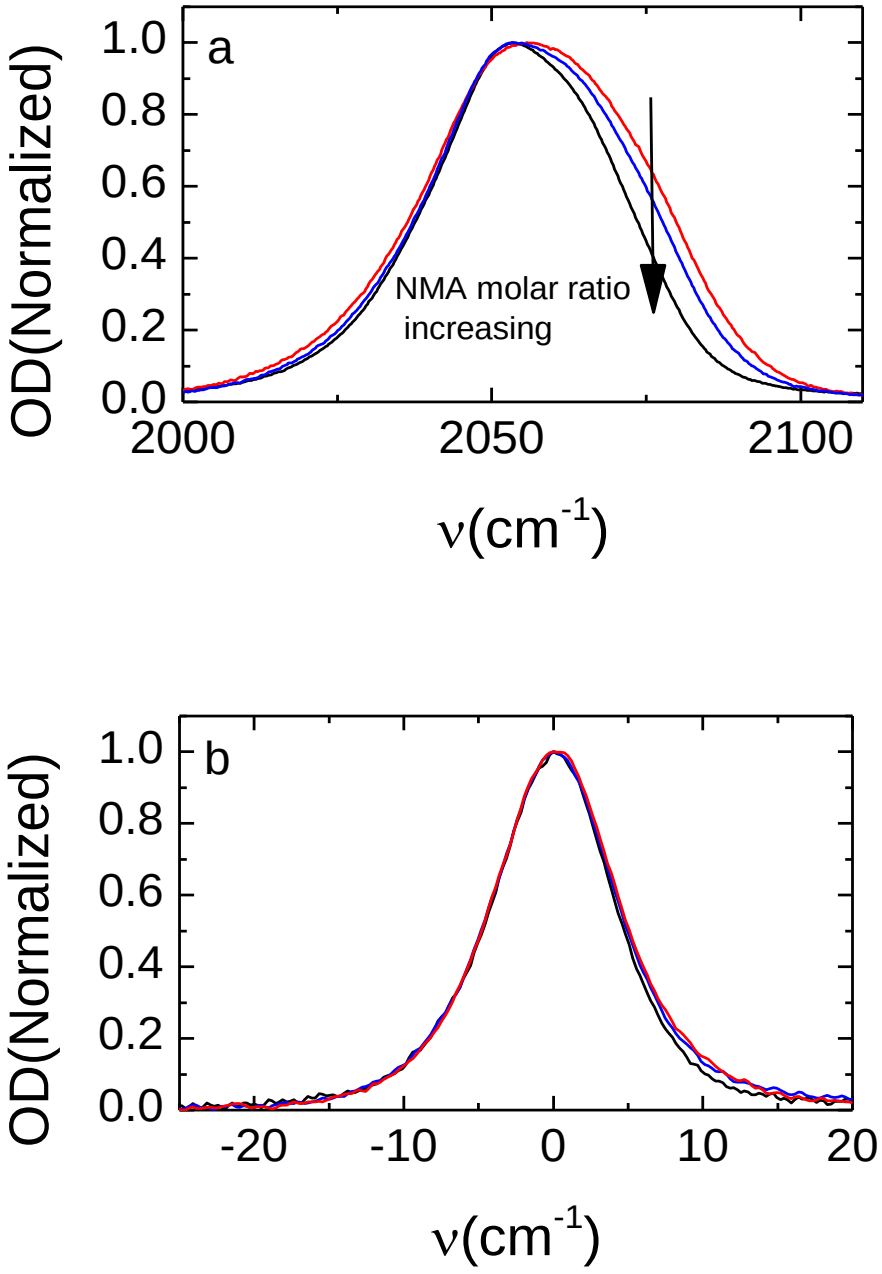

Figure 5.13. Normalized TFIR spectra of TBASCN (a) BSCN (b) probe in NMA (black), DES4 (blue), and DES2 (red).

profiles. Among them, the spectra of DES with 2:1 ratio is centered at 2056 cm^{-1}, while the other spectra are centered at 2054 cm^{-1}. The probe in NMA has the narrowest profile, and with the concentration of NMA decreasing in DESs, the peak becomes broader from the blue-side of the peak, while leaving the red-side almost the same for all the samples.

The spectra after background subtraction and normalization of BSCN as a probe in DES and NMA are slightly asymmetric, and the central frequencies of NMA, DES2, and DES4 are 2155.2 cm^{-1}, 2155.7 cm^{-1}, and 2155.9 cm^{-1}, respectively. The spectra of DES2 and DES4 have the same lineshape. Comparing the spectra of NMA, the width of the spectra of DESs are slightly broader.

The structure and dynamics of NMA-LA systems were also studied with infrared probed by 2DIR spectroscopy. Figure 5.14 shows the 2DIR spectra for the nitrile stretch region of the thiocyanate ion in the DESs and NMA as a comparison as well. The positive and negative peaks are separated by ~23 cm^{-1}, the anharmonicity of the vibrational potential of the thiocyanate nitrile stretch, which agrees previous published.[20] At T_w = 0 ps, the positive and negative peaks of all the spectra are tilted and elongated along the diagonal line. All the spectra at this time are similar to each other. With longer waiting times, the peaks acquire rounder shapes and become less tilted. At the later waiting times, the spectra of NMA are nearly round or square shape, while the spectra of DES4 and DES2 are still slightly tilted. The shapes of the spectra show clear evidence that cross peaks exist in the 2DIR, which are absent at T_w = 0 ps.

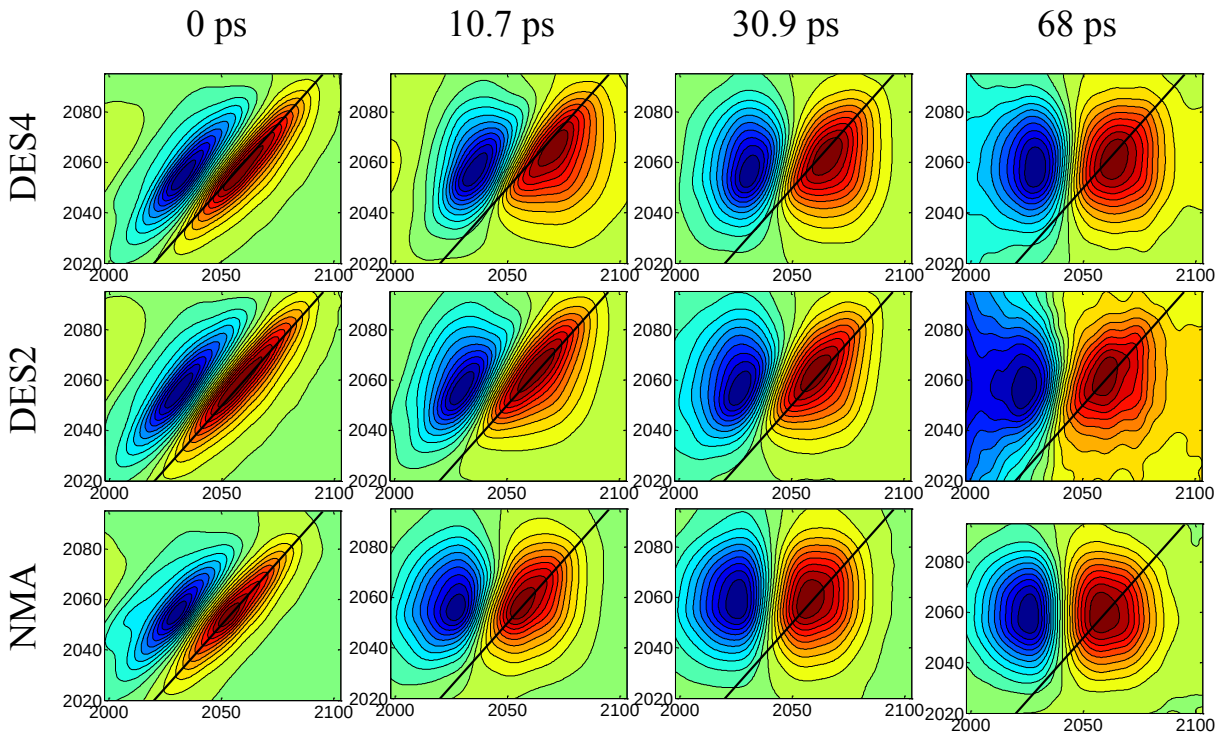

Figure 5.14. 2DIR spectra of TBA SCN in DES4 (top), DES2 (middle), and NMA (bottom) at Tw = 0 ps, 10.7 ps, 30.9 ps, and 68 ps.

With benzyl thiocyanate as the molecular infrared probe, in DES4, DES2, and NMA were measured with 2DIR spectroscopy, and the 2DIR spectra are given in figure 5.15. Compared with ionic thiocyanate probe, the spectra have larger anharmonicities, ~25 cm^{-1}. Similar to the 2DIR spectra of TBA SCN probe, the spectra of the molecular probe in DESs and NMA present tilted and elongated ellipsis along the diagonal line at short or no waiting time. With the waiting time evolution, the spectra exhibit almost upright and round shapes. The spectra of BSCN in NMA already looks round from Tw = 68 ps on, while the probe in DES2 and DES4 still exhibit slightly elongated shapes. In the 2DIR spectra of BSCN in DESs and NMA, no obvious cross peaks appear within 100 ps of waiting time.

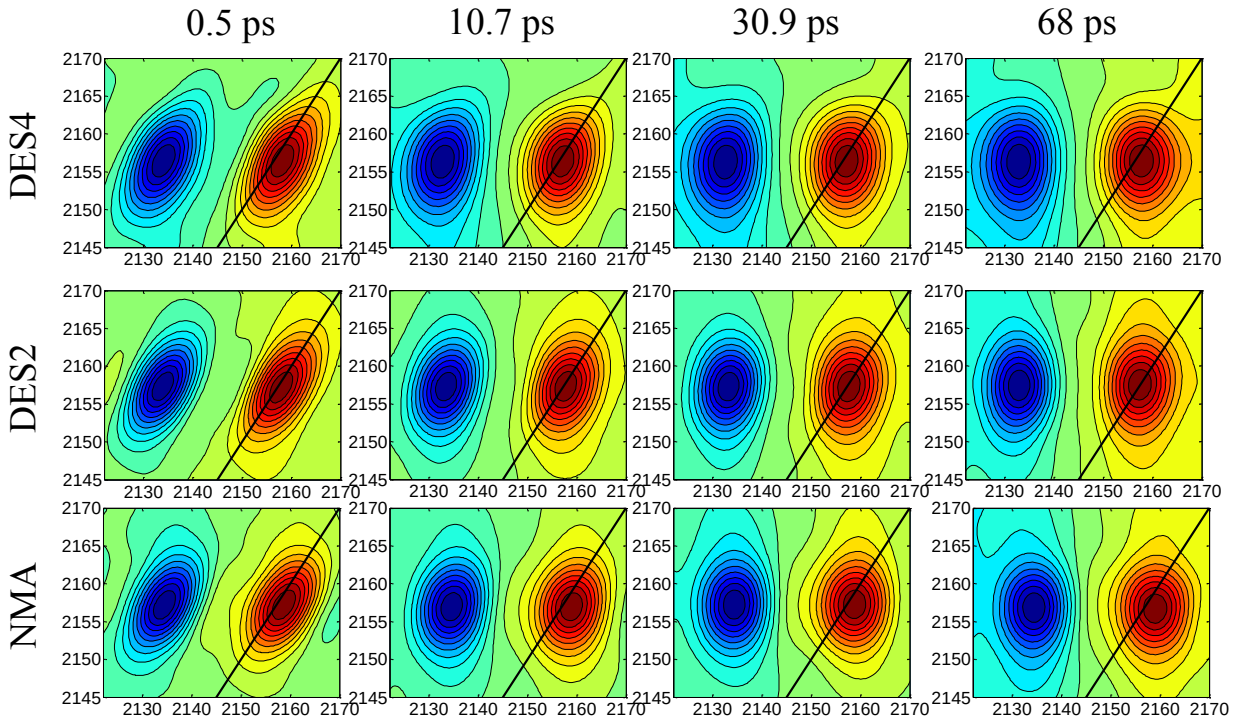

Figure 5.15. 2DIR spectra of BSCN in DES4 (top), DES2 (middle) and NMA (bottom) at Tw = 0.5 ps, 10.7 ps, 30.9 ps, and 68 ps.

The spectral diffusion of the ionic and molecular probes with time is shown in figure 5.16, and the parameters of the exponential decay fitting are shown in table 5.4. Compared to probes in NMA, we observe the slowdown of the time constant in both probes, similar to what has been observed in reverse micelles. These results confirm the confinement effect, showing the confined dynamics from the other domain. For the ionic probe, we observed the larger characteristic time of DES2 than that of DES4, where DES4 has a lower concentration of LA. However, the time constants of correlation decay in DES2 and DES4 with the molecular probe are identical. There are two possible explanations: one is the probe location in the DES is in the center of the polar domain where it is not sensing the confinement from the region near interface; the other reason could be that the probe is not sensitive enough to show the difference in time.

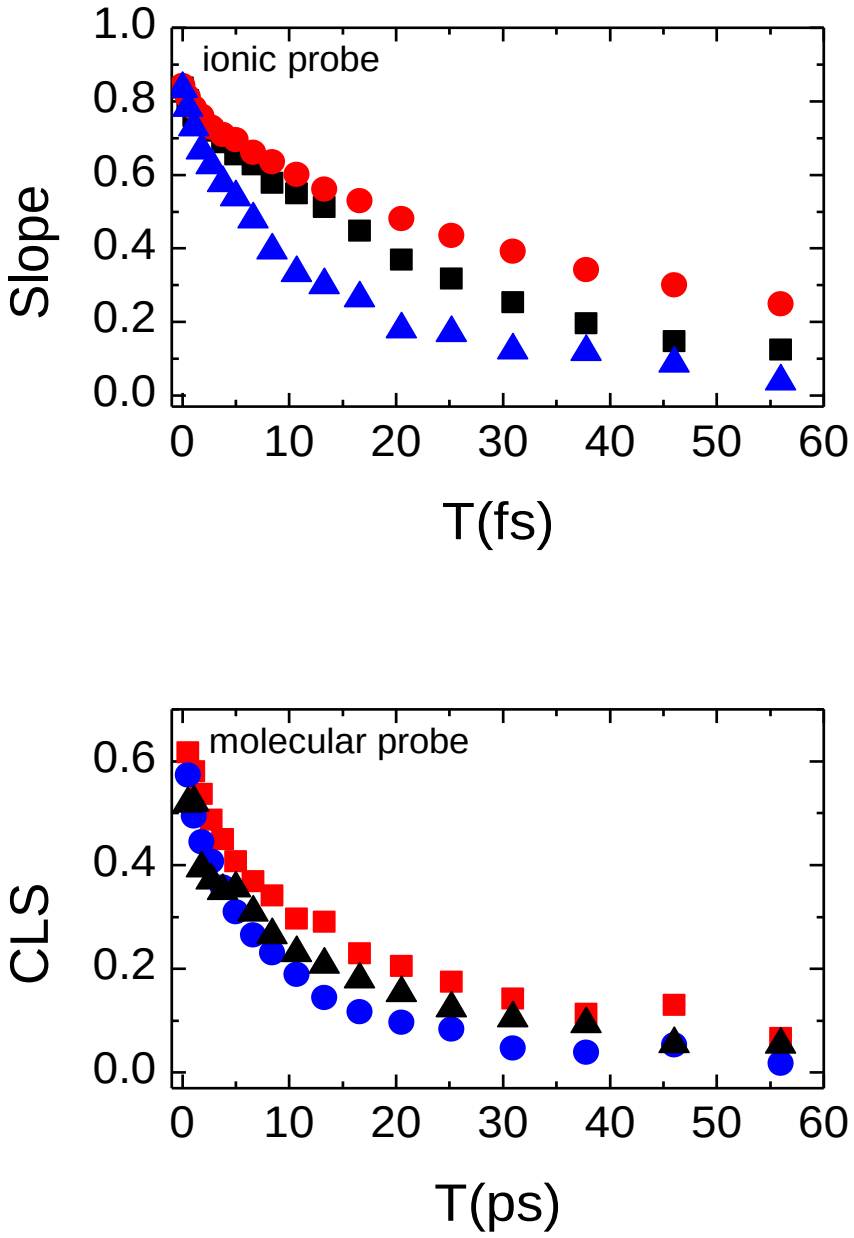

Figure 5.16. Frequency-frequency correlation decay of thiocyanate ion in DES2 (red), DES4 (black), and NMA (blue) solution.

Table 5.4. Exponential decay fitting parameters of FFCF dynamics of SCN^- 2DIR spectra

	Ionic probe			Molecular probe				
	y_0	A	τ	y_0	A_1	τ_1	A_2	τ_2
DES2	0.15±0.01	0.64±0.01	30±1	0.07±0.01	0.19±0.04	2.7±0.9	0.41±0.04	19±3
DES4	0.01±0.02	0.80±0.01	27±1	0.02±0.02	0.19±0.04	1.4±0.7	0.39±0.03	19±3
NMA	0.06±0.01	0.73±0.02	12±1	0.03±0.01	0.16±0.03	1.0±0.4	0.46±0.02	10±1

The cross peak growing with waiting time in 2DIR of TBA SCN in DESs and NMA is shown in figure 5.17. The cross peak intensity is fitted with an exponential function, $f(t) = A(1 - e^{-t/\tau})$, and fitting data are in table 5.5. The time constants for all the DESs are statistically the same, while that of the NMA sample is a little bit slower. The cross peaks of SCN ion in DESs show that the hydrogen bond dynamics around the probe are similar regardless of the mixing ratio of components, indicating ionic probes are probing polar pool.

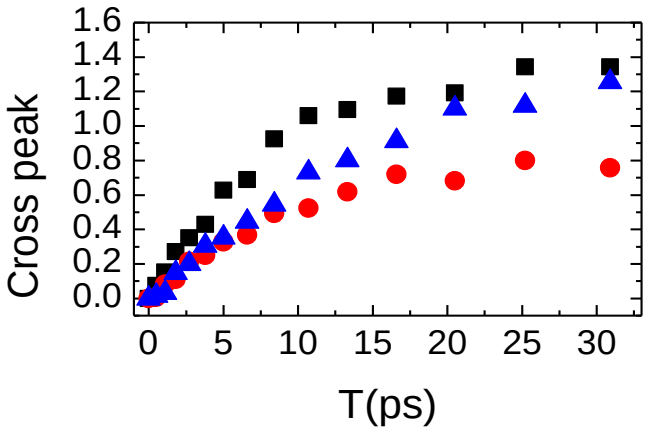

Figure 5.17. Cross peak intensity changes with waiting time of ionic SCN probe in DES2 (red), DES4 (black), and NMA (blue).

Table 5.5. Exponential fitting parameters of the cross peak intensity of 2DIRspectra of TBA SCN in DESs and NMA.

	A	t / ps
DES2	-0.84±0.03	9.6±0.9
DES4	-1.39±0.04	8.4±0.6
NMA	-1.52±0.06	17±1

5.5. Summary

In the DES composed of N-methylacetamide and lauric acid, the interactions and dynamics of NMA and LA in the DES with the different molar ratios were investigated by linear and time-resolved infrared spectroscopy. With the probe of C=O group both in NMA and LA, the interactions between components in DESs are revealed. Inside the DES, C=O group of NMA can form one hydrogen bond, two hydrogen-bond, or free of the hydrogen-bond, and the carbonyl of the acid can form one hydrogen bond or none. The interactions between self-species and inter-species are observed in FTIR studies. Based on the interactions between components and dynamics probed by free amide I bond, as well as introducing ionic and molecular probe, we proposed the NMA-LA system possesses a heterogeneous structure. The dynamics of probes is confined by the smaller pool size, which is similar to the well-studied confined water dynamics in reverse micelles. Our observation of slowing down dynamics of probes in a lower molar ratio of NMA in the DES provides the indirect evidence of the heterogeneous structure. The study of the NMA-LA system with the non-polar region and X-ray spectroscopy of the DES are expected to be conducted in order to provide direct evidence.

5.6. References

1. Guthrie, F., On Eutexia. *Proceedings of the Physical Society of London* **1884**, *6*, 124.

2. Abbott, A. P.; Barron, J. C.; Ryder, K. S.; Wilson, D., Eutectic-Based Ionic Liquids with Metal-Containing Anions and Cations. *Chemistry-A European Journal* **2007**, *13*, 6495-6501.

3. Abbott, A. P.; Capper, G.; Davies, D. L.; Munro, H. L.; Rasheed, R. K.; Tambyrajah, V., Preparation of Novel, Moisture-Stable, Lewis-Acidic Ionic Liquids Containing Quaternary Ammonium Salts with Functional Side Chainselectronic *Chemical Communications* **2001**, 2010-2011.

4. Abbott, A. P.; Boothby, D.; Capper, G.; Davies, D. L.; Rasheed, R. K., Deep Eutectic Solvents Formed between Choline Chloride and Carboxylic Acids: Versatile Alternatives to Ionic Liquids. *Journal of the American Chemical Society* **2004**, *126*, 9142-9147.

5. Smith, E. L.; Abbott, A. P.; Ryder, K. S., Deep Eutectic Solvents (Dess) and Their Applications. *Chemical reviews* **2014**, *114*, 11060-11082.

6. Zhang, Q.; Vigier, K. D. O.; Royer, S.; Jérôme, F., Deep Eutectic Solvents: Syntheses, Properties and Applications. *Chemical Society Reviews* **2012**, *41*, 7108-7146.

7. Zhao, H.; Baker, G. A., Ionic Liquids and Deep Eutectic Solvents for Biodiesel Synthesis: A Review. *Journal of Chemical Technology and Biotechnology* **2013**, *88*, 3-12.

8. Francisco, M.; van den Bruinhorst, A.; Kroon, M. C., Low-Transition-Temperature Mixtures (Lttms): A New Generation of Designer Solvents. *Angewandte Chemie international edition* **2013**, *52*, 3074-3085.

9. Welton, T., Room-Temperature Ionic Liquids. Solvents for Synthesis and Catalysis. *Chemical reviews* **1999**, *99*, 2071-2084.

10. García, G.; Aparicio, S.; Ullah, R.; Atilhan, M., Deep Eutectic Solvents: Physicochemical Properties and Gas Separation Applications. *Energy & Fuels* **2015**, *29*, 2616-2644.

11. Singh, B.; Lobo, H.; Shankarling, G., Selective N-Alkylation of Aromatic Primary Amines Catalyzed by Bio-Catalyst or Deep Eutectic Solvent. *Catalysis letters* **2011**, *141*, 178-182.

12. Yang, H.; Guo, X.; Birbilis, N.; Wu, G.; Ding, W., Tailoring Nickel Coatings Via Electrodeposition from a Eutectic-Based Ionic Liquid Doped with Nicotinic Acid. *Applied Surface Science* **2011**, *257*, 9094-9102.

13. Gómez, E.; Cojocaru, P.; Magagnin, L.; Valles, E., Electrodeposition of Co, Sm and Smco from a Deep Eutectic Solvent. *Journal of electroanalytical chemistry* **2011**, *658*, 18-24.

14. Abbott, A. P.; Capper, G.; Davies, D. L.; McKenzie, K. J.; Obi, S. U., Solubility of Metal Oxides in Deep Eutectic Solvents Based on Choline Chloride. *Journal of Chemical & Engineering Data* **2006**, *51*, 1280-1282.

15. Leron, R. B.; Li, M.-H., Solubility of Carbon Dioxide in a Choline Chloride–Ethylene Glycol Based Deep Eutectic Solvent. *Thermochimica acta* **2013**, *551*, 14-19.

16. Shahbaz, K.; Mjalli, F.; Hashim, M.; AlNashef, I., Using Deep Eutectic Solvents Based on Methyl Triphenyl Phosphunium Bromide for the Removal of Glycerol from Palm-Oil-Based Biodiesel. *Energy & Fuels* **2011**, *25*, 2671-2678.

17. Carriazo, D.; Serrano, M. C.; Gutiérrez, M. C.; Ferrer, M. L.; del Monte, F., Deep-Eutectic Solvents Playing Multiple Roles in the Synthesis of Polymers and Related Materials. *Chemical Society Reviews* **2012**, *41*, 4996-5014.

18. Fortenberry, D. I.; Pojman, J. A., Solvent-Free Synthesis of Polyacrylamide by Frontal Polymerization. *Journal of Polymer Science Part A: Polymer Chemistry* **2000**, *38*, 1129-1135.

19. Cui, Y.; Li, M.-C.; Wu, Q.; Pojman, J. A.; Kuroda, D. G., Synthesis-Free Phase-Selective Gelator for Oil-Spill Remediation. *ACS Applied Materials & Interfaces* **2017**, *9*, 33549-33553.

20. Cui, Y.; Fulfer, K.; Ma, J.; Weldeghiorghis, T.; Kuroda, D., Solvation Dynamics of an Ionic Probe in Choline Chloride-Based Deep Eutectic Solvents. *Physical Chemistry Chemical Physics* **2016**, *18*, 31471-31479.

21. Perkins, S. L.; Painter, P.; Colina, C. M., Experimental and Computational Studies of Choline Chloride-Based Deep Eutectic Solvents. *Journal of Chemical & Engineering Data* **2014**, *59*, 3652-3662.

22. Das, A.; Biswas, R., Dynamic Solvent Control of a Reaction in Ionic Deep Eutectic Solvents: Time-Resolved Fluorescence Measurements of Reactive and Nonreactive Dynamics in (Choline Chloride+ Urea) Melts. *The Journal of Physical Chemistry B* **2015**, *119*, 10102-10113.

23. Wagle, D. V.; Baker, G. A.; Mamontov, E., Differential Microscopic Mobility of Components within a Deep Eutectic Solvent. *The journal of physical chemistry letters* **2015**, *6*, 2924-2928.

24. D'Agostino, C.; Harris, R. C.; Abbott, A. P.; Gladden, L. F.; Mantle, M. D., Molecular Motion and Ion Diffusion in Choline Chloride Based Deep Eutectic Solvents Studied by 1 H Pulsed Field Gradient Nmr Spectroscopy. *Physical Chemistry Chemical Physics* **2011**, *13*, 21383-21391.

25. van Osch, D. J.; Zubeir, L. F.; van den Bruinhorst, A.; Rocha, M. A.; Kroon, M. C., Hydrophobic Deep Eutectic Solvents as Water-Immiscible Extractants. *Green Chemistry* **2015**, *17*, 4518-4521.

26. Das, A.; Das, S.; Biswas, R., Density Relaxation and Particle Motion Characteristics in a Non-Ionic Deep Eutectic Solvent (Acetamide+ Urea): Time-Resolved Fluorescence

Measurements and All-Atom Molecular Dynamics Simulations. *The Journal of chemical physics* **2015**, *142*, 034505.

27. Woutersen, S.; Mu, Y.; Stock, G.; Hamm, P., Hydrogen-Bond Lifetime Measured by Time-Resolved 2d-Ir Spectroscopy: N-Methylacetamide in Methanol. *Chemical Physics* **2001**, *266*, 137-147.

28. Asplund, M.; Zanni, M. T.; Hochstrasser, R. M., Two-Dimensional Infrared Spectroscopy of Peptides by Phase-Controlled Femtosecond Vibrational Photon Echoes. *Proceedings of the National Academy of Sciences* **2000**, *97*, 8219-8224.

29. DeFlores, L. P.; Ganim, Z.; Nicodemus, R. A.; Tokmakoff, A., Amide I′− Ii′ 2d Ir Spectroscopy Provides Enhanced Protein Secondary Structural Sensitivity. *Journal of the American Chemical Society* **2009**, *131*, 3385-3391.

30. Lim, M.; Hochstrasser, R. M., Unusual Vibrational Dynamics of the Acetic Acid Dimer. *The Journal of Chemical Physics* **2001**, *115*, 7629-7643.

31. Rubtsov, I. V.; Wang, J.; Hochstrasser, R. M., Dual-Frequency 2d-Ir Spectroscopy Heterodyned Photon Echo of the Peptide Bond. *Proceedings of the National Academy of Sciences* **2003**, *100*, 5601-5606.

32. Kim, Y. S.; Hochstrasser, R. M., Applications of 2d Ir Spectroscopy to Peptides, Proteins, and Hydrogen-Bond Dynamics. *The Journal of Physical Chemistry B* **2009**, *113*, 8231-8251.

33. Ganim, Z.; Chung, H. S.; Smith, A. W.; DeFlores, L. P.; Jones, K. C.; Tokmakoff, A., Amide I Two-Dimensional Infrared Spectroscopy of Proteins. *Accounts of chemical research* **2008**, *41*, 432-441.

34. Wang, L.; Middleton, C. T.; Zanni, M. T.; Skinner, J. L., Development and Validation of Transferable Amide I Vibrational Frequency Maps for Peptides. *The Journal of Physical Chemistry B* **2011**, *115*, 3713-3724.

35. DeCamp, M.; DeFlores, L.; McCracken, J.; Tokmakoff, A.; Kwac, K.; Cho, M., Amide I Vibrational Dynamics of N-Methylacetamide in Polar Solvents: The Role of Electrostatic Interactions. *The Journal of Physical Chemistry B* **2005**, *109*, 11016-11026.

36. Hamm, P.; Zanni, M., *Concepts and Methods of 2d Infrared Spectroscopy*; Cambridge University Press, 2011.

37. Fayer, M., Dynamics of Liquids, Molecules, and Proteins Measured with Ultrafast 2d Ir Vibrational Echo Chemical Exchange Spectroscopy. *Annual review of physical chemistry* **2009**, *60*, 21-38.

38. Kim, Y. S.; Wang, J.; Hochstrasser, R. M., Two-Dimensional Infrared Spectroscopy of the Alanine Dipeptide in Aqueous Solution. *The journal of physical chemistry B* **2005**, *109*, 7511-7521.

39. Fulfer, K.; Kuroda, D., A Comparison of the Solvation Structure and Dynamics of the Lithium Ion in Linear Organic Carbonates with Different Alkyl Chain Lengths. *Physical Chemistry Chemical Physics* **2017**, *19*, 25140-25150.

40. Besley, N. A., Ab Initio Modeling of Amide Vibrational Bands in Solution. *The Journal of Physical Chemistry A* **2004**, *108*, 10794-10800.

41. Cunha, A. V.; Salamatova, E.; Bloem, R.; Roeters, S. J.; Woutersen, S.; Pshenichnikov, M. S.; Jansen, T. L., Interplay between Hydrogen Bonding and Vibrational Coupling in Liquid N-Methylacetamide. *The journal of physical chemistry letters* **2017**, *8*, 2438-2444.

42. Zanni, M. T.; Asplund, M. C.; Hochstrasser, R. M., Two-Dimensional Heterodyned and Stimulated Infrared Photon Echoes of N-Methylacetamide-D. *The Journal of Chemical Physics* **2001**, *114*, 4579-4590.

43. Kwac, K.; Cho, M., Molecular Dynamics Simulation Study of N-Methylacetamide in Water. Ii. Two-Dimensional Infrared Pump–Probe Spectra. *The Journal of chemical physics* **2003**, *119*, 2256-2263.

44. DeFlores, L. P.; Ganim, Z.; Ackley, S. F.; Chung, H. S.; Tokmakoff, A., The Anharmonic Vibrational Potential and Relaxation Pathways of the Amide I and Ii Modes of N-Methylacetamide. *The Journal of Physical Chemistry B* **2006**, *110*, 18973-18980.

45. Torii, H.; Tatsumi, T.; Tasumi, M., Effects of Hydration on the Structure, Vibrational Wavenumbers, Vibrational Force Field and Resonance Raman Intensities of N-Methylacetamide. *Journal of Raman Spectroscopy* **1998**, *29*, 537-546.

46. Guerin, A. C.; Riley, K.; Rupnik, K.; Kuroda, D. G., Determining the Energetics of the Hydrogen Bond through Ftir: A Hands-on Physical Chemistry Lab Experiment. *Journal of Chemical Education* **2016**, *93*, 1124-1129.

47. Fecko, C.; Eaves, J.; Loparo, J.; Tokmakoff, A.; Geissler, P., Ultrafast Hydrogen-Bond Dynamics in the Infrared Spectroscopy of Water. *Science* **2003**, *301*, 1698-1702.

48. Woutersen, S.; Pfister, R.; Hamm, P.; Mu, Y.; Kosov, D. S.; Stock, G., Peptide Conformational Heterogeneity Revealed from Nonlinear Vibrational Spectroscopy and Molecular-Dynamics Simulations. *The Journal of chemical physics* **2002**, *117*, 6833-6840.

49. Ghosh, A.; Hochstrasser, R. M., A Peptide's Perspective of Water Dynamics. *Chemical physics* **2011**, *390*, 1-13.

50. Chung, J. K.; Thielges, M. C.; Fayer, M. D., Dynamics of the Folded and Unfolded Villin Headpiece (Hp35) Measured with Ultrafast 2d Ir Vibrational Echo Spectroscopy. *Proceedings of the National Academy of Sciences* **2011**, *108*, 3578-3583.

51. Ghosh, A.; Remorino, A.; Tucker, M. J.; Hochstrasser, R. M., 2d Ir Photon Echo Spectroscopy Reveals Hydrogen Bond Dynamics of Aromatic Nitriles. *Chemical physics letters* **2009**, *469*, 325-330.

52. Singh, P. K.; Kuroda, D. G.; Hochstrasser, R. M., An Ion's Perspective on the Molecular Motions of Nanoconfined Water: A Two-Dimensional Infrared Spectroscopy Study. *The Journal of Physical Chemistry B* **2013**, *117*, 9775-9784.

53. Tan, H.-S.; Piletic, I. R.; Riter, R. E.; Levinger, N. E.; Fayer, M., Dynamics of Water Confined on a Nanometer Length Scale in Reverse Micelles: Ultrafast Infrared Vibrational Echo Spectroscopy. *Physical review letters* **2005**, *94*, 057405.

54. Moilanen, D. E.; Fenn, E. E.; Wong, D.; Fayer, M. D., Water Dynamics in Large and Small Reverse Micelles: From Two Ensembles to Collective Behavior. *The Journal of chemical physics* **2009**, *131*, 014704.

55. Moilanen, D. E.; Fenn, E. E.; Wong, D.; Fayer, M., Water Dynamics at the Interface in Aot Reverse Micelles. *The Journal of Physical Chemistry B* **2009**, *113*, 8560-8568.

APPENDIX A: COPYRIGHT RELEASE 1

Solvation dynamics of an ionic probe in choline chloride-based Deep Eutectic Solvents

Cui, Y., K. D. Fulfer, J. Ma, T. K. Weldeghiorghis, and D. G. Kuroda. *Physical Chemistry Chemical Physics* **2016**, 18, 31471-31479.

DOI: 10.1039/C6CP06318G

http://pubs.rsc.org/-/content/articlehtml/2016/cp/c6cp06318g

The following is a proof of copyright permission.

From: Gill Cockhead [mailto:CockheadG@rsc.org]
Sent: Tuesday, April 3, 2018 1:42 AM
To: Yaowen Cui <yyaowe1@lsu.edu>
Subject: RE: Reuse text of paper

Dear Yaowen

The Royal Society of Chemistry (RSC) hereby grants permission for the use of your paper(s) specified below in the printed and microfilm version of your thesis. You may also make available the PDF version of your paper(s) that the RSC sent to the corresponding author(s) of your paper(s) upon publication of the paper(s) in the following ways: in your thesis via any website that your university may have for the deposition of theses, via your university's Intranet or via your own personal website. We are however unable to grant you permission to include the PDF version of the paper(s) on its own in your institutional repository. The Royal Society of Chemistry is a signatory to the STM Guidelines on Permissions (available on request).

Please note that if the material specified below or any part of it appears with credit or acknowledgement to a third party then you must also secure permission from that third party before reproducing that material.

Please ensure that the thesis states the following:
Reproduced by permission of the PCCP Owner Societies
and include a link to the paper on the Royal Society of Chemistry's website.

Please ensure that your co-authors are aware that you are including the paper in your thesis.

Regards
Gill Cockhead
Publishing Contracts & Copyright Executive

Gill Cockhead
Publishing Contracts & Copyright Executive
Royal Society of Chemistry,
Thomas Graham House,
Science Park, Milton Road,
Cambridge, CB4 0WF, UK
Tel +44 (0) 1223 432134

Follow the Royal Society of Chemistry:
www.rsc.org/follow

APPENDIX B: COPYRIGHT RELEASE 2

Evidence of molecular heterogeneities in amide-based Deep Eutectic Solvents

Cui, Y., & Kuroda, D. G., *Journal of Physical Chemistry A.* 2018, 122, 1185−1193

DOI: 10.1021/acs.jpca.7b10264

https://pubs.acs.org/doi/abs/10.1021/acs.jpca.7b10264

4/2/2018 Rightslink® by Copyright Clearance Center

Copyright Clearance Center RightsLink®

Home | Create Account | Help

ACS Publications Most Trusted. Most Cited. Most Read.

Title: Evidence of Molecular Heterogeneities in Amide-Based Deep Eutectic Solvents

Author: Yaowen Cui, Daniel G. Kuroda

Publication: The Journal of Physical Chemistry A

Publisher: American Chemical Society

Date: Feb 1, 2018

Copyright © 2018, American Chemical Society

LOGIN

If you're a copyright.com user, you can login to RightsLink using your copyright.com credentials.

Already **a RightsLink user** or want to learn more?

PERMISSION/LICENSE IS GRANTED FOR YOUR ORDER AT NO CHARGE

This type of permission/license, instead of the standard Terms & Conditions, is sent to you because no fee is being charged for your order. Please note the following:

- Permission is granted for your request in both print and electronic formats, and translations.
- If figures and/or tables were requested, they may be adapted or used in part.
- Please print this page for your records and send a copy of it to your publisher/graduate school.
- Appropriate credit for the requested material should be given as follows: "Reprinted (adapted) with permission from (COMPLETE REFERENCE CITATION). Copyright (YEAR) American Chemical Society." Insert appropriate information in place of the capitalized words.
- One-time permission is granted only for the use specified in your request. No additional uses are granted (such as derivative works or other editions). For any other uses, please submit a new request.

BACK | CLOSE WINDOW

Copyright © 2018 Copyright Clearance Center, Inc. All Rights Reserved. Privacy statement. Terms and Conditions.
Comments? We would like to hear from you. E-mail us at customercare@copyright.com

VITA

Yaowen Cui finished his undergraduate study and obtained the Bachelor of Engineering degree in the major of Chemical Engineering and Technology from Harbin University of Science and Technology in 2007. He entered US to pursue higher education in Western Kentucky University in 2010. He got his M.S. degree in chemistry in 2012. The next year, he came to Louisiana to continue his studying under the guidance of Dr. Daniel Kuroda in physical chemistry. He plans to graduate in summer of 2018.